UNIVERSITA' DEGLI STUDI DI PADOVA

Facoltà di ingegneria

Corso di laurea specialistica in bioingegneria

TESI DI LAUREA

A MULTIMODAL NEUROIMAGING STUDY OF SOMATOSENSORY SYSTEM

Laureanda

Elisa Leonardelli

Mat. 586358

Relatrice

Prof. Alessandra Bertoldo

Correlatori

Prof. Christoph Braun

Dott. Christos Papadelis

(CIMeC-Università degli studi di Trento)

Padova, 26 ottobre 2010

Anno accademico 2009/2010

Preface

This thesis is the result of a ten months training by the magnetoencephalography laboratory (MEG-lab) of the Center for Brain/Mind science (CIMeC) of the University of Trento.

One of the first paper I read about MEG was titled "Magnetoencephalography: the art of finding a needle in a haystack". This sentence, a part scaring me, let me very surprised: is this art or science? MEG is a subtle and challenging science, I realized. I took care of projecting, developing and analyzing an entire experiment and every step I did, was not granted. For this reason the aim of this thesis is not only the results, but the whole procedure is also essential part of the thesis. Indeed, finding a needle in a haystack is not a everyday finding.

First of all I want to say thanks to the staff people of the MEG-lab, who helped me a lot and who involved me in laboratory life, permitting me not only to develop this thesis but also to participate actively in the research life and to live a precious human and working experience.

A particular thanks to the Prof. Alessandra Bertoldo from the University of Padova, who followed my thesis and supported me.

I want to thank also the University of Trento, the CIMeC and the University of Padova that gave me this opportunity.

Last, I want to thank my parents and tell them that … yesss, finally … I graduate! Thank you once again!

Elisa Leonardelli

Contents

Introduction

Magnetoencephalography (MEG) is a neuroimaging technique able to detect the minuscule changes in the magnetic fields produced by small changes in the electrical activity within the brain. It is a noninvasive direct measurement of neural activity and provide a sub-millisecond temporal accuracy able to unraveling the dynamics of the brain. In addition it provides a good spatial resolution especially for superficial sources, on the order of mm at the level of the cortex.

The generators of the recorded MEG signals are debated. Two separate basic neuronal events are possible candidates accounting for the generation of the measurable magnetic field: action potentials traveling along the axon away from the soma and postsynaptic currents at the apical dendrites of neurons. MEG is generally considered to be sensitive only to the slow (below 100Hz) postsynaptic potentials in pyramidal neurons of the cerebral cortex, that are lined-up along mainly tangential orientation. Recently it has been shown that synchronized population of action potentials may contribute to very high frequency MEG signals. Direct evidence for high-frequency brain activity in humans in the 200–800 Hz range was identified from EEG and MEG data for strong electrical stimulation of different sensory nerves. Often called high-frequency oscillations (HFOs), this activity was identified after averaging many hundreds or thousands of trials.

Starting point of the study described in this thesis is a Brief Communication titled “Impulse Propagation along Thalamocortical Fibers Can Be Detected Magnetically outside the Human Brain”, (Kimura 2008),[12]. In [12] MEG detection of impulse propagations, i.e. intracellular depolarizing action current, along the fibers from the thalamus to the somatosensory cortex was reported. Is MEG capable to capture activities from the subcortical brain areas and to follow the neural information flow up to the cortex?

Aim of the study described in this thesis and executed by the MEG-lab of the Center for Mind/Brain Sciences of the University of Trento and me, is to repeat and improve the quality of the findings reported in [12]. Moreover, in order to validate the findings we integrated the data collected with MEG with MRI, diffusion MRI and functional MRI data.

A first goal of this thesis is to describe and motivate the project and development of the experiment. In the first chapter the theoretical basis of MEG are given, from the physiological and physical point of view. In this chapter also the sophisticated

instrumentation used in MEG technique is described. In the second chapter a few fundamental neuroscientific notions are given and the scientific question is addressed. In third chapter the experimental setup and motivation of the main setup choices are exposed.
Further goal of this thesis is the analysis of the collected data. The analysis here exposed is not meant to be exhaustive since many different topics can be pursed on the collected data and alternative analysis can and will be executed. Here, in order to find the propagation of neuronal activation along the thalamo-cortical pathways, the activation trajectory was studied using neuromagnetic source imaging based on MEG recordings. In order to take localization errors into account then Monte-Carlo simulation of the founded sources was performed. Then the trajectory of neuronal sources, as obtained with MEG, was superimposed to the anatomical fiber tracts, as reconstructed by DTI. This analysis is described in chapter four: the pre-processing of MEG, MRI and diffusion MRI data, the coregisteration of the two different modalities (MEG and MRI), the source localization performed with MEG and the fiber tracking with DTI data. Finally, in chapter 5 and 6 the results from the analysis performed in chapter 4 and a brief discussion of the results are given.

Chapter 1

1.1 The physiological basis of MEG signals

1.2 Biophysical foundation of MEG

1.3 Instrumentation for magnetoencephalography

1.1 The physiological basis of MEG signals

Neurons generate time-varying electrical currents when activated. The physical principles of MEG are based on the fact that an electrical current generates a surrounding circular magnetic field. Since impulses propagating in the brain are generated by electrical currents, small local magnetic fields will be generated.

MEG technique measures thus these minuscule changes in the magnetic fields produced by small changes in the electrical activity within the brain. It is therefore a direct measurement of neural activity.

In the following sections a brief description is given of the basic physiological aspects of how magnetic signals are generated in the brain.

1.1.1 The neuron

The fundamental task of a nerve cell is to receive and propagate information. Neurons carry signals from sensory organs to the central nervous system, the spinal cord and the brain. In the peripheral and central nervous system, neurons interact. The strongest interactions take place on the level of the brain by forming networks of enormous complexity, allowing the brain to analyze, interpret and respond to afferent signals. In addition, efferent neurons carry information from the central nervous system to the muscles and effector organs.

Neurons have different shapes depending on their function, but every neuron consists of a cell body (soma), an axon and dendrites. The cell body contains a nucleus and the cytoplasm and is dedicated to metabolic control. The axon is a long fiber, which conducts signals away from the cell body toward distant target cells. Short, branching dendrites extend from the cell and provide an enlarged surface area to receive signals from the axons of other neurons. They propagate the electrochemical stimulation received from other neural cells to the soma via depolarization of the cell membrane. The contact areas between axons and the consecutive dendrites to which the neuronal signal is conveyed, are called synapses. They are located at various points throughout the dendritic arbor.

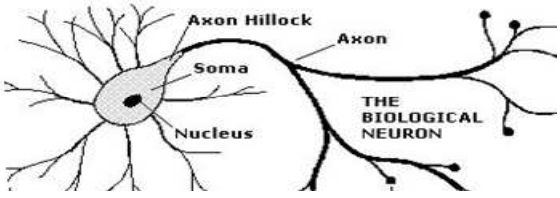

Figure 1.1:

Schematic of a neuron

1.1.2 The membrane resting potential

All these portions of the neuron are contained within the neural membrane. This insulating membrane divides the tissue into intracellular and extracellular compartments and consists of a double layer of phospholipids spanned by proteins.

The proteins embedded in the membrane can be ion channels or ion pumps. The ion channels have a channel that allows certain ions to cross the cell membrane, thus making the membrane selectively permeable to several ion species. Ionic pumps on the membrane that pump continuously selected ions against the concentration gradient. The most important is the Na-K pump, which moves three Na^+ ions out and two K^+ ions into the cell in one duty cycle. There are also active carriers.

This mechanism produces results in a different concentration of ionic populations inside and outside the cell: in particular, K^+ ions are much more abundant inside the membrane than outside, whereas Na^+ and Cl^- are more abundant outside. This imbalance of ionic concentrations creates an electrical potential across the membrane, with the interior of the cell negative with respect to the exterior. This membrane potential is referred to as the resting potential.

The Nernst equation permits calculation of the voltage difference across the neuron membrane based on the imbalance of the concentrations inside and outside the neuron: the resulting transmembrane resting potential is about −70mV.

Every electrical signal in the brain is the consequence of variations of this potential.

1.1.3 The action potential

Neurons propagate signals from one neuron to the next or to the target organ in the form of action potentials (AP). The AP is a short-lasting event: a rapid depolarization front in which the electrical membrane potential of a cell rises, followed by an almost equally fast repolarization front, where the membrane potential falls. Each AP is followed by a refractory period during which it is impossible to evoke another AP.

The axon hillock is believed to be the site of action potential initiation. It is a specialized part of the soma that connects to the axon. The membrane potential propagated from synaptic inputs are summated before being transmitted to the axon, an action potential is initiated when the voltage at the axon hillock reaches the firing threshold of about 40 mV.

Although the Na^+ - K^+ pump gives rise to a current through the membrane, the increase of the resting voltage due to this current is only a few mV. The basic mechanism of depolarization and repolarization of the neural membrane in the cycle of an action potential can be essentially explained by taking into account the displacement of Na^+ and K^+ ions due to the ability of the membrane to alter its permeability to these ions. The so called voltage-gated ion channels allow passage of ions only when they are in a specific configuration, depending on the membrane potential that can change as a result of an approaching action potential.

During the action potential, the interior of the cell is positive for a short time. This change of potential triggers the neighboring region, the action potential has thus the particular feature of being self-propagating.

The propagation of action potentials along axons is also unidirectional. Each action potential is followed in fact by a refractory period (1ms) during which it is impossible to evoke another action potential, so that the patch of axon behind the actively spiking part is refractory, but the patch in front, not having been activated recently, is capable of being stimulated by the depolarization from the action potential.

The excitation propagates along the neuron at a high speed with undiminished amplitude. Note that when the excitatory input becomes stronger, the amplitude remains the same but the frequency of firing increases.

The complete phenomenon that includes a depolarization of the membrane and its successive repolarization lasts less than 3 ms. The refractory period lasts 1 ms.

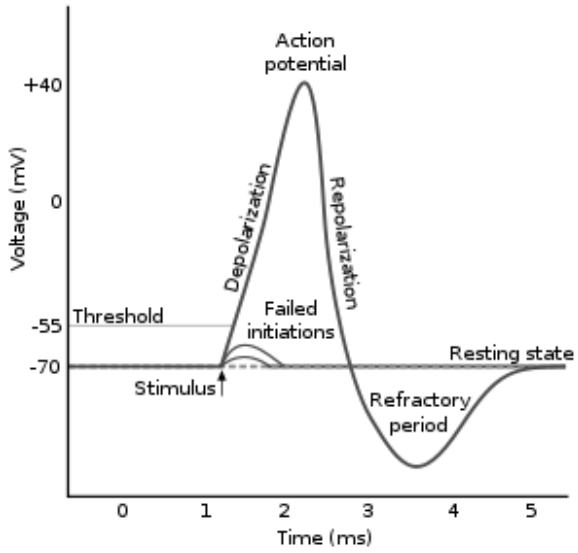

Figure 1.2:

An action potential is initiated when the voltage at the axon hillock reaches the firing threshold of about 40 mV. An action potential consists of three phases.

1. Depolarization.
2. Repolarization.
3. Refractory period

1.1.4 Post synaptic potential

Post synaptic potential (PSP) consist of a slow depolarization wave, followed by a much slower repolarization and its function is to initiate or inhibit action potentials. In comparison with the action potential, the postsynaptic potential may last several tens or hundreds of milliseconds.

When an action potential arrives along the axon of the presynaptic cell, neurotransmitter molecules are liberated from the synaptic vesicles into the 50 nm wide synaptic cleft and the permeability of the membrane of the post-synaptic cell, for specific ions is altered. The ensuing flow of electrical charges is called transmembrane current and changes the membrane potential of the postsynaptic cell in the vicinity of the active synapse. The event is called postsynaptic potential and two main kinds should be distinguished: the excitatory and the inhibitory potential.

If the synapse is excitatory, the permeability of the membrane to positive ions is increased causing a flow of positive ions inward. The potential difference is reduced and the cell is depolarized with respect to the resting state. The resulting change in transmembrane potential is called excitatory postsynaptic potential (EPSP).

Similarly, if the synapse is inhibitory, hyperpolarization will occur, due to a flow of negative ions inward. This represents an inhibitory postsynaptic potential (IPSP).

At the synapse, the change in permeability initiates a change in the membrane potential that will spread onward from this point. Because the cell is conductive, the depolarization (or hyperpolarization) causes current flow within the cell, the so called intracellular current that diminishes exponentially with time and distance.

In the case of EPSP the transmembrane current is carried by positive ions inwards (e.g. Na^+) whereas in the case of the IPSP it is carried by negative ions inwards (e.g. Cl^-) or positive ions outwards (K^+). Thus the positive electric current is directed to the extracellular medium in the case of an EPSP and it is directed from inside the neuron to the outside in the case of an IPSP.

In general, the dendrites and the soma have typically thousands of synapses from other neurons. If multiple postsynaptic potentials travel along the dendrites separated by an interval less than a couple of 100 ms, there will be temporal and spatial summation.

Both inhibitory postsynaptic potentials and excitatory postsynaptic potentials are summed in the axon hillock. If several such events occur in a short time, the axon hillock may

become sufficiently depolarized for triggering an action potential that propagates through the rest of the axon.

Conservation of electric charges imposes that the current loop be closed with extracellular currents flowing even through the most distant part of the volume conductor. Intracellular currents are called also primary or impressed currents, while extracellular currents are known as secondary, return, or volume currents.

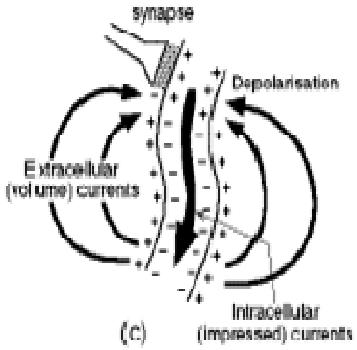

Figure 1.3: currents generate by an EPSP

1.1.5 What MEG measures

The currents associated with the PSPs generated at the dendrites are believed to be at the source of most of the signals detected in MEG and also EEG for the following reasons.

Firstly, the current patterns associated with the action potential and the postsynaptic potentials have a fundamental importance for the generation of the magnetic field. The PSP typically last longer than the rapidly firing action potentials and temporal summation of currents flowing in neighboring fibers is much more effective, while the action potentials are in general too small and too unsynchronized to be caught by the MEG technique.

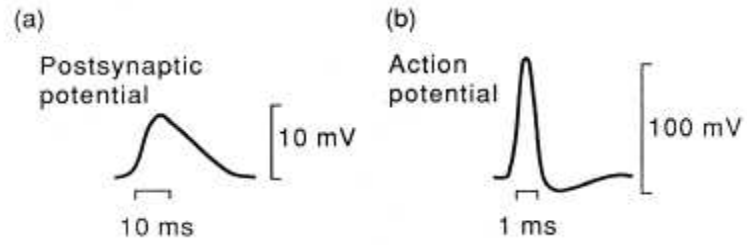

Figure 1.4: Postsynaptic potential and action potential in function of time

Moreover, the AP pattern can be represented by two oppositely oriented current dipole while the PSP pattern can be represented by one current dipole. In fact, the action potential represents a rapid depolarization process followed by a repolarization process and during the repolarization the overall current pattern is reversed, with the intracellular current

pointing backward and the extracellular current pointing in a forward direction. Both, the depolarization and repolarization fronts, move rapidly along the axon and are linked together and separate by less than a few milliseconds in time, and less than a few millimeters in space. Over straight portions of nerve fiber of uniform thickness, the action potential can be approximated by two oppositely oriented current dipoles and since the two dipoles are opposite, they form a current quadrupole. By contrast, the current pattern associated with postsynaptic potentials generated at the apical part of the dendrites is basically the one originating from the much slower repolarization process and can be approximated by a single dipole. A dipolar field produced by synaptic current flow, decreases with distance as $1/r^2$, more slowly than the $1/r^3$ dependent quadrupolar field generates with an AP. Thus EEG and MEG signals are produced in large part by synaptic current flow, which is approximately dipolar and lasts more, allowing temporal summation.

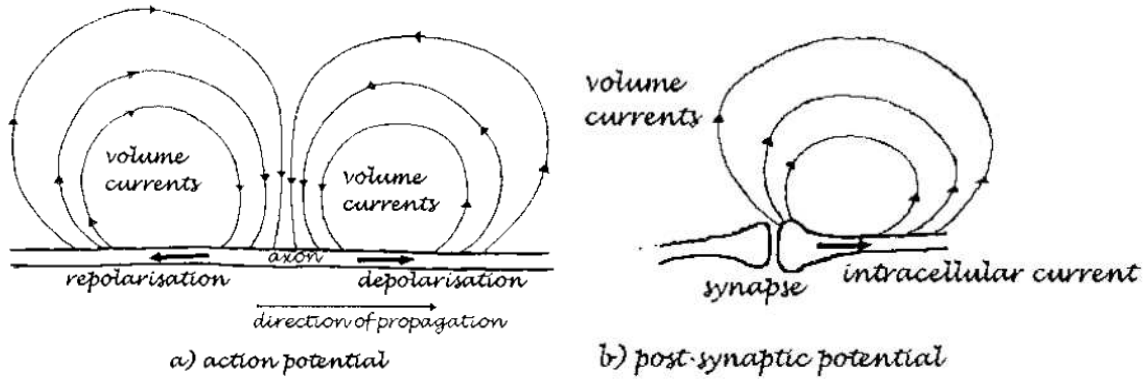

Figure 1.5, adapted from Magnetoencephalography—a noninvasive brain imaging method with 1 ms time resolution, C. Del Gratta, V. Pizzella, F. Tecchio, G. Romani
Schematic current pattern of :
a) action potential
b)Postsynaptic potential

The intracellular current is represented by an arrow (it can be represented through the model source a current dipole). The transmembrane current follows a radial pattern, the extracellular current flows backward in the surrounding medium in order to close the loop. In the AP repolarization and depolarization are linked together and separated by less than a few milliseconds in time, and less than a few millimeters.

In the PSP, primary and secondary currents contribute to magnetic fields outside the head. To calculate the magnetic field outside the head, the geometry and the electrical properties of the brain tissue, the cerebrospinal fluid, the skull and the scalp have to be modeled. As a first approximation, the head can be modeled by a spherical conducting medium. In this case the tangential currents produce a magnetic field outside the head and the MEG signal

represent the magnetic field corresponding to the primary currents. Any radial currents do not contribute to the magnetic field because of cancellation effects.

The magnetic field due to the current of a single excited neuron is too small to be measured by MEG. Thus, spatially structured arrangements of cells are of crucial importance to obtain a measurable superposition of the magnetic fields. Macrocolumns of tens of thousands pyramidal cortical neurons that are synchronously activated, are believed to be the main generators of MEG. In fact in the cortex, pyramidal cells have a well ordered distribution of their large dendritic trunks, locally oriented in parallel and their dendritic current due to cell depolarization (or hyperpolarization) flows roughly perpendicular to the cortex. This means that longitudinal intracellular currents flow along them, as in a wire, and thus generate magnetic fields around them according to the right-hand rule of electromagnetism.

As mentioned above, only tangential currents produce magnetic field. The fact that the cortex is folded, forming gyri and sulci, implies that some populations of neurons have apical dendrites that are perpendicular to the overlying, whereas others are parallel to the skull. MEG “sees” only those magnetic fields that are perpendicular to the skull.

The observed magnetic fields are generated thus by intracellular currents that are oriented tangentially to the skull, in contrast those that are oriented radially to the skull do not generate a magnetic field outside the head but contribute to EEG (EEG is also sensitive to volume currents).

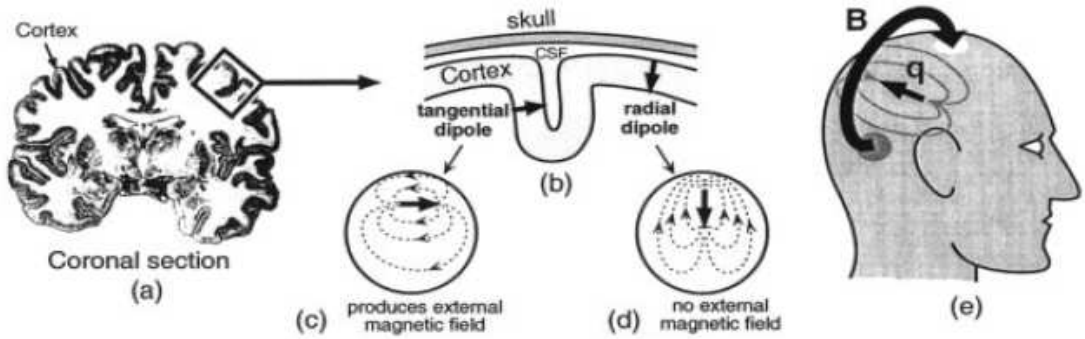

Figure 1.6, adapted from Signal Processing in Magnetoencephalography, Jiri Vrba and Stephen E. Robinson

The extracranial magnetic field measured by MEG reflects postsynaptic intracellular current within the apical dendrites of pyramidal cells oriented parallel to the skull surface.

1.2 Biophysical foundation of MEG

1.2.1 The forward problem in neuromagnetism: general formulation

The forward problem in neuromagnetism consists in calculating the distribution of magnetic fields B (r) outside the head and electric fields E(r) on the head surface, as generated by a configuration of sources of known strength and position.

The variation in time of the biological signals of interest is relatively slow. The frequency range of neural activity is typically below 1 kHz. It is assumed that the time-derivatives of the associated electric and magnetic fields are sufficiently low and can be ignored in Maxwell's equations. Thus, the electric and magnetic fields of the brain can be accounted for by the quasi-static Maxwell's equations.

In the quasi-static approximation the integral equation relating B(r) and an the current density J(r) is the integral form of the Biot–Savart law

$$B(r) = \frac{\mu_0}{4\pi} \int J(r') \times \frac{r - r'}{\left\| r - r' \right\|^3} dV \qquad (1),$$

where the integral is taken over the complete volume of conductor G. μ_0 is the susceptibility of empty space.

We can assume that the current density J(r) produced by neuronal activity is divided into volume currents $J^v(r)$ and primary currents $J^p(r)$: $J(r) = J^p(r) + J^v(r)$.

Volume currents are the result of the electric field in the volume on extracellular charge carriers and flows passively everywhere in the medium. Volume current is defined as: $J^v(r) = \sigma(r)E(r)$, where $\sigma(r)$ is the conductivity profile of the head tissue and, under the quasi-static assumption, E=-div(V). Everything else is the primary current $J^p(r)$. The primary current is mainly inside or in the vicinity of the cell and its flow is largely determined by the electrical characteristic of the cell membranes, being good electrical insulators. Finding the primary current means locate the source of brain activity.

$$J(r) = J^p(r) + \sigma E(r) = J^p(r) - \sigma \nabla V(r) \qquad (2)$$

The head comprises different tissues each having its own characteristic conductivity. Assume that the conductivity in the volume conductor is piecewise constant, for instance let's assume that the head consists of a set of only three contiguous regions each of constant isotropic conductivity $\sigma_i, i = 1,...,3$, representing the brain, the skull and the scalp. This is the so called Boundary Element Method (BEM). We can rewrite the Biot-Savart of above as a sum of contributions from primary and volume currents:

$$B(r) = B_0(r) + \frac{\mu_0}{4\pi}\sum_{ij}(\sigma_i - \sigma_j)\int_{S_{ij}} V(r')\frac{r-r'}{\|r-r'\|^3}\times dS_{ij}' \quad (3)$$

where $B_0(r)$ is the magnetic field due to primary currents only and the second term is the volume current contribution to the magnetic field formed as a sum of surface integrals over the brain-skull, skull-scalp, and scalp-air boundaries.

In order to calculate expression (3) one need to know V(r) on all surfaces.

We can create a equation similar to Eq.(3) for the potential itself that yields through a similar way that for reasons of expositions we don't write, to:

$$(\sigma_i + \sigma_j)V(r) = 2\sigma_0 V_0(r) - \frac{1}{2\pi}\sum_{ij}(\sigma_i - \sigma_j)\int_{S_{ij}} V(r')\frac{r-r'}{\|r-r'\|^3}\times dS_{ij}' \quad (4)$$

for the potential on surface S_{ij}, where V_0 is the potential at r due to primary current distribution.

The two equations (3), (4), represent the integral solution to the forward problem.

If we specify a primary current $J^p(r)$ we can calculate a primary potential V_0 and a primary magnetic field B_0, as:

$$B_0(r) = \frac{\mu_0}{4\pi}\int J^p(r')\frac{r-r'}{\|r-r'\|^3}dr' \qquad (5)$$

$$V_0(r) = \frac{1}{4\pi\sigma_0}\int J^p(r')\frac{r-r'}{\|r-r'\|^3}dr' \qquad (6)$$

V_0 is used to solve Eq.(4) for the potentials for all surfaces (the forward problem of EEG). These surface potentials and B_0 are then used to calculate the external magnetic fields of Eq.(3).

Unfortunately solving the equations for the conditions of a real head is complicated. First of all, for a general source configuration and an arbitrary head shape there is no analytical solution to these equations. Secondly, the conductivities are poorly known.

Assuming homogenous conductivities in the different compartments, one can use the Boundary Element Method (BEM) to solve the equations, used in Eq. (3). In this case as sub-volumes three regions are distinguished in the head: the brain, the skull and the scalp. The realistic shapes of the surfaces Sn are obtained using the anatomical information from other data modalities as MRI and CT. However, this procedure is rather time consuming.

For what concerns the conductivity values of the different layers, these are complicated to estimate. These values can be estimated either in vivo or in vitro. Different conductivity

estimation techniques have been performed, and have, unfortunately, resulted in greatly varying values. With MEG these problems can be avoided by assuming the head shape to be spherical and the source to be a dipole source. This special case is addressed in the next section.

1.2.2 Source model

The source model is the type of model used to describe the primary current distributions. Computation of the scalp potentials and magnetic fields requires solution of the forward Eq.(3) and (4) for a particular source model.

Neuronal current in the cortex flows predominantly perpendicular to the cortical surface. The intracellular current vectors of nearby cortical columns sum linearly and can be represented without too much loss of information by an equivalent dipole current vector. Areas with up to 3 cm in diameter can be modeled very accurately by a single equivalent dipole. This is the canonical source model in MEG data analysis.

An equivalent current dipole (ECD) is specified by three parameters. First its location, i.e. the equivalent center of the modeled gray matter patch. Second, its orientation, i.e. the net direction of the modeled neuronal current. The orientation of a dipole therefore indicates the local orientation of the pyramidal cells in the gray matter and it is not to be confused with a direction of signal propagation across the brain. The orientation of a dipole is symbolized by an arrow or a short line. The third parameter of an equivalent current dipole is its strength or amplitude, reflecting the modeled net current flow. Its units are that of a dipole moment, i.e. nAm (nano-Ampere x meter). It can be thought of as the product of the total current flow (in nA) and the length over which this current is flowing (on the order of the length of a pyramidal cell in meters).

The temporal evolution of the dipole moment is called the source waveform and is an important outcome of source analysis.

It should be noted that the use of such a simple model does not mean oversimplification of the problem: the idea of schematically representing the activity of population of neurons by means of an equivalent dipole provides a tool which is mathematically accessible and sufficiently realistic as well.

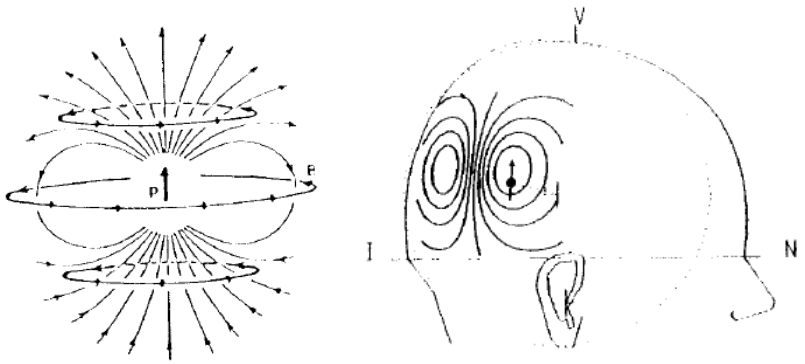

Figure 1.7:

Left: the location and orientation of a current dipole and its current distribution, when immersed in an infinite medium with homogeneous conductivity. The dark arrow represents the primary current. The outer lines are the volume currents which, flowing in the surrounding medium, close the loop. The transverse circles printed in bold represent the magnetic field lines.

Right: Distribution of the component of the magnetic field normal to the sphere surface as produced by a tangential dipole source 0.3 units of radius deep.

Mathematically, the current dipole may be viewed as a short element of current, characterized by an intensity J of the current, and a vector L, indicating the direction and the length of the element. The current dipole moment Q is defined as Q = JL. Let us assume a small patch of activated cortex centered at location r_q and that the observation point r is some distance away from this patch. The primary current distribution in this case can thus be approximated by an equivalent current dipole represented as a point source $J_p(r') = Q\delta(r'-r_q)$, where δ is Dirac delta function and the moment is $Q = \int J_p(r')dr'$.

The current dipole model is the most used model in clinical and research applications to MEG and also EEG source localization.

1.2.3 Spherical head model

Predicting the magnetic field produced by an elementary source model at a given sensor array requires also the a head model: it is a model of the head geometry and electric and magnetostatic properties of head tissues, that affects the magnetic fields measured outside the head.

In EEG for instance, it is quite intuitive that the skull would form a barrier of lower conductivity that strongly distorts and attenuates the electric potentials and consecutively the electrical currents at the scalp and at the cortical surface. Since the magnetic fields

measured outside the head depend also on the intracranial current distribution, geometry and conductivity are also relevant for MEG

It is useful to note, that most heads fit reasonably well inside a sphere centered about 5 cm above the plane defined by the usually defined anatomical fiducials used in MEG: the nasion and the pre-auricular points. Spherical models of the head have thus been extensively investigated. The spherical geometry has demonstrated very attractive properties in MEG.

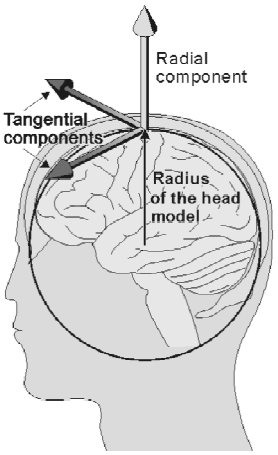

Figure 1.8:

The MEG is sensitive only to the two tangential components.

A main fact when the head shape is assumed to be spherical, is that the radial field component outside the head, $B_r = B(r) \cdot e_r$, can be obtained without explicit reference to the volume currents. The contribution of volume currents to the radial field component vanishes and Eq.(3) becomes:

$$B_r = B(r) \cdot e_r = B_0(r) \cdot e_r + \frac{\mu_0}{4\pi} \sum_{ij} (\sigma_i - \sigma_j) \int_{S_{ij}} V(r') [n(r') \times \frac{r - r'}{\|r - r'\|^3}] \cdot e_r dS'_{ij} = B_0(r) \cdot e_r \qquad (7)$$

Where n(r') is the vector normal to the surface. Thus, in the case of spherical head model, for a radially oriented MEG sensor, we don't have to solve surface potential V(r) on all surfaces and the MEG forward problem can be solved directly and because B_0 is independent of the conductivities, the radial component of B(r) is independent from the conductivities.

Consider the case of a current dipole of moment q located at r_q in a spherical head. The magnetic field of the dipole in a homogenous medium is:

$$B_0(r) = \frac{\mu_0}{4\pi} q \times \frac{r - r_q}{\|r - r_q\|^3} \quad (8)$$

Note that this magnetic field measurement is linear in the dipole moment q but highly non linear with respect to its location r_q.

Very important, from Eq. (7) and (8), we can find out that if the primary current is radial, B vanishes. A source in the center of the sphere or dipole with radial orientation will produce no magnetic field outside. Therefore, signals from currents at the crests of the gyri and depth of the sulci are attenuated in the MEG data.

1.2.3 Algebraic formulation of the forward problem

With the introduction of source and head models, we can now provide a linear algebraic model for the forward problem.

We can model the source with a ECD defined by three factors: location represented by the vector r_q, dipole magnitude $q \equiv \|q\|$ and orientation $\Theta = q/\|q\|$. As seen in Eq.(8), the magnetic field measurements are linear with respect to the dipole moment **q**, and nonlinear with respect to the location r_q. The forward field $m(r)$ on each MEG sensor generated by a dipole at location r_q, can algebraically be expressed by a vector $a(r, r_q, \Theta)q$, where $a(r, r_q, \Theta)$ is formed as the solution of the magnetic forward problem for dipole with unit amplitude and orientation Θ.

For the simultaneous activation of p dipoles located at r_{qi} and by linear superposition, we can simply sum the individual contributions to obtain $m(r) = \sum_i a(r, r_{qi}, \Theta_i) q_i$ and for simultaneous MEG measurement made at N sensors we obtain:

$$m(r) = \begin{bmatrix} m(r_1) \\ \vdots \\ m(r_N) \end{bmatrix} = \begin{bmatrix} a(r_1, r_{q1}, \Theta_1) \cdots a(r_1, r_{qp}, \Theta_p) \\ \vdots \\ a(r_N, r_{q1}, \Theta_1) \cdots a(r_N, r_{qp}, \Theta_p) \end{bmatrix} \begin{bmatrix} q_1 \\ \vdots \\ q_p \end{bmatrix} = A(\{r_{qi}, \Theta_i\}) S^T$$

m(r) is a set of N measurements, S is a matrix of source amplitudes and A is called forward field matrix and relates a set of p dipoles to the set of N sensors locations.

This is the forward model for one time instant. When considering a time window, consisting of T discrete time instants, the forward model becomes a matrix $M \in \Re^{N \times T}$. This spatiotemporal forward model depends on how the dipole parameters, i.e. location and moment, change over time. For p sources and T discrete time samples, the spatio-temporal model can therefore be represented as

$$M(r) = \begin{bmatrix} m(r_1, 1) \cdots m(r_1, T) \\ \vdots \\ m(r_s, 1) \cdots m(r_s, T) \end{bmatrix} = A(\{r_i, \Theta_i\}) \begin{bmatrix} s_1^T \\ \vdots \\ s_p^T \end{bmatrix} = A(\{r_i, \Theta_i\}) S^T$$

Where the corresponding time series for each dipole are the columns of the time series matrix S.

Because the location and orientation of the dipole are not a function of time, this type of model is often referred to as a “fixed” dipole model. In general three possibilities can be distinguished: the case of above, where the location and orientation of a stationary dipole are fixed over time, though the amplitude can change; the orientation and amplitude of a

rotating dipole changes over time, while its location is fixed; a moving dipole has varying amplitude, a varying location and a varying orientation over time.

1.3 Instrumentation for magnetoencephalography

The challenge for biomagnetic instrumentation is the detection of extremely weak magnetic signals, from 1 fT to 100 pT, in the presence of a very noisy background of 10 μT and above.

Properly designed instrumentation must therefore be endowed with sensitive magnetic field detectors and noise cancellation techniques.

In the next sections a detailed description of the most relevant parts of MEG systems is given.

1.3.1 MEG history

MEG signals were first measured in 1968, before the availability of the SQUID, by physicist David Cohen, University of Illinois. He used a copper induction coil as detector.

Figure 1.9: a modern MEG device

Superconducting quantum interference devices (SQUIDs) were first used for MEG in 1972 and since there are the core of the MEG systems. They are still the most sensitive detectors of magnetic flux currently available.

In 1972 Cohen used one of the first SQUID detectors, just developed by James E. Zimmerman, a researcher at Ford Motor Company, to measure MEG signals.

At first, a single SQUID detector was used to successively measure the magnetic field at a number of points around the subject's head by using single-channel devices.

In the 1980s-early 1990s, MEG manufacturers began to arrange multiple sensors into arrays to cover a larger area of the head: systems with 5 to 7 channels, then systems with 20 to 40 sensor arrays. Finally, the first helmet-MEG systems were introduced in 1992 and, present-day, MEG systems have several hundred channels (typically 100-300), that are set in a helmet-shaped Dewar arrangement that covers most of the head. In this way, MEG signals of a subject can now be accumulated rapidly and efficiently.

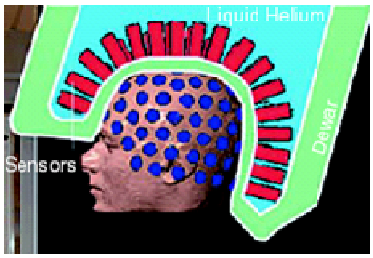

Figure 1.10: Sensor array

Today about 100 institutions worldwide currently use neuromagnetic systems.

1.3.2 Overview of MEG installation

A typical MEG system is a complex installation, as showed in the schematic diagram below.

The SQUIDs work with superconductivity and are thus positioned inside a helmet-shaped container called Dewar that is cooled with liquid helium at a temperature close to absolute zero (4.2K) to maintain the superconductivity state of SQUIDs.

The mechanical system supporting the Dewar is called the gantry. It allows adjusting the elevation and angle of the Dewar to comfortably accommodate subjects of different heights and in different measurement positions (seated or supine).

The SQUIDs system and the subject are usually positioned in a magnetically shielded room (MSR) to eliminate environmental magnetic interference.

The electronics system necessary for recording the magnetic activity from a patient are located outside the MSR. These systems include the SQUIDs processing electronics and the computer for data analysis and archiving.

MEG measurement can be supplemented by EEG data acquisition.

The MEG system is accomplished also with stimulus delivery equipment (electrical, visual, auditory, etc.).

The installation is completed with a video camera and intercom for communication with the subject in the shielded room.

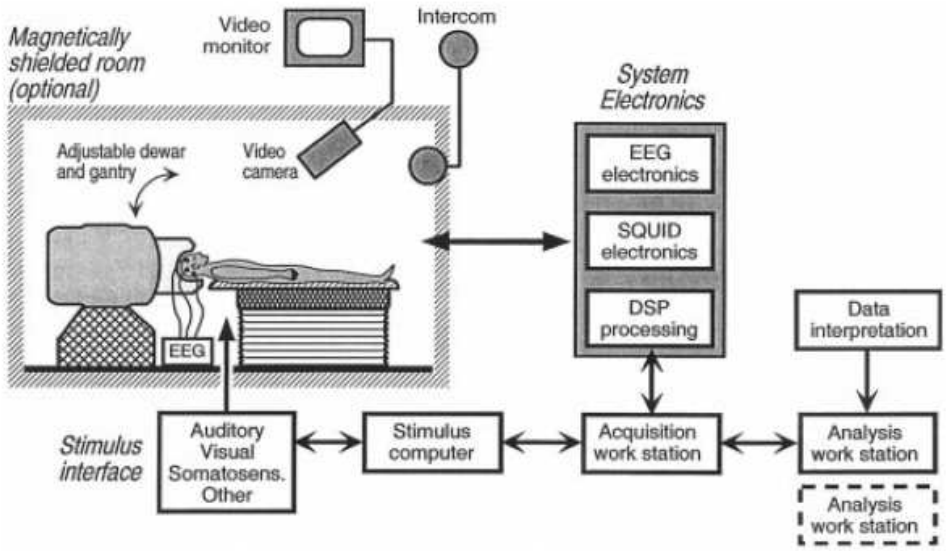

Figure 1.11, *adapted from: Signal Processing in Magnetoencephalography, Jiri Vrba and Stephen E. Robinson*

Schematic diagram of an MEG installation

1.3.3 The SQUIDs

*T*he challenge in biomagnetism is the detection of extremely weak magnetic signals (1fT to 100 pT) in the presence of a very noisy background (~10μT and above). Superconducting Quantum Interference Devices (SQUIDs) are the most sensitive detectors of magnetic flux currently available. The SQUIDs act as flux-to-voltage transducer. They are amazingly versatile, being able to measure any physical quantity that can be converted to a flux, for example magnetic field, current, voltage, magnetic susceptibility.

The most common type of SQUID used in MEG technique is the dc-SQUID, from now on simply referred to as SQUID. It consists of two Josephson junctions connected in parallel in a superconducting loop. A Josephson junction consists of two superconductors separated by a thin insulating barrier.

SQUIDs combine two physical phenomena observed in superconductors: the first is the flux quantization, the property of a supercurrent that the magnetic flux passing through any area bounded by such a current is quantized. The quantum of magnetic flux is a physical constant, as it is independent of the underlying material as long as it is a superconductor. Its value is $\Phi_0 = \frac{h}{2e} = 2.067\,833\,636 \times 10{-}15$ Wb, where h is the Planck constant and *e* is the charge of the electron. Thus, the flux enclosed by the superconducting loop must be an integral number of the flux quanta. The second phenomenon is the so called Josephson effect. Indeed, the first SQUIDs were built after the prediction by Josephson in 1962 that in superconductors the so called Cooper pairs, a pairs of electrons, which are the charge carriers of the supercurrent, may tunnel across an insulating barrier and also maintain their phase coherence. This phenomenon is named the Josephson effect, and the barrier is named the Josephson junction.

Figure 1.12 :
Schematic diagram of a dc SQUID.
Two junctions are connected in parallel on a superconducting loop of inductance L.
The Josephson junction is denoted by a cross.
The capacitor is due to the stray capacity of the junction.
The resistor is added to remove the hysteric behavior of the junction itself.
In fact the Josephson junction has a hysteric current-voltage characteristic: as the current is increased from zero the voltage switches abruptly to a nonzero value when I exceeds Ic, but returns to zero only when I is reduced to a value much less than Ic. This hysteresis must be eliminates and one does so by shunting the junction with an external shunt resistance.

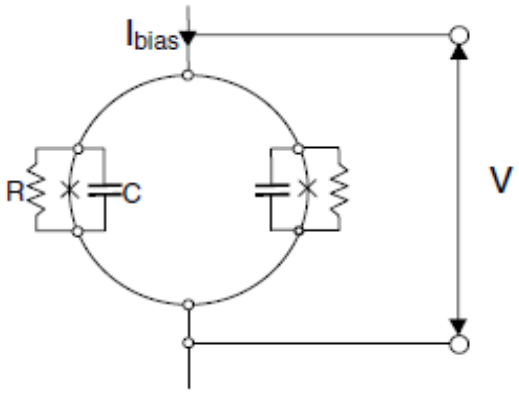

The electrical proprieties of a Josephson junction are described by the Josephson equations *(Josephson 1962)*:

$$1) I(t) = I_c \sin(\phi(t)) \quad , \quad 2) V(t) = \Phi_0 \frac{\partial \phi}{\partial t}$$

Where $V(t)$ and $I(t)$ are the voltage and current across the Josephson junction.

In practice, there is a capacitance C and a resistance R across the junction and the resistively shunted models becomes

$$I = \frac{V}{R} + I_c \sin\theta + C\frac{dV}{dt} \quad .$$

The dc SQUIDs principle of operation is based on the interference of the phase of the wave function describing the condition of the Cooper pair across each junction.

Eq.1) is the current-phase relation in which the current is proportional to the sine of the phase difference across the junction $\phi(t) = \phi_1 - \phi_2$. I_c is a constant and represents the critical current of the junction, I may take values between - I_c and I_c. Higher currents $I > I_c$ result in a voltage across the junction according to the voltage-frequency relation shown in Eq. 2).

The applied current I controls ϕ between the phases according to the current-phase relation of above. Thus, an external field or flux variation changes the phase difference across the Josephson junctions due to flux quantization. In fact, in order to keep the flux constant, the loop will compensate the external flux variation Φ_{ex} by generating a screening current $J = \Phi_{ex} / L$, where L is the inductance of the loop. In so doing the loop is able to remain in its current flux quantum state, until the external flux is increased to the point in which an additional flux quantum can enter the loop and raise it to the next flux quantum state.

The applied bias current is the sum of currents through the two junctions $I_B = I_1 + I_2$. The screening currents J are superimposed on the bias current at which the SQUID operates. The two junctions are identical arranged symmetrically on the loop and the bias current is swept from zero to a value above the critical current of the two junctions. In the absence of any applied flux or with $\Phi = n\Phi_0$, there is no current circulating around the loop and the bias current divides equally between the two junctions. The measured critical current is $2Ic$.

If we apply a magnetic flux Φ_{ex}, the flux in the loop will be quantized and will generate a current $J = -\Phi_{ex} / L$. The current adds to the bias current flowing through one junction and

subtracts from that flowing through the other junction. The critical current of one junction is reached when $I/2 + J = Ic$, at which point the current flowing through the other junction is $I/2 - J$. Thus the SQUID switches to the voltage state when $I = 2Ic - 2J$. As Φ_{ex} is increased to $\Phi_0/2$, J increases to $\Phi_0/2L$, and the critical current falls to $2I_c - \Phi_0/L$. As the flux is increases beyond $\Phi_0/2$ however, the SQUID makes a transition from the flux state n=0 to n=1 and J changes sign. As we increase Φ_{ex} to Φ_0, J is reduced to zero and critical current is restored to its maximum value $I_m = 2Ic$. In this way the critical current oscillates as a function of Φ_{ex}.

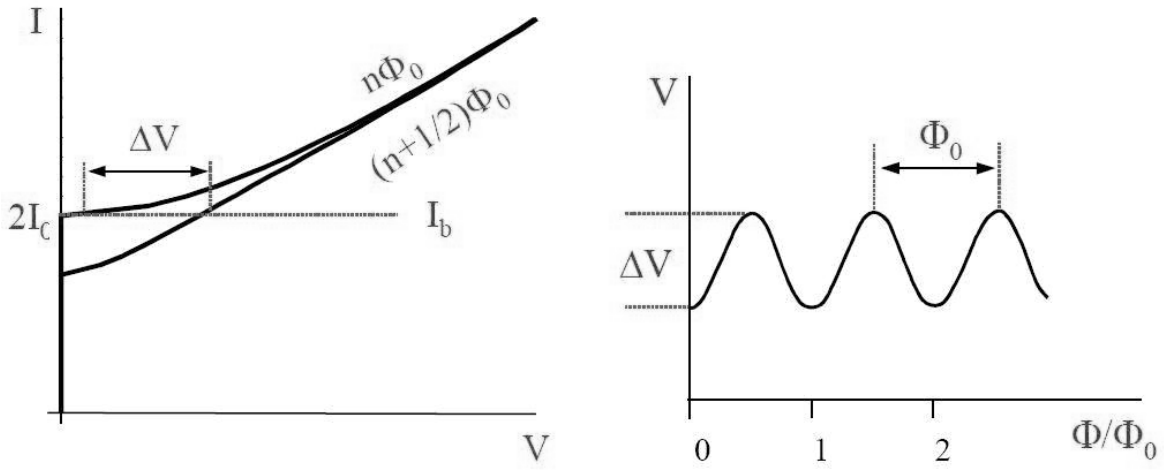

Figure 1.13:
Left: current-voltage characteristic of a dc SQUID. For $\Phi_{ext} n\Phi_0$ the critical current I_c is maximum. For $\Phi_{ext} = (n+1/2)\Phi_0$, I_c is minimum .
Right: V vs Φ/Φ_0 at constant bias current I. The period is equal to a flux quantum Φ0

1.3.4 SQUID Electronics

The periodic response of the SQUID to applied field, i.e. the $\Phi - V$ characteristic showed in the previous Figure, must be linearized. In order to make the sensor output a linear function of the applied flux, the SQUID must be operated in a flux-locked- loop mode (FLL), where negative feedback is used to keep the working point of the SQUID constant.
A schematic diagram of the FLL circuit is shown in figure. Because the SQUID output signal does not exceed amplitudes of a few μV, it is directly coupled to a low-noise preamplifier and integrator circuit. The scheme must take into account the impedance mismatch between the SQUID and the preamplifier and this is done thanks to a flux modulation technique or applying a positive feedback.

The amplified output voltage is then converted into a current by using a feedback resistor (Rfb). This current is fed back to a coil (Mfb) which, positioned close to the SQUID, converts the current into magnetic flux. An applied field is thus fed back and generates an opposing flux which keeps constant the flux in the SQUID. The output voltage V is directly proportional to the external Φ_{ext} applied, by a constant factor Rfb/Mfb. The extension of the dynamic range by using the flux periodicity of the SQUID transfer function works in the following manner: the loop is locked at a certain point on the SQUID transfer function and remains locked for the applied flux in the range of $\pm \Phi_0$. When this range is exceeded, the loop lock is released and the locking point is shifted by $1\,\Phi_0$ along the transfer function. The flux transitions along the transfer function are counted and are merged with the signal from the digital integrator.

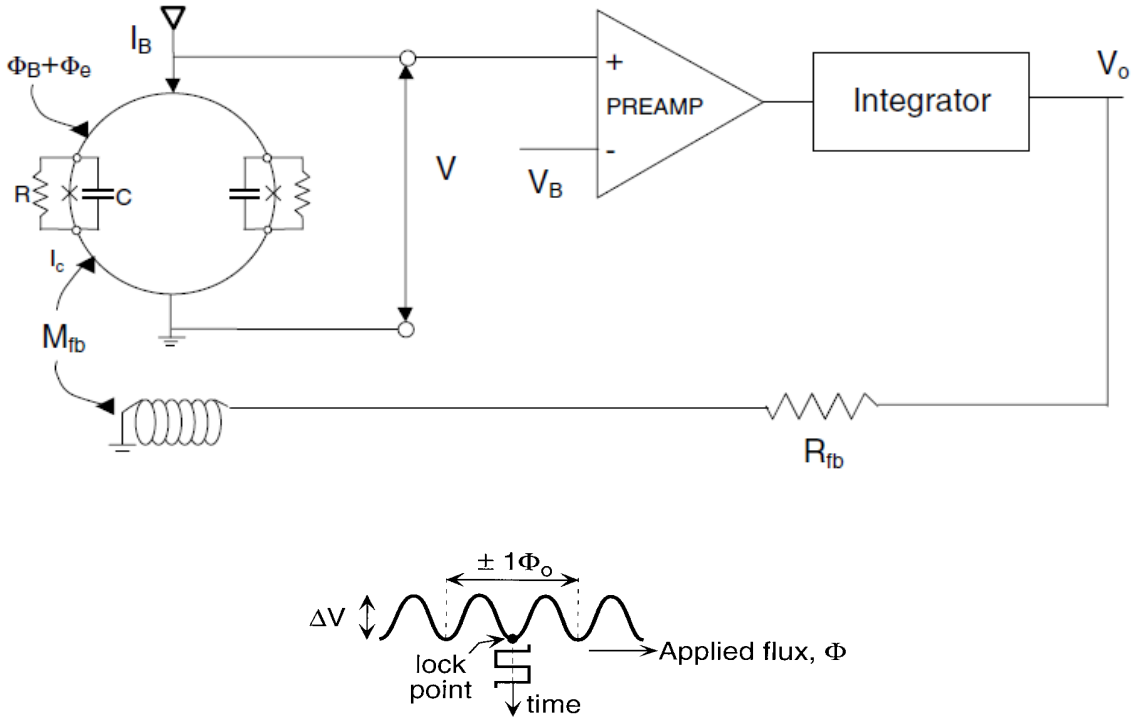

Figure 1.14:
Above: Simplified scheme of the FLL configuration
Below: Working point of the SQUID, maintained fixed by a negative feedback.

1.3.5 Flux transformers

In order to increase overall magnetic field sensitivity, it is not convenient to use the SQUID loop to directly sense the field. SQUIDs effective flux capture area is small, leading to low magnetic field resolution. Furthermore the SQUID inductance must be small in order to minimize the noise of the detector. Additionally, it is convenient to use a

separate detection coil to sense the external magnetic field, because in this way it is possible to change the field spatial sensitivity of the device without affecting the SQUID design. For all these reasons, is useful to couple inductively the SQUID sensors to the measured signals with a flux transformer, like a simple wire wound flux transformer.

It consists of a pick-up coil at one end and an input coil, conductively coupled the nearby SQUID loop, at other end. The external magnetic field B_{ex} threading the pick-up coil L_d excites a shielding current i_{sh} and, hence, a flux in the primary coil L_s: this flux is coupled, via the mutual inductance M, into the SQUID loop.

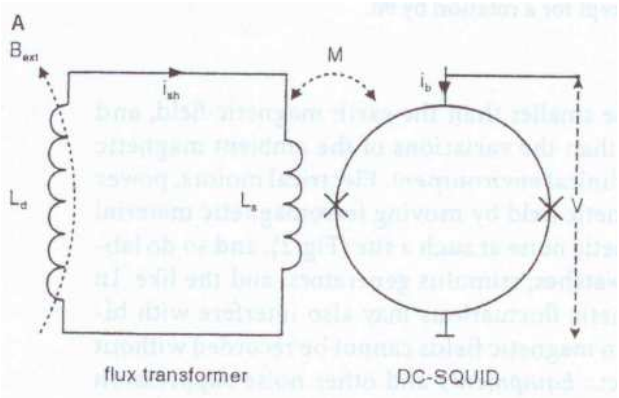

Figure 1.15:
Principle of sensing by SQUIDs

The entire flux transformer, detection coil and input coil, is a superconducting loop. Thus, the external magnetic field induces a current in this loop which is proportional to the field itself, it doesn't generate noise and its gain is noiseless.

The flux transformer pickup coils can have diverse configurations. The simplest detection coil consists of a single loop of superconducting wire and is called magnetometer and is sensitive to the magnetic field component perpendicular to its area. If the magnetic field is constant over the coil area, the current flowing in the loop is simply proportional to the field intensity. The important advantage of this simple type of detection coil is that it is easy to integrate within the SQUID chip, thus simplifying the construction of complex multichannel biomagnetic systems.

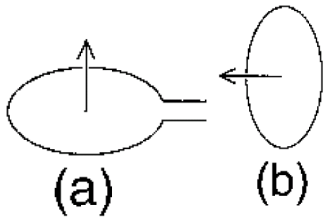

Figure 1.16:
The flux transformers orientation assumes that the scalp surface is at the bottom of the figure.
a) Radial magnetometer
b) tangential magnetometer

From the sensitivity point of view, specific geometries for the detection coil may reduce conveniently the sensitivity to noise sources, with little loss of sensitivity for the biomagnetic sources of interest.

Two magnetometer loops can be combined with opposite orientation and connected by the same wire. These pickup coils are called first-order gradiometers.

This arrangement is insensitive to an homogeneous magnetic field, like the fields generated by distant noises. In fact an homogenous magnetic field imposes an opposite net flux through the lower, the pickup coil, and the upper coil. By contrast the first-order gradiometers are effective in measuring the inhomogeneous magnetic fields produced by the brain signal sources. In fact the field of a dipole, such as what we assume to measure, decays with distance as $1/r^3$. If the pickup coil is close to the subject's head and the distance between the two coils is at least 4-5 cm, the magnetic field produced by the brain is sensed essentially by the lower coil only. In general, an adequate base line for an axial gradiometer is 1-2 times the typical distance to the source. This provides sufficient far-field rejection without severe attenuation of the signal.

The two coils of the first-order gradiometer may be displaced along their common axis, producing an axial gradiometer, or in their common plane, producing a planar gradiometer. Due to the configuration of the coils, planar gradiometers give the strongest response over the current source, whereas the axial gradiometer gives the maximum response on both sides of the source.

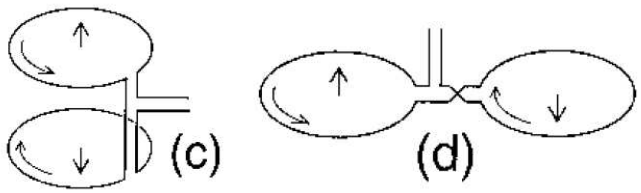

Figure 1.17:
c) Axial first-order gradiometer
d) Planar first-order gradiometer

Similarly, first-order gradiometers can be combined with opposing polarity to form second-order gradiometers so that the detection coil is insensitive to both homogeneous fields and uniform field gradients. And second-order gradiometers can be combined to form third-order gradiometers. Other configurations are possible but not widely used in MEG practice.

1.3.6 Cryogenics

As seen in the section about the SQUIDs, these sensors need to operate in superconductivity state. Unfortunately, superconductivity shows up only at a very low temperature, therefore the MEG sensing elements (SQUIDs, flux transformers and their interconnections) must be immersed in a cooling medium. In all the MEG commercial system low-temperature superconductivity is used, hence liquid helium is used as cooling fluid to reach a temperature of 4.2 K.

A special thermally insulated container for the helium is used, called Dewar, after its inventor James Dewar. The Dewar tail end, which is in contact with the patient, has a helmet like shape and the inner vessel of the Dewar is covered with the primary sensor flux transformer.

The Dewar is a critical part of the instrument and requires elaborate thermal isolation: the distance of the detection coils from the head of the subject must be as small as possible, and simultaneously it has to maintain a very high temperature difference (2-3 cm between the subject's head at body temperature and the location of the SQUID sensors close to absolute zero). It is a device that incorporates various forms of thermal insulation, heat conduction and radiation shielding, inside of which SQUIDs can operate. It comprises two concentric vessels with a vacuum jacket and radiation shields in between. The vacuum prevents heat conduction from outside to inside vessel, the shields block thermal radiation. The Dewar has to be of course strictly nonmagnetic in order not to influence the fields being measured.

Despite the extreme thermal isolation, there is still a small heat leakage into the inner vessel, causing the liquid helium to slowly evaporate. The gaseous helium exits the Dewar along an exhaust line which guides the gas out of the system and the shielded room. The helium gas is either collected into pressurized containers for re liquefaction or just let out into the open air outside the building.

A typical whole-head MEG system boils 10-20 liter of liquid helium per day. The helium reservoir of the Dewar is usually 70-90 liters, thus intervals of about 7 days are allowed before the loss of helium by vaporization requires a refill. This is a major cost factor. Liquid helium is transferred from a storage Dewar by means of a vacuum isolated siphon. The storage is pressurized by gaseous helium to "push" the liquid along the siphon into the MEG Dewar.

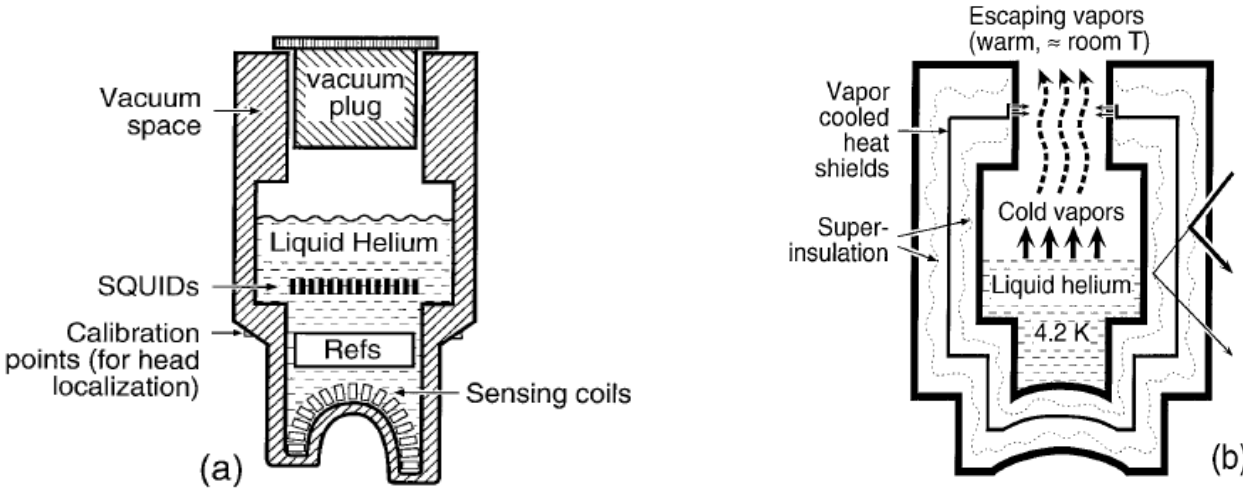

Figure 1.18: Principle of the Dewar operation.
Left :An example of how the components may be organized within the Dewar.
Right: The He Dewar is an evacuated double-walled vessel. The thermal differential between the environment and the He liquid is about 300, thermal radiation losses, which are proportional to T4, are an important factor in the overall Dewar heat budget. To protect the cryogen from the thermal radiation multiple layers of superinsulation are placed into the Dewar vacuum space.
The cold gases from the evaporating He carry out energy that is captured in the Dewar neck and conducted by heat shields back into the Dewar vacuum space to help reduce the thermal gradient between the He and the environment.

1.3.7 Noise cancellation

Noise is a major concern for MEG. Noise at the output of MEG sensors can be divided into three categories: sensors noise, brain noise, and environmental noise.

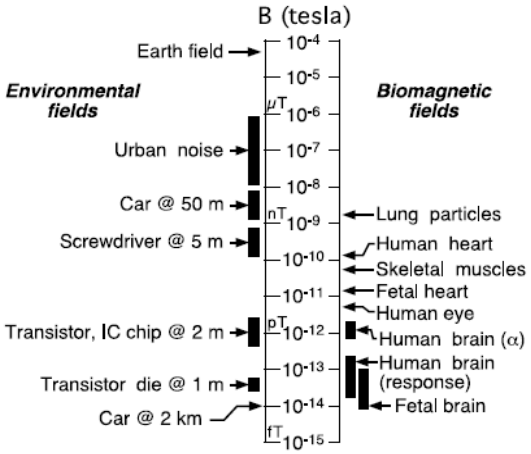

Figure 1.19: *adapted from Magnetoencephalography: the art of finding a needle in a haystack- J. Vrba:* Comparison of biomagnetic fields and environmental (unshielded) fields.

Sensors noise can be controlled by careful design of the SQUID and primary flux (minimized by the use of superconducting materials and immersing the sensing setup in a Dewar cooled with liquid helium).

Brain noise, if it is considered noise, can be controlled or reduced by spatial filtering methods.

The environmental noise is caused by moving magnetic objects (cars, people, trains), or by electrical equipment (power lines, computers, etc.). It is usually generated at larger distances from the MEG system and the magnetic interference magnitudes at urban locations or even at rural areas are many orders of magnitude larger than the magnetic fields of the brain.

If the primary MEG sensors are gradiometers, the effect of the environmental noise is reduced. Noise sources distant from the gradiometer produce magnetic fields with small spatial gradients and hence are effectively attenuated using this mechanism. Such an approach is beneficial but it is not sufficient, and additional methods for environmental noise elimination have been the subject of intense study during MEG history.

Enclosing the MEG system within a shielded room is the traditional and most straightforward method for reduction of environmental noise.

The shielding properties of such a room at low frequencies are attributable to the high-permeability mu-metal, an alloy consisting mostly of nickel and iron, which diverts the flux of the impinging magnetic field with a low-reluctance path along the walls of the room, thus reducing the field strength within the room. At higher frequencies the shielding relies on the eddy currents flowing in a high-conductivity material, usually aluminum. To allow both shielding methods to work efficiently, the walls are typically made of a combination of mu-metal and aluminum plates. Practical shielded rooms employ multiple such shells to increase the shielding factor, mostly shielded rooms comprise 2 or 3 shells.

A different approach to environmental noise reduction may consist in an active noise compensation by using of simple, integrated SQUID magnetometers plus additional reference sensors displaced at a convenient distance from the main array to sense the environmental noise. After that the measurement of the magnetic field has been carried out with the standard SQUID electronics, the noise may be subtracted on line, as well as off line during signal processing.

Hardware noise cancellation such as shielding or active compensation can be integrated with others methods, implemented in software or firmware. Higher-order gradiometers or adaptive systems can be synthesized using the additional reference sensors.

Furthermore spatial filtering methods like signal-space projection or beamformers can be employed.

Chapter 2

2.1 The somatosensory system

2.2 Event related fields

2.3 Topic of the experiment

2.1 The somatosensory system

Sensory systems represent the input part of the nervous system that provides the individuum with information from inside and also from its environment. Commonly recognized sensory systems are those for vision, hearing, somatic sensation, taste and olfaction. A sensory system consists of sensory receptors, neural pathways, and sub-cortical and cortical brain areas that transfer the sensory input to a sensory percept.

The somatosensory system provides information from the skin about touch, vibrations, temperature and pain. Touch may be considered as one of five human senses; however, when a person touches something or somebody, this gives rise to various feelings: the perception of pressure (shape, softness, texture, vibration, etc.), temperature and even pain. Thus, the somatosensory modality comprises several sub-modalities.

The somatosensory system is composed of different peripheral receptors: mechanoreceptors, thermoreceptores, nociceptors, and chemoreceptors. The receptors are embedded in the skin and epithelia, skeletal muscles, bones and joints, internal organs, and the cardiovascular system.

2.1 Somatosensory pathways

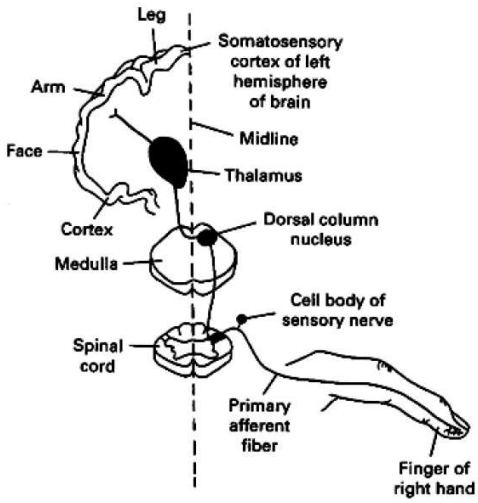

Figure 2.1:

Somatosensory pathways from peripheral receptors to cortex, via spinal cord, midbrain and thalamus

When receptors are stimulated, the information is propagated via peripheral nerves to the dorsal root ganglia in the spinal cord. Fibers from the dorsal root ganglia project along the dorsal columns of the spinal cord ipsilateral to the stimulation site to the dorsal column nuclei in the medulla. From these nuclei fibers cross to the other side of the body and to the posterior part of the ventro-lateral thalamus. Consecutively information is conveyed to the primary somatosensory cortex the post-central sulcus situated in the parietal cortex. The cortical somatosensory system consists of a distributed network of specialized, interconnected brain regions. Note that the pathways of the brain are crossed; the left side of the cortex relates to the right side of the body and right side to the left.

2.1.2 Brodmann map

Based on cytoarchitectonic differences, anatomists of the nineteenth and the early twentieth centuries formulated classifications according to which the cerebral cortex can be divided into distinct regions. The map of Brodmann (1909) has prevailed over time; it is relatively simple and allows animal and human cortices to be compared. The morphologically different cortical regions have proved to be also functionally dissimilar .

2.13 The primary somatosensory area S1

Primary sensory areas are the main cerebral areas that receive sensory information from thalamic nerve projections. There are nine cortical areas with mainly somatosensory function: the primary somatosensory cortex S1, comprising Brodmann areas 3a, 3b, 1 and 2, the second somatosensory area S2 located along the superior bank of the lateral sulcus, the granular insula and retroinsular cortex, and in the posterior parietal cortex areas 5 and 7b. Since in the present we are interested in S1, we focus only on this area.

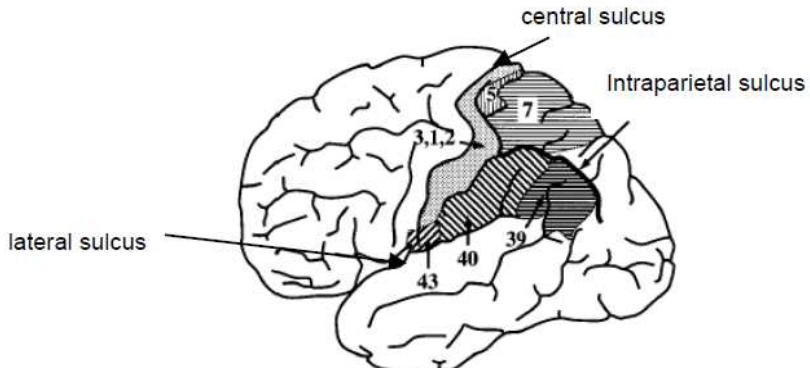

Figure 2.2:

Anatomical subdivisions of human parietal cortex. Primary somatosensory cortex is located in the posterior bank of the central sulcus and the postcentral gyrus and comprises areas 1,2,3.
Somatosensory regions in posterior parietal cortex include areas 5 and 7b.
The secondary somatosensory cortex is located in the upper bank of the lateral sulcus.

For the somatosensory system, the primary somatosensory cortex S1, is the main sensory receptive area for the sense of touch and is located posterior to the central sulcus in the parietal lobe. It is organized somatotopically, i.e. neighboring areas on the skin are represented as close neighbors in the cortex. Due to the preservation of the neighborship of body regions the representation is referred to as the little man, the so-called ‘homunculus’. Each part of the body is represented in brain volume in proportion to its relative

importance in sensory behavior. The somatotopic map is distorted with an exaggerated representation of the hand, mouth and foot, which are important sensors of the properties of objects and have the highest density of touch receptors.

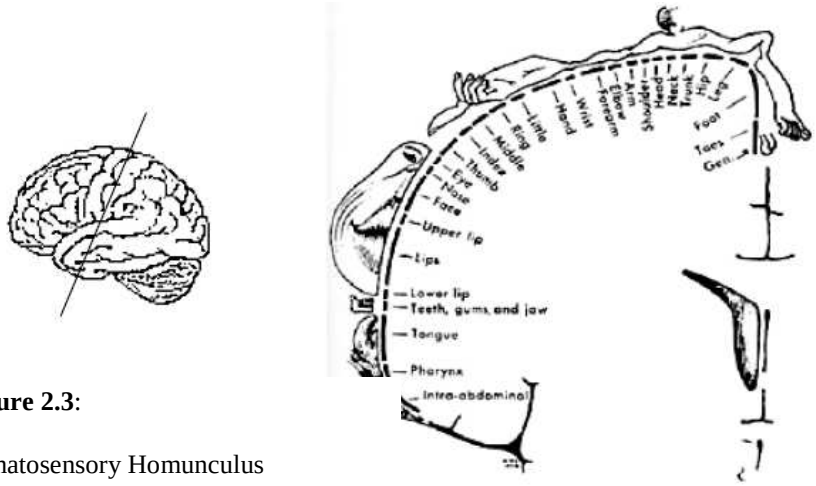

Figure 2.3:

Somatosensory Homunculus

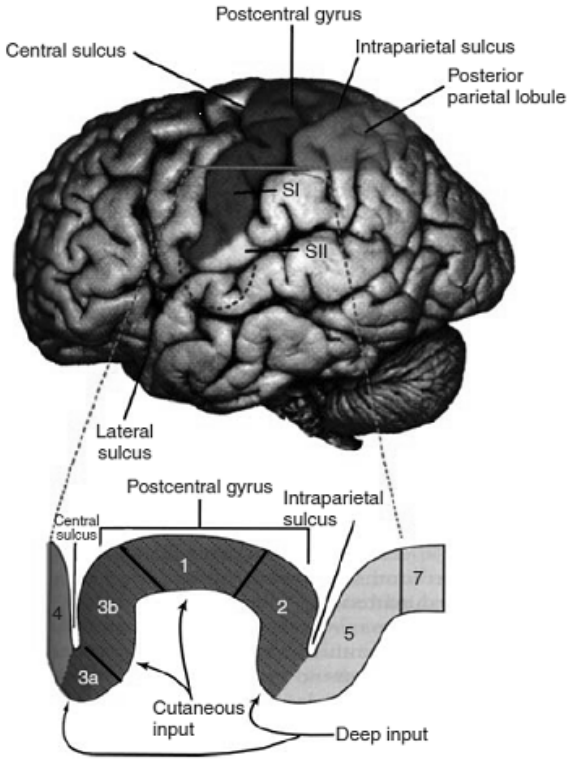

Figure 2.4: Anatomy of the primary somatosensory cortex

The region called S1, consists of four different architectonic fields that are called Brodmann's areas 3a, 3b, 1 and 2. The term S1 is for the cortical representation of touch that was discovered and described first. The name became useful when other cortical representations of touch were discovered, starting with the second representation, S2. The four different areas of S1, all of which receive afferents from the ipsilateral thalamus, differ in cytoarchitecture and process different submodalities of the somatosensory system.

Each of these areas has its own representation of the body, but only the area 3b representation has the defining characteristics of S1: a representation that is almost exclusively responsive to the activation of touch receptors. While area 3a is dominated by

inputs from muscle spindle receptors for proprioception, and area 2 also has major inputs from proprioreceptors, area 1 and at least much of area 2 respond well to light touch.

2.2 Event-related fields (ERFs) and somatosensory evoked fields (SEFs)

2.2.1 Event-related fields

The brain generates spontaneous oscillatory activity. It consists of rhythmical activity in the frequency range of 0.5-70 Hz and can be categorized into four groups relatives to their frequency. The oscillatory activity is assumed to emerge from feedback loops. In addition to the spontaneous oscillatory activity, activity following the presentation of stimuli can be recorded as evoked response. Usually, the stimulus related activation reflecting the processing of stimulus information is rather small and hidden in the spontaneous brain activity. To study the processing of stimuli MEG studies have focused thus on evoked responses, i.e. neural activation that occurs phase-locked, with respect to stimulus presentation or task onset. In EEG, the changes in potentials that are time-locked to sensory, motor, or cognitive events are known as event related potentials (ERPs). The corresponding magnetic field changes are termed event-related fields (ERFs). Evoked responses are typically detected within about 1 s from the stimulus presentation or execution of the task and consist of precisely timed sequences of waves of varying field strength and polarity. The observed peaks trough the waveform are referred to as components that represent a certain step of the information processing chain. In EEG, the components are described by their polarity P (positive) or N (negative) and a number representing the mean peak latency in milliseconds from the stimulus onset in the normal population. For example, N20 is a negativity that typically peaks at 20 milliseconds after the stimulus. To address components in MEG recordings the latency is preceded by the letter “M”. Usually, the polarity is not specified. The normal latency value for a component in a particular individual may be different from that implied by the component's name.

Given the background activity of the brain, the evoked responses are small and often difficult to detect in single trials. Brain noise, environmental noise etc. cause a very low signal to noise ratio. Thus, to acquire an ERP or ERF, the time-locked signals from several trials are averaged. Assuming that the noise is uncorrelated to the stimulus and its mean is zero, repetition of the same stimulus and averaging the evoked response will maintain the stimulus related activity while the background activity cancels. Note, if the time-locked rhythmical brain activity is not phase-locked over trials, then ERF/ERP signals might

cancel each other. Also it has to be assured that the time interval between two succeeding stimuli is sufficiently long to let the system return to its initial state.

The earliest salient responses, i.e. those of shortest latency, are typically transient (short-lasting) and tightly locked to the stimulus, and thus yield sharp responses even when averaged across multiple trials. The longer-latency responses tend to progressively increase in duration and are likely to exhibit more jitter with respect to the stimulus timing; in the average, they appear as sustained responses with slow fade-in and fade-out phases.

It is possible to estimate the location of an ERF generator by assessing the distribution of the magnetic field over the array of sensors, just as with ERPs. The fact that the skull is essentially transparent to magnetic fields and does not cause them to spread laterally like the electrical potentials, allows more accurate ERFs source localization, if compared to localization performed on ERPs. The effect of the noise on ERF recording is however problematic and limits the effectiveness of ERF localization techniques. Very different sets of hypothetical generator locations can often lead to a very similar voltage-magnetic field distributions at the surface; the noise level must be small with respect to the bandwidth of the voltage distributions or magnetic field in order for one to distinguish between the different hypothetical generator configurations. For example, a component that is broadly distributed across the scalp could arise from the activation of a large area of cortex near the surface or from a small area of cortex relatively deep in the brain; distinguishing between those alternatives can be an extremely difficult computational problem. The SNR in ERF averages is a function of the square root of the number of trials; doubling the SNR therefore requires a fourfold increase in the number of trials. Reducing noise levels beyond a certain point is therefore difficult because one can quadruple the number of trials only so many times without creating an unreasonably long experiment.

2.3.2 The somatosensory evoked magnetic fields (SEFs)

The somatosensory evoked magnetic field (SEF), represents the averaged magnetic activity following somatosensory stimulation and consists of a series of waves that reflect sequential activation of neural structures along the somatosensory pathways. They were first reported in 1978 (Brenner et al., 1978) and since there many studies have been conducted, and their number continues to increase.

The evaluation of averaged MEG signals following somatosensory stimulation, is one of the most useful methods for investigating the human somatosensory system. Our knowledge of the functional anatomy of somatosensory areas in humans has long been

limited by the difficulty in assessing, with adequate resolution in time and space, the sequential activation of cortical areas during processing of afferent somatosensory inputs. The spatial resolution of MEG is almost the same as that of functional magnetic resonance imaging and positron emission tomography, but the temporal resolution is much better. Therefore, we can analyze MEG responses to somatosensory stimulation for not only detecting cortical sources but also measuring the time taken for signals to transfer in the brain in the order of milliseconds. The SEFs provide thus information on the anatomical distribution of the sources and on their activation timing.

SEFs can be recorded for stimulation of various parts of the body: lower limb, upper limb, urogenital organs, the truncus, the neck , shoulder, face. SEF components typically are named by their polarity and typical peak latency in the normal population. However, the normal latency value for a component in a particular individual may be different from that implied by the component's name, because the lengths of the peripheral nerve and spinal conduction pathways, which vary with the patient's stature, influence the latencies of the SEF components.

A large number of studies have utilized computerized bit-mapped images of scalp topography of somatosensory evoked responses in attempts to elucidate each identifiable component. However, scalp-recorded EEG could not provide enough resolution and it is difficult to estimate the location of the electrical source in the brain, because the quality of reconstruction depends on the exact knowledge of the electrical and topological properties of the different head tissues which are not easily accessible. As already mentioned, MEG has several theoretical advantages over EEG in localizing cortical sources. MEG offers a very good localization accuracy of a few millimeters especially for superficial cortical sources such as those located in the primary somatosensory cortex. For example, in a study titled “Somatosensory Homunculus as drawn by MEG”, (Nakamura, 1998) a detailed somatosensory representation map of the human primary somatosensory cortex using MEG is given: SEFs following stimulation of 19 sites were recorded (tongue, lower lip, upper lip, thumb, index finger, middle finger, ring finger, little finger, radial palm, ulnar palm, forearm, elbow, upper arm, chest, thigh, ankle, big toe, second toe and fifth toe). The equivalent current dipoles (ECD) on the MRI of each subject was estimate. These representative areas were generally arranged in the above order from inferior to superior, lateral to medial, and anterior to posterior and the changes in the coordinates were compatible with the anatomy of the central sulcus and the homunculus. The location of the ECD for the upper lip could be distinguished from that on the lower lip, and each

representation of the thumb, index finger, middle finger, ring finger and little finger was distinguishable. The moment of each ECD, which suggested the size of the cortical areas responsive to the stimulation, was also compatible with the bizarre proportion of the homunculus with a large tongue, lips, and fingers. According to these results, a large part of the somatosensory homunculus was quantitatively reproduced on an individual brain MRI.

2.3.1 SEFs following median nerve stimulation

SEF following upper limb stimulation is usually recorded following stimulation of the median nerve at the wrist or fingers.

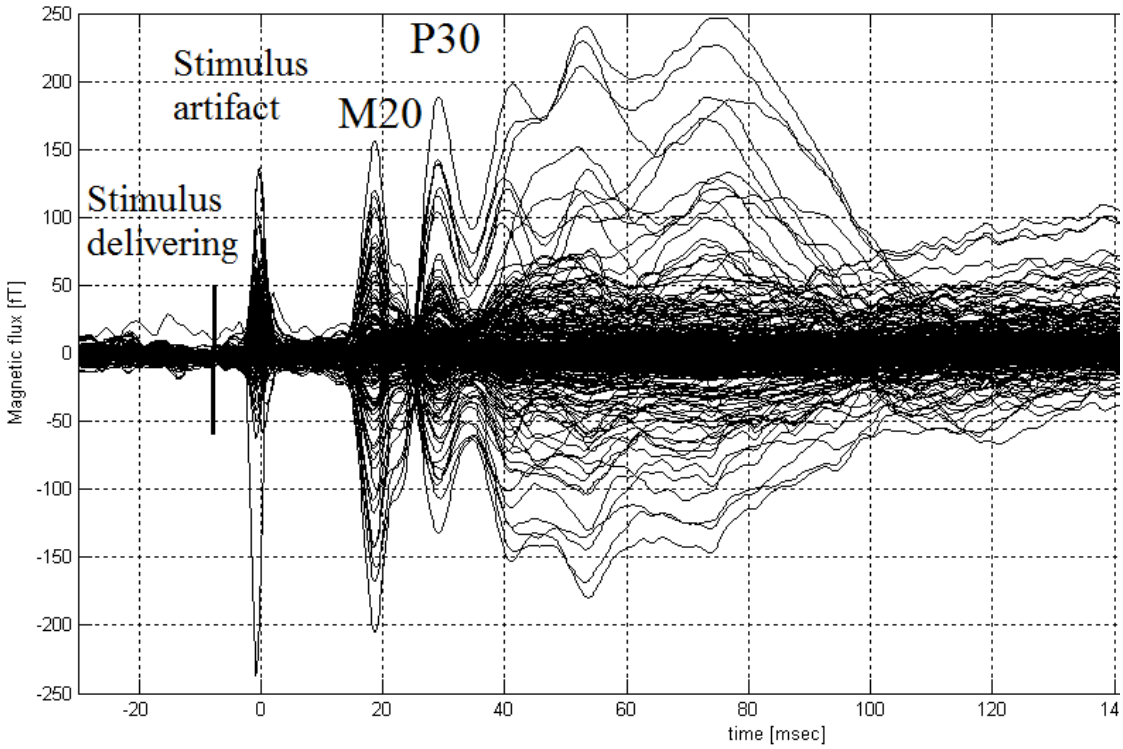

Figure 2.5: Superimposition of all recording channels in the 200 ms post-stimulus period.

The recorded SEFs following median nerve stimulation are generally classified by their post-stimulus latencies, as short-latency responses, less than 40 ms after stimulus onset, and long-latency responses (40–300 ms after stimulus onset).

The morphology of the short-latency SEFs has been consistently reported as two prominent peaks, one around 20±1 ms (M20) and the second at 32±3 ms (M30).

In the experiment described in this thesis we are interested in the short-latencies, thereby for sake of simplicity only short-latencies components are described here. Long-latency

components show a large inter-individual variability; it is however to outline that SEF morphology is very stable in the same subject, when tested in successive independent sessions.

The anatomic generators of short-latency human somatosensory responses have been the subject of considerable debate. There is a general agreement that the generators of M20 and M30 are located in the hand area of the SI contralateral to the stimulus. The specific region involved is probably area 3b.

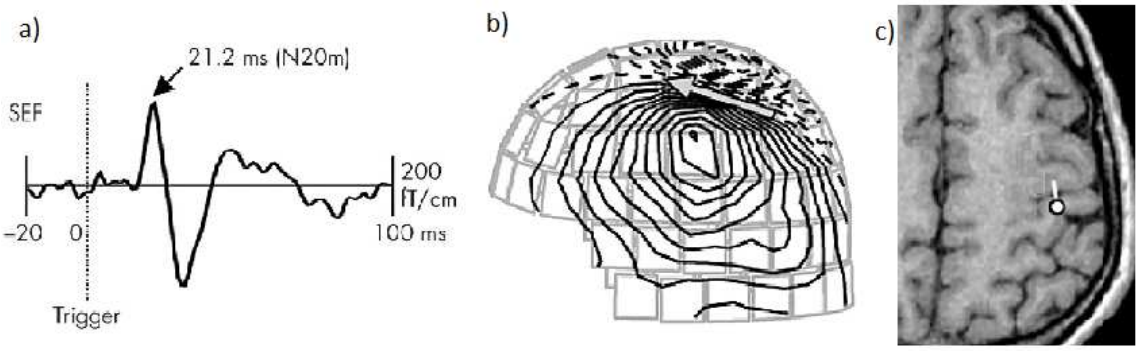

Figure 2.6:

a) Signal after median nerve stimulation

b) Magnetic field patterns at different M20. The arrows represent the ECDs that best account for the field pattern.

c) equivalent current dipole location at M20 (area S1)

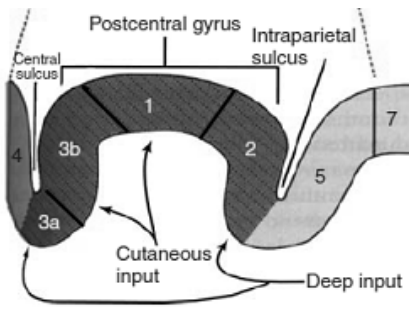

Figure 2.7: detail of area S1

When considering MEG signals the limits of the technique has to be kept in mind. There are four main limits. The first limit is that it is difficult for MEG to detect brain dipoles radial to the skull, which are mainly generated in the gyrus. In other words, dipoles tangential to the skull generated in the wall of the sulcus, i.e. area 3b , which are located on the posterior and anterior bank of the central sulcus, are easily detected by MEG, but dipoles in area 1 or 3a, which is located on the crown and the bottom of the central sulcus, respectively, are not. The second is that activities in the white matter are not detected by MEG, since it is assumed that the signal recorded by MEG is generated by the apical dendrites of cortical pyramidal cells. The third disadvantage is that it is difficult for MEG to detect dipoles in the deep brain areas, since magnetic fields recorded from outside of the scalp rapidly decrease with increasing depth. The fourth one is that it is difficult for MEG to disentangle multiple generators.

2. 3 Topic of the experiment

2.3.1 Scientific background

As seen in chapter 1, two separate basic neuronal events are possible candidates accounting for the generation of a measurable magnetic field: action potentials traveling along the axon away from the soma and postsynaptic currents at the apical dendrites of neurons.

Yet, action potentials are not very likely to generate MEG signals. The contribution of action potentials is assumed to be minimal compared to that of synaptically meditated activity and other slow waves. First, since action potentials form a travelling quadrupole the influence of action potentials on recordings at a distance attenuates much more strongly than postsynaptic potentials. Second, the probability that action potentials of different cells synchronize precisely is rather low, since action potentials are very short and there is always a considerable jitter between the discharges of different cells.

Excluding action potentials and ignoring the possibility of large-scale synchrony of elemental events, led researchers to believe that no normal physiological processes generate a macroscopic MEG signal at frequencies above 100 Hz. Much of the thinking behind previous MEG studies was dominated by this view. Hence, high-frequency "contamination" continues to be routinely eliminated by averaging and filtering of the data. Slow postsynaptic events in the apical dendrites of pyramidal neurons are very likely generating that part of the MEG signal that remains after averaging and filtering the data below 100 Hz. However, theoretical considerations and accumulating evidence from invasive electrophysiological recordings and new imaging modalities for cellular neuroimaging suggest that a faster neuronal mechanism may also contribute to the MEG signal at frequencies well above 100 Hz.

Direct evidence for high-frequency brain activity in humans in the 200–800 Hz range was identified from EEG and MEG data for strong electrical stimulation of different sensory nerves. Often called high-frequency oscillations (HFOs), this activity was identified after averaging many hundreds or thousands of trials.

Somatosensory response, if measured with a wide enough pass band, comprises the traditional low-frequency responses and a high-frequency burst-like response around 600 Hz, which react to experimental manipulations differently and likely reflect partially different neural events.

For the median nerve stimulation, HFOs latency is almost the same as that of the primary component (M20) of SEF and also generated close to its source. Interestingly, the HFOs are much reduced in amplitude during sleep, while in contrast, the underlying M20

magnetic field increases its amplitude during sleep. Consequently, it has been suggested that the M20 response and the HFOs reflect different cortical sources.

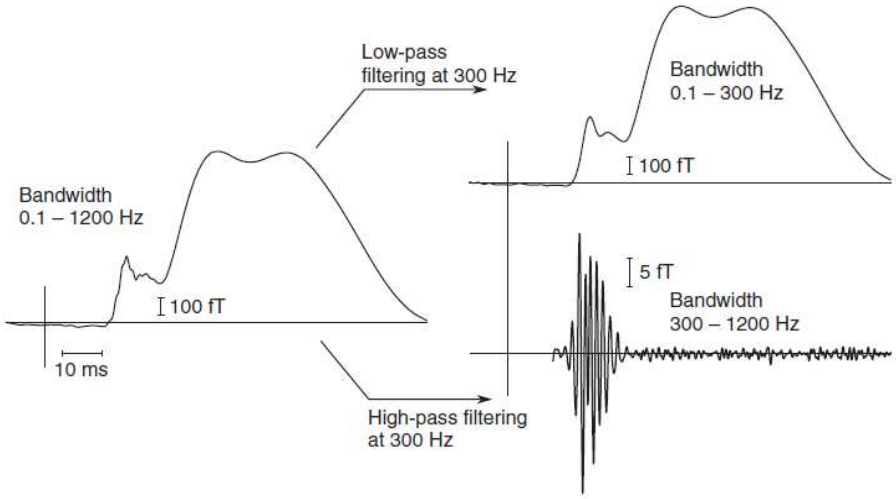

Figure 2.8:
Separating the low- and high-frequency components of somatosensory evoked responses to electric median nerve stimulation. HFOs are one of the recent topics of SEF study.

Early HFOs are thought to be generated by thalamo-cortical afferents, and late HFOs by inhibitory interneurons in parietal area 3b. But their origin is still matter of debate.

Synchronous neuronal activity is increasingly being implicated in theories explaining the effective transmission of information in the brain. In this context, detecting oscillatory activity of the brain offers new insights in the functioning human brain. In general, slow oscillations involve long-range networks, whereas fast oscillations involve short-range networks, i.e., the distance between the recruited neuronal pools is inversely related to their frequency (Buzsaki, 2006). It has been shown that orchestrating cortical network activity with synchronous oscillations of neurons across distant regions of the brain is a basis for human cerebral information processing (Knight, 2007) and monkeys (Saalmann et al., 2007; Womelsdorf et al., 2007). Oscillatory neuronal activity in defined frequency ranges supports synchronous interactions between anatomically distinct regions of the mammalian brain during cognitive tasks that require deliberate or automatic attention, memory, or visual processing. Frequencies of oscillatory activities depend, to a considerable extent, on the length and conduction velocity of the tracts connecting the neural areas that participate in oscillations.

Figure 2.9: adapted from *"Impulse Propagation along Thalamocortical Fibers Can Be Detected Magnetically outside the Human Brain", T. Kimura, 2008:*
Dipole localization for the M15 component from 14.9ms to 16.7ms

A Brief Communications titled "Impulse Propagation along Thalamocortical Fibers Can Be Detected Magnetically outside the Human Brain", (T. Kimura, 2008) [12], reported a MEG experiment on 3 subjects, following median nerve stimulation, where a "new" magnetic field component, labeled M15 was found. M15 changed dynamically within 1.6 – 1.8 ms before the onset of magnetic M20, the first component of SEF localized in S1, and was supposed to correspond to the signal propagation in the thalamocortical fibers, i.e. to intracellular depolarizing action current. In this report the MEG impulse propagations along the fibers from the thalamus to the somatosensory cortex was visualized (see Fig. above). Also the mean conduction velocity of the thalamocortical volleys was calculated (29 m/s). So far, the impulse propagation along the fiber tracts in the white matter had never been visualized in humans. The common belief was that MEG measures signal generated from the slow postsynaptic potentials generated by aligned neurons in the cortex and that MEG detection is almost blind to deep and radial sources, owing to the cancellation by the magnetic field of the secondary volume currents.

No previous studies on MEG have disclosed impulse propagations within the white matter in the human brain. An alternative hypothesis which could explain the results of the source localization showed in figure 2.9, and thus contradicting what reported in [12], is the existence of two sources, one in the thalamus and one in S1, slightly shifted in time. Since the thalamic one is much deeper, fitting the results with two sources doesn't detect the deep one, but fitting the data with only one source would produce the movement that we see. The major theme against this hypothesis is that in this case the dipole movement should follow a straight line, which is not the case reported in [12]. Still, the frequencies

considered could play an important role in distorting eventually the trajectory of the dipoles.

2.5 Aim of the experiment

Aim of this study is to reproduce and improve what reported in [12], i.e. that MEG is able to visualize impulse propagations along the fibers from the thalamus to the somatosensory cortex. Thus, we designed and performed the same experiment described in [12], but improved: higher SNR, higher number of subjects investigated, higher frequency sample during the recording of the signal. In addition the same day of the MEG experiment we collected MRI anatomical data of the subject, Thanks to a coregistration procedure between the MRI and MEG techniques, information collected with MRI allows improving the power of MEG source localization by taking into account the real shape of the head of the subject, and allows also visualization of the results of MEG source localization into the subject's proper anatomy.

Further goal of this study is to validate the results obtained with MEG source localization. For this we collected also diffusion MRI data of the subject, in order to reconstruct the trajectory of the fibers of interest in the brain of the subject. The idea is to superimpose the results obtained with MEG source analysis with the information obtained from diffusion MRI, in order to evaluate the reliability of the MEG findings. In the following chapters design, development and data analysis of this experiment are described.

Chapter 3

3.1 Overview of the experimental setup

3.2 The stimulation

3.3 Data acquisition

3.4 Head position defining and coregistration with MR- images

3.1 Experimental setup

Subjects

Thirteen healthy subjects (ten males, two females; 26 ± 3.5 years), participated in the study. They gave their written informed consent before the experiment, which was first approved by the Ethical Committee of University of Trento.

Stimulation paradigm

Electrical pulses at two different stimulation levels, motor threshold (MT) and sensory threshold (ST) , were randomly applied to the left and right median nerves, thus producing 4 conditions: left motor (LM), left supra (LS), right motor (RM), right supra (RS). The intensity levels were adjusted to different values based on the subject feedback before, and fixed throughout the experiment.

The stimulation was delivered through rectangular current pulses with duration 0.2 ms. The time interval between two stimuli varied randomly between 200-300 ms.

The electrical pulses were generated using a constant current stimulator.

For every subject we collected 3000 trials per condition. The experiment was divided into 15 block of 800 trials (200 trial per condition collected at every block). Every block had a duration of about 200s for a total duration of the experiment of 50 minutes.

Data acquisition

Before the experiment, the subject was asked to change his clothes and wear a disposable pajama and shoe covers, in order to avoid any possible magnetic interference.

During the recording, the subjects were instructed to relax and keep their eyes open fixating a small cross ahead.

SEFs were recorded with a Elekta Neuromag system, 306-channel whole-head array consisting of 102 magnetometers and 204 planar gradiometers arranged in 102 triplets. MEG signals were bandpass filtered between 0.01 and 1000 Hz, sampled at 5000 Hz.

To assess the exact location of the head with respect to the sensors, current was led into four head position indicator (HPI) coils pasted on the scalp and the resulting magnetic fields were measured. A 3D-digitiser (Isotrak 3S1002, Polhemus Navigation Sciences, Colchester, VT, USA) was used to determine the locations of these coils and the head shape with respect to anatomical landmarks (nasion, left and right preauricular points). We collected in fact about 1000 additional skin points from the skull and also from the nose tip along the midline to the inion and laterally from the preauricular points to the cheek bones.

Mri scanning

For each subject, the same day a scan session was performed using a 4.0 Tesla Bruker Medspec scanner equipped with an eight-channel multi-receive head RF system.

A structural MRI with a T1- weighted sequence of 176 sagittal slices (MP-RAGE; 1x1x1 mm3, acquisition matrix: 256x224x176) was acquired.

A set of diffusion weighted images (DWI) was acquired. The DWI was acquired by using 30 diffusion encoded directions. Five images with null b-value were taken before starting the acquisition with gradients, in order to obtain reference images without diffusion sensitizing gradients. Imaging parameters were: Bvalue=1000, image resolution 2x2x2, acquisition matrix 128x128x50, TE/TR=94/7900.

Coregistration MEG-MRI

For allowing coregistration of the two imaging modalities, markers were placed at the three anatomical landmarks (nasion, left and right preauricular points defined in MEG coordinates) on the subject's skin. This points good references since usually there is no fat and are quite stable, independently if the subject is seated, like in the MEG modality, or lies, like in the MRI scanner.

The markers are circular stickers of 1.5 cm diameter and 0.3 cm thickness with a circular hollow center of 0.5 cm diameter (MM 3005, IZI Medical Products Corp., Baltimore, MA). They are clearly visible in the MR images. Once the subject had finished the MEG study, the coils enabling the measurement of subjects' head position in the MEG were removed and replaced with additional markers of the same type as used for the anatomical landmarks. Then the subject was sent to the scanner. This positional information together with the scalp shape as taken by the digitization of the head it is used to verify goodness of coregistration and for further improvements of the coregistration results.

3.2 The stimulation

3.2.1 Electrical Stimulation

The human somatosensory system can be stimulated peripherally and noninvasively by touching the skin mechanically, by heating and cooling, and by applying brief electric pulses to directly activate the sensory nerves. The most used ones are electrical or mechanical stimulation.

In mechanical stimulation, tactile stimuli are usually delivered by pneumatic devices with multiple channels to stimulate different fingers. Pressurized air is fed directly to skin or to a small container with an elastic membrane in contact with the skin. The SNR ratio following mechanical stimulation is smaller than that for electrical stimulation, thus the recorded waveforms are noisy and not very sharp. Moreover due to the dispersion of the pressure wave, these stimuli have significant rise and fall times (on the order of 20 ms) and it is difficult to record short-latency components. For these reasons we used electrical stimulation.

By electrical stimulation, nerves are stimulated directly: electric pulses applied via cutaneous electrodes evoke tactile sensations and, by passing a local electric current through the skin, trigger action potentials in the nerve fiber.

One big problem when recording SEFs following electrical stimulation, is the presence of stimulus artifacts caused by the stimulation. The stimulation currents generate a magnetic fields around them. The strength of the field due to a current is directly proportional to the strength of the current and therefore, to minimize the interference, the stimulation currents must be kept as low as possible. However, the stimulus artifacts from an electric stimulator can be too large to record clear SEF. Luckily, the duration of stimulus artifacts is very short, usually less than 5 ms following stimulation, to return to the baseline of the waveform. Nevertheless, when sites very close to the magnetic coils are stimulated, for example, facial skin and tongue, it is frequently impossible to record clear SEFs, especially the short-latencies, due to large stimulus artifacts. In such a case, mechanical stimulation is frequently used.

3.2.2 Stimulus location and intensity

The sites typically used for recording of SEFs with electrical stimulation are the median nerve at the wrist, the common peroneal nerve at the knee, and the posterior tibial nerve at the ankle.

Either sensory nerves or mixed nerves (sensory and motor) can be stimulated. The stimulation of the mixed nerve is preferred generally because it allows regulating the intensity of the stimulus based on the motor response. Moreover, stimulation of the mixed nerve evokes bigger answers than stimulation of only sensory nerves, because during mixed nerve stimulation also the fibers afferent to muscles are activated.

For recording median nerve SEFs, the nerve is stimulated at the wrist. In order to reproduce stimulus locations and intensities among subjects, before the experiment began, the anode and cathode were placed so that, a motoric response, i.e. a consistent twitch of the thumb, was produced. This location of stimulus delivery was maintained throughout the experiment. During the experiment subjects were stimulated at the motor threshold (MT) and sensory threshold (ST). The thresholds were determined by varying the stimulus intensity and by asking the subject whether he/she had felt the stimulus or whether he/she showed a muscular reaction. MT was adjusted individually so that a clear twitch of the thumb was seen and fixed as:

MT=first motor answer+0.28*(first motor answer – sensory perception).

Sensory perception is the lowest point at which response to a stimulus can be perceived. The corresponding condition ST was fixed as:

ST=sensory perception+0.28*(motor answer-sensory perception).

3.2.3 Timing

The number of experimental conditions, the number of trials per condition, the stimulus duration, the inter-trial interval and the total duration of the experiment depend mutually on each other. For each condition there were 3000 trials. The high number of stimulus repetitions was chosen in order to obtain a good signal-to-noise ratio. In general, a good SNR is the prerequisite for further data analysis like in single subject analysis and source modeling. In stimulus-locked, evoked brain responses, 100 accepted trials per condition are regarded to be sufficient. Assuming that 15–20% of the trials are contaminated by eye blinks or other types of artifact signals, the total number of trials per condition should be around 120. In cognitive tasks, in which each trial may be fairly long and one needs to limit the total duration of the experiment in order to keep the subjects alert and motivated, 60–80 accepted trials is what can be reached at most, however on the cost of a bad SNR. In the present experiment, a number of 3000 trials are necessary in order to have a SNR high enough to reveal evoked high frequency oscillations in addition to the SEF responses.

The interstimulus interval (ISI) should be long enough to allow the neural responses to return to the baseline level. In the case of evoked responses it should last at least 200 ms. With a large number of trials, a small ISI was required, in order to have a reasonable duration of the experiment.

The choice between fixed or variable ISI is at the discretion of the experimenter. A randomly changing interstimulus interval is recommended, in order to avoid habituation and to maintain subjects' vigilance. We have chosen an ISI of 250 ± 50 ms.

3.2.4 The Stimulator

Delivering stimuli without interfering with the MEG signals is often challenging, as the devices used for generating the required sensory input also produce unwanted magnetic signals that are picked up by the MEG. In addition, stimulus delivery has to be temporally precise: sloppy timing yields smeared responses, particularly in the primary sensory areas. Developing, selecting and applying stimulators are a large undertaking.

The stimulator we used is a stimulator that allows the use of up to 5 independent channels for stimulation. It is driven by a computer through a DA-card, thus allowing the generation of almost every desired signal shape even with changing polarities. For security reasons the current supply of the stimulator is realized by an internal battery.

Electrical stimuli are delivered by using either constant voltage or constant current stimulator. The stimulator we have used operates by keeping the current constant, independently from the skin and cable impedance, provided this is not too high. The constant current drive has the advantage to be less affected by changes in the electrode impedance, and for this reason it is more widely used.

When stimulating the median nerve at the wrist, the current at the motor threshold is typically 2–7 mA. The strength of the field due to a current is directly proportional to the strength of the current and therefore, to minimize the interference, the currents must be kept as low as possible. Contact impedances of the stimulating electrodes should be kept low in order to minimize the electrical stimulus artifacts in the recorded data and also to minimize patient discomfort.

3.3 Data acquisition

3.3.1 The Elekta system

The MEG owned by Cimec in the MEG-lab of Mattarello (Trento), is an 306-channel whole-head array produced by Elekta Neuromag (VectorView, Elekta Neuromag, Helsinki, Finland). The device operates inside a 3-layered magnetically shielded room. A data acquisition system outside of the shielded room collects and routes the data to a UNIX workstation, which controls the measurement and performs on-line processing of data.

The main peculiarity of this 306 channels-system is the ingenious geometry of the triple-sensor element: every sensor comprises two orthogonal planar gradiometers and one magnetometer. The sensor combines thus the focal sensitivity of planar gradiometers, measuring the sideways gradients of the normal component Bz, and the widespread, spatially less specific, sensitivity of the magnetometers, measuring the normal component Bz.

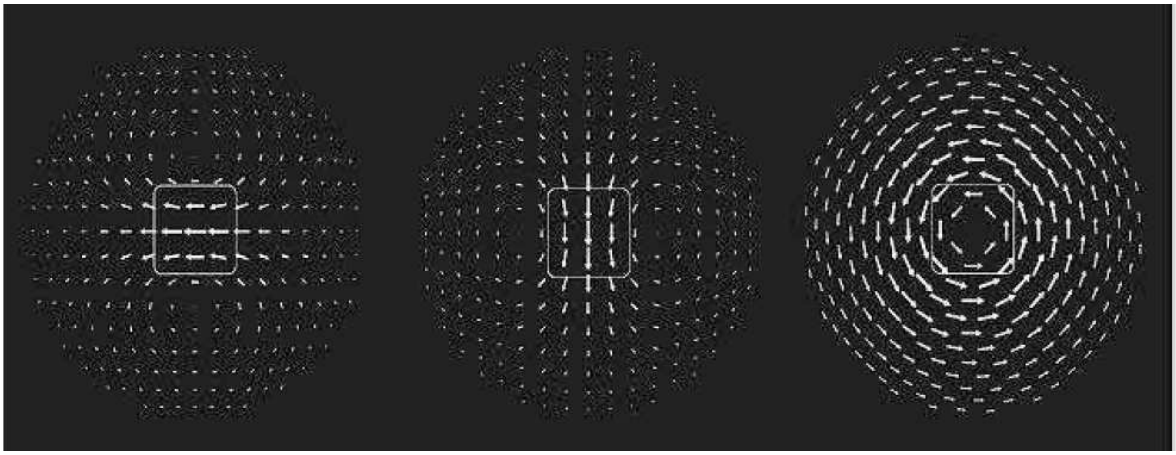

Figure 3.1:
The lead fields (sensitivity patterns) of the two gradiometer and the magnetometer integrated on one sensor unit. The lead fields of the three channels in such a sensor element are orthogonal to each other. This means that despite of the overlapping pick-up loops the three channels of the sensor element convey orthogonal information. The signal in any one of the three channels cannot be predicted from the signals of the other two.

Furthermore this design enables the densest spatial sampling of the magnetic field in the industry: the field is measured at 510 locations above the cortex by 510 coils configured into 306 independent MEG channels and the total sampling area of the pick-up loops is 1543 cm^2, 27% more than the total area covered by the array. This is possible because the pick-up loops in the triplet sensor element partially overlap and provide three orthogonal, independent channels of information. This feature is not feasible in wirewound axial gradiometer or magnetometer based arrays. In other MEG systems using only axial sensor

arrays, the amount of information sampled does not grow after about 200 channels because the increasing of the channel count leads to decreased sensor size and decreased sensitivity of the individual sensors.

3.3.2 Temporal Sampling

According to the sampling theorem it is sufficient to sample the continuous signal at a rate that is twice the frequency of any component of the signal, and yet to perfectly reconstruct the original signal from the discrete samples. All signal components, whether of interest or noise, must be below the Nyqvist frequency, half the sampling rate, in order to avoid aliasing. Those signals that are above will fold along the frequency axis to appear as lower frequencies. This undesirable phenomenon can be avoided by low-pass filtering the signal before sampling to ensure that there is no signal above half the sampling rate (anti-alias filtering).

Given the MEG signal frequencies and the Nyqvist condition, the sampling rates range between 300 Hz and 4 kHz.

It is often desirable to temporally oversample the signal of interest to avoid the non-idealities of the anti-alias filters such as phase distortion and the finite fall-off rate, and also for an easier reconstruction of the original signal by linearly interpolating the values between the samples, instead of using the optimal, but computationally expensive, sinc-interpolation.

3.3.3 Triggering

By recording of event related fields a stimulus defines the time epoch of interest within the data array. Each epoch is called a trial. MEG signal is recorded continuously and triggers are necessary to time-lock the MEG data to the stimulus presentation, in order to know when and which certain stimulation happened. During the recording, triggers are sent to the data recording system and the occurrence of the trigger will be recorded as a temporal marker in the MEG data. In process of the collected data, off-line time-locked signal average is calculated across trials epochs for each condition. Note that on-line average could be also performer. This is useful in order to have a real-time look on the data quality. However off-line average is the standard procedure, since it allows cleaning the data before averaging.

3.3.4 Filtering

Before ERFs measurements are made, it is useful to apply SNR-enhancing filters that incorporate assumptions about frequency, timing, and spatial distribution of the component of interest. Though signal averaging attenuates unsynchronized noise at every frequency, as it improves SNR, MEG data can be improved by limiting the window of frequencies so that only the band where the response's energy lies is retained. Frequency filters are commonly applied prior to component measurement; these filters are useful whenever the frequency of the noise is different from that of the signal.

The frequency range of MEG responses typically contains frequencies up to about 100 Hz. As seen in chapter 2, more recently the higher frequency bands have also received attention following the discovery of fast oscillatory.

The 600-Hz burst response to electric nerve stimulation contains probably the highest-frequency oscillatory components so far detected by MEG and we are interested in this signal.

When measured with a wide enough pass band, the somatosensory responses comprise the traditional low-frequency responses and a high-frequency burst-like response around 600 Hz.

Since the continuous acquisition mode is employed, we applied a generous bandpass in the data acquisition (0.1-1000 Hz). Off-line digital filtering will be performed during the data analysis for separating lower- and higher-frequency components.

3.4 Head position defining and coregistration with MR images

Accurately defined head position is a prerequisite for all source modeling approaches. In addition, the estimated MEG source is usually visualized superimposed on the anatomical MR-image of the subject and can be mapped into a normalized space, such as Talairach or Montreal Neurological Institute (MNI) standard brain. Thus, accurate coregistration between MEG and anatomical MRI is fundamental.

The MEG measurements are taken at locations known only with respect to the MEG device itself, unlike MRI. The subjects' head location inside the helmet is unknown since head movements as large as a few centimeters are possible. Therefore, MEG devices include a subsystem to determine the position of the head with respect to the MEG sensors.

Definition of the head position and its successive coregistration with a structural MR image is based on three pieces of information.

First, head digitization is carried out prior to measurement. Three to five small indicator coils, called Head position Indicator (HPI), are placed at known locations on the scalp of the subject. The location of the anatomical landmarks (preauricular points and nasion) as well as the locations of the head position indicator coils with respect to the anatomy are digitized prior to the measurement with a 3D digitizer. Additional digitized points of the surface of the scalp can also be taken during this step.

Second, the location of the head relative to the helmet is recorded during MEG measurement by energizing the head position indication coils. The HPI are fed with small currents, either sequentially or simultaneously at different frequencies, generating magnetic fields. The MEG sensor array can be used to localize the elicited magnetic field, just like it is used to localize neural currents in the brain, and the coils locations can be estimated. In standard studies the coils are activated prior to the data acquisition, at the beginning of each recording block. Note that with this method, movement of the subject during the recording severely distorts MEG data. Usually with cooperative and healthy subjects this is not a problem. It can be a problem with small children or epileptic patients. The analysis of such data requires movement compensation which consists of dynamic recording of head position.

Third step, the three digitized anatomical landmarks are visually identified from MR images. In MR images the landmarks are visualized by MR compatible markers. The three correspondent digitized points are aligned to these. Matching of the spatial reference systems can be performed by identifying at least three corresponding points, by which the registration parameters can be estimate and a strict known correspondence between the MEG space and the MRI space is defined and each point in the first space corresponds to a known point in the second space. In this step coordinate system can be adjusted to ensure that the additional digitized points match to the surface of the scalp. If the anatomical landmarks would be accurately identifiable on MR images, this step would be sufficient to provide us with a coordinate transformation between the MEG device coordinate system and the MRI device coordinate system. Unfortunately anatomical landmarks are difficult to exactly indentify on an MR image. For this reason, before digitizing the anatomical landmarks, with the Pholemus we placed three markers on the skin of the subject. These markers are visible in the MRI. In this way it is possible (theoretically) to easily identify the three anatomical landmarks on the MRI image and coregister MEG and MRI. Moreover, once the subject was completed with the MEG study, the coils were removed

and replaced with other markers, the same used for the anatomical landmarks, and the subject was sent to the scanner.

The four markers in correspondence of the coils and the additional digitized points give additional information about the goodness of the coregistration performed based on match the three anatomical landmarks and can also be used for improving it.

Note that, although we put much effort in performing coregistration, we found same problems that will be treated in next chapter. Also more details about head positioning are given in next chapter: since we used for every subject average among different blocks, in the post-processing part we performed a software called Head Position Correction for re-align the head position of a subject through all runs.

Chapter 4

4.1 MEG data pre-processing

4.2 Anatomical MRI pre-process

4.3 Coregistration between MEG and MRI

4.4 Source analysis – part 1: theory

4.4 Source analysis - part 2: source analysis in the data

4.6 Monte Carlo simulation

4.7 Diffusion MRI

4.1 MEG Data Pre-processing

Prior to the analysis of specific features of the magnetic brain activity, the raw MEG data normally undergoes several preprocessing steps like artifact detection and removal, filtering, and averaging.

In my project the pre-process of the raw consists of: alignment of the different runs of the same subject for different head position, cleaning, filtering and averaging of the raw data. At the end for each subject I will obtain four somatosensory evoked fields (SEFs). Later, source localization will be performed on these datasets.

4.1.1 Softwares for MEG data analysis

The offline analysis of MEG data were mainly performed with BESA Reseach 5.3 (MEGIS Software GmbH, Graefelfing, Germany). BESA is versatile software for signal processing of EEG and MEG data and covers the whole range of signal processing and analysis. It allows also integration with BrainVoyager, which I will use for the analysis and coregistration of anatomical MRI data. BESA also has a direct interface to MATLAB, which I will use for performing Monte Carlo simulations.

Apart from BESA, I used also Maxfilter as data pre-processing tool. This tool is provided by Elekta Neuromag (the producer of the MEG device). This package provides various functions for pre-processing the MEG data (filtering, averaging, automatic artifact rejection etc.) and it also provides a direct interface to other Elekta Neuormag programs for source analysis and MRI analysis.

I choose to use BESA as main software for the analysis, since it allows for easy interactive source modeling that is the central part in present analysis.

I used Maxfilter for centering head position into a common frame in order to align data between the runs of the same subject.

4.1.2 Artifacts rejection and bad channels exclusion

The presence of artifacts in the signal can be due to external causes, e.g. moving vehicles, moving iron objects (buttons, buckles, necklaces etc.). Also the subject is a source of artifacts: small movements, eye movement and blinks. Attempts to control this kind of artifact by instructing subjects to be still and fixate their gaze on a point or not to blink help but often are not sufficient. The presence of these interferences produce electrical potentials and magnetic fields that are often much larger than those deriving from brain

sources. Removal of this artifact is good praxis. Several paradigms have been developed for automatic artifact rejection.

Since the magnetic artifacts are not problem as long as they are not synchronized to the events to which the averaging of single trials is locked to, and since I had a big number of trial per condition, I decided to proceed with manual artifact removing, i.e. inspecting visually the whole raw data recordings for artifacts and eventually removing contaminated parts.

Good praxis is also to exclude the so called “bad channels”, i.e. noisy or spiky channels. Up to 3-7 bad channels per measurement are acceptable. Bad channels were identified by visual inspection and excluded from the data set if needed. In the rare runs were the bad channels were more than 7, the run was discarded.

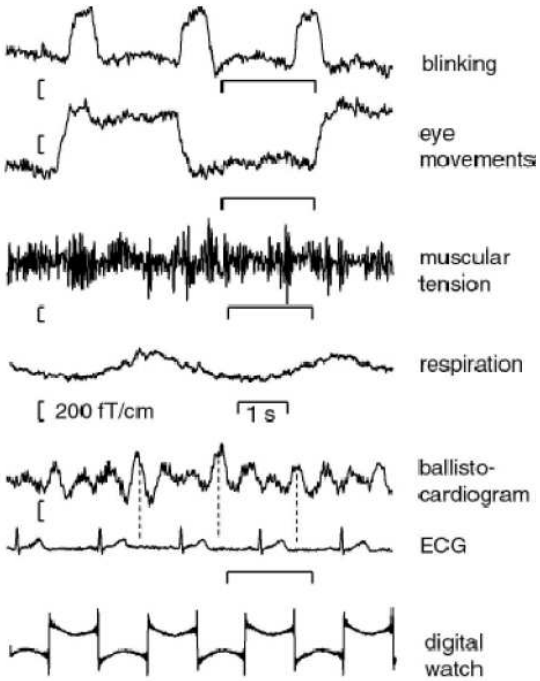

Figure 4.1, adapted from Hari, 2000:

4.1.3 Filtering

I applied a digital filter 0.1-1000 Hz. i.e. I kept the same filter applied in the data recording. Further filtering can be done also later, when performing source analysis, in order to separate the high and low frequencies.

4.1.4 Averaging

Single evoked responses have a poor signal-to-noise ratio (SNR). The MEG signal amplitude is affected by several factors: the extend of the activated area, the level of neuronal synchrony, the anatomical location and orientation of the source, and cancellation

effects due to opposing coincident nearby activations. MEG response amplitudes can span the range from few femtotesla to a picotesla. Noise from several sources hampers MEG: brain activity not of interest, biological noise from sources other than the brain, instrumentation and ambient magnetic interference, all contribute to the noise seen in MEG recordings. The relative strengths of these sources depend on the frequency: in rough terms, at the lowest frequencies (below 1 Hz) the ambient and biological noise are usually most prominent; the mid-frequency band (1–100 Hz) is dominated by brain noise (except at the line frequency of 50/60 Hz), and at higher frequencies most of the noise originates in the MEG instrument itself.

In order to improve the SNR and allow accurate detection and localization of the underlying sources, multiple responses can be averaged to remove random noise, given the possibility of acquiring multiple realizations of the event of interest.

By recording event related fields (see chap.2), a stimulus defines the time epoch of interest within the data array. The event is repeated, each repetition is called a trial, and a time-locked signal average is calculated across trials epochs for each time point of the epoch.

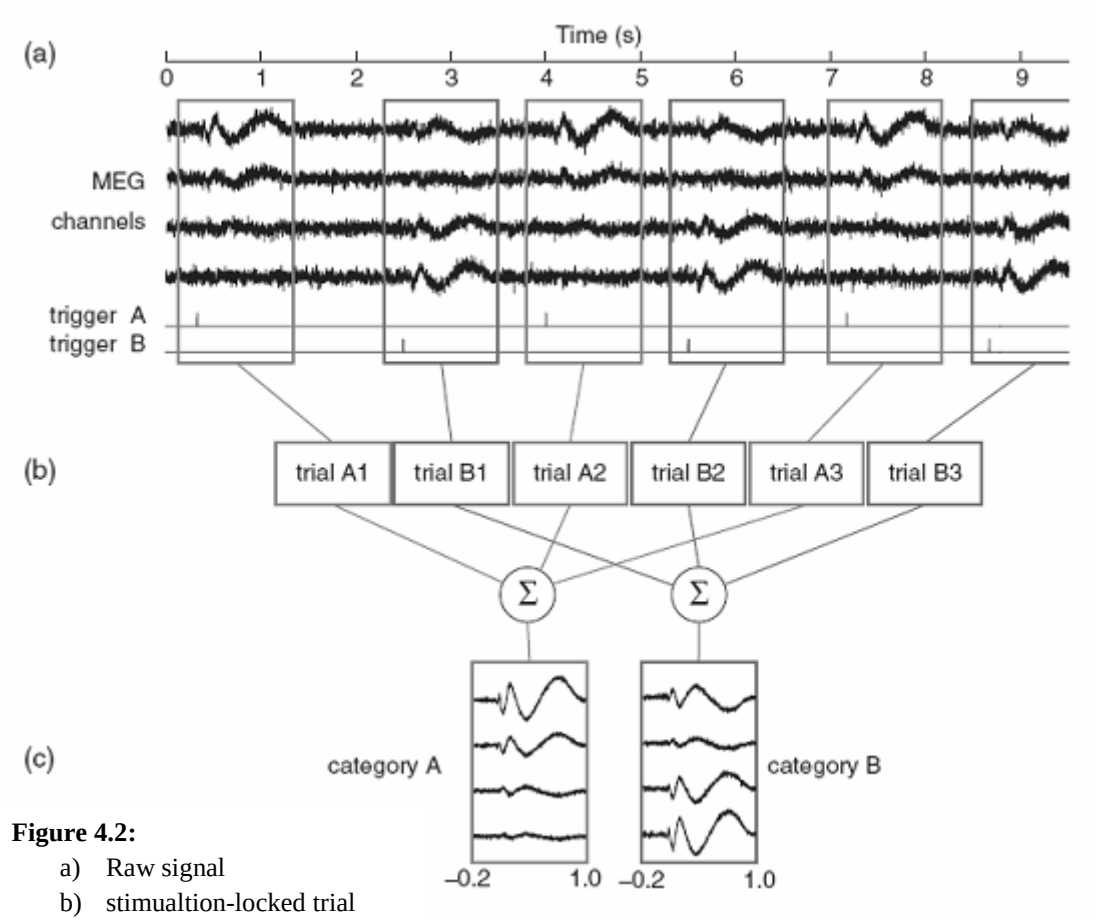

Figure 4.2:

a) Raw signal
b) stimualtion-locked trial
c) averaged signal

Assuming that noise is uncorrelated with the stimulus and its mean is zero, if we repeat the same stimulus after a time interval sufficiently long to assume that the system is returned to its initial state, the new evoked response will be essentially the same as the precedent.
Note that the assumption that the signal is invariant across trials is violated when the latency of the ERF component of interest varies from trial to trial or due to habituation of the subject to the stimulus. Also the assumption that background MEG noise is random noise, is only an approximation to the truth.

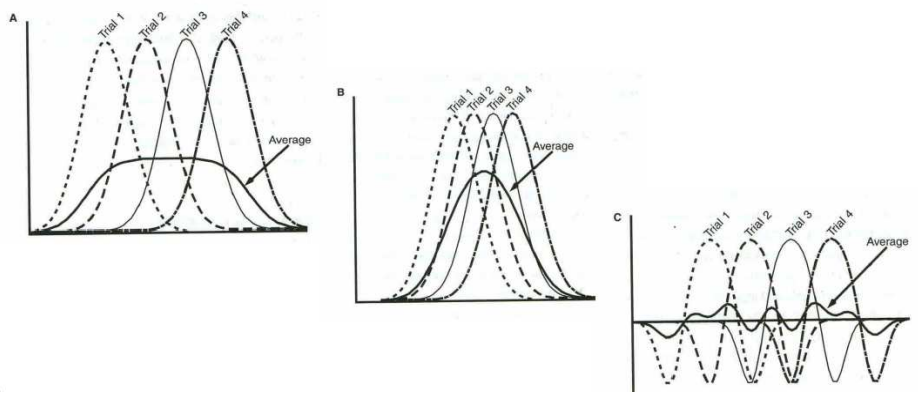

Figure 4.3: Trial-to-trial variability of the component's latency: by averaging signals might cancel each other.

increasing number of trials, averaging reduces the noise with a decrement of $1/\sqrt{N}$, where N is the number of averaged trials. This relation only holds provided that the noise in the data is temporally uncorrelated from trial to trial. Since the response amplitude often decreases with frequent presentations of the same stimulus, and biological noise may increase with a prolonged measurement (frequent eye blinks, muscle artifacts due to neck tension etc.), the SNR improvement in practice is somewhat worse than predicted by the formula above.

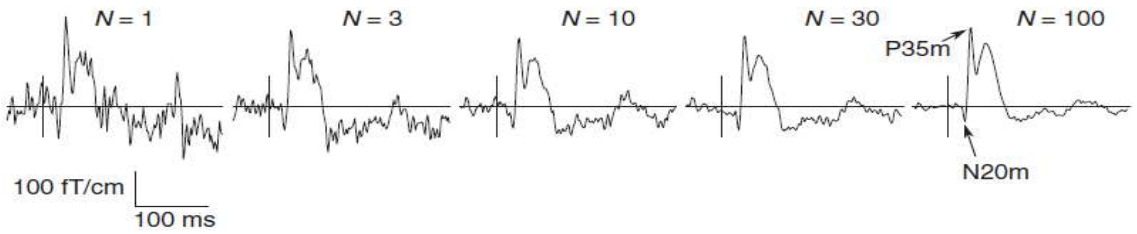

Figure 4.4, adapted from *MEG: an introduction to methods P. Hansen, M. Kringelbach, R. Salmelin.* Averaging of somatosensory evoked fields. N refers to the number of trials averaged. The responses are elicited by electric stimulation of the median nerve at the wrist of a healthy adult.

Averaging was performed separately for all conditions in one run (200 trials, less the trials rejected because of artifact rejections). Then averaging was performed across all the runs of the same subject resulting in four SEFs for every subjects, every one obtained by the average of about 3000 trials (less the rejected trials by prior artifact rejections).

4.1.5 Alignment of Different Head Positions among runs of the same subject

Different head positions of the subjects with respect to the measurement device hamper the comparison or averaged data obtained from different measurement sessions. In order average across runs signals have to be aligned to correspond to a standard head position.

In this analysis the interest is in source localization performed on the average of all the runs of the same subject. During experiment recordings, the head position was measured before the starting of every block and the subject was instructed not to move during the block. This means that between runs the head has a different position with respect to the device. Thus, before averaging, I need to re-calculate the brain activity at the channel positions of a template sensor configuration.

In a first step of the analysis I calculated averages across runs for every subject without aligning the different head position. In this case the source localization of the M20 component, that is usually localized in primary somatosensory cortex, even with much less averaged trials, was incorrectly localized along the vertical direction. In contrast, localizations for every single run were correctly performed and yielded consistent results. The error found for source localizations without realigning the head position across runs corresponds to the slipping of the subject's head out of the helmet of the Dewar that is often observed along MEG studies when subjects start to relax.

In order to correct for the localization error, I went a step back in the analysis and applied head position alignment between runs on the raw data. For every subject I used as standard position for the alignment, the position of the head during the seventh run. Once obtained these new aligned signals, artifacts rejection, filtering and averaging were performed again and S1 was localized correctly for every subject.

To "convert" a measured signal, it has to be transformed into a device-independent representation attached to the coordinate system of the head, and a virtual signal that would have been measured from a standard head position is calculated. A recently proposed method called Signal Space Separation (SSS) transforms multichannel MEG signals into an idealized form. This method is implemented in the MaxFilter software.

In SSS, multipole expansion is used as device-independent source model. The data are expressed as two multipole expansions: the multipole components are calculated for contribution from inside the helmet and for the outside contribution. Then, the virtual signals are calculated using both multipole components, or the component corresponding to the inside helmet part only. The foundation of SSS is a basis spanning all multichannel signals of magnetic origin. It is based on Maxwell's equations and the geometry of the sensor array, with the assumption that the sensors are located in a current free volume. For more details see [*Applications of the Signal Space Separation Method*, S. Taulu, J. Simola, M. Kajola; *Spatiotemporal signal space separation method for rejecting nearby interference in MEG measurements*, S Taulu and J Simola].

SSS method provides a way of standardization of different positions of the subject. It can also provide suppression of external interference signals, by taking only the contribution from the inside helmet. However, since in the present study the SNR is very good, I decided to perform only head alignment taking into consideration the whole signal and not to apply this spatial filter.

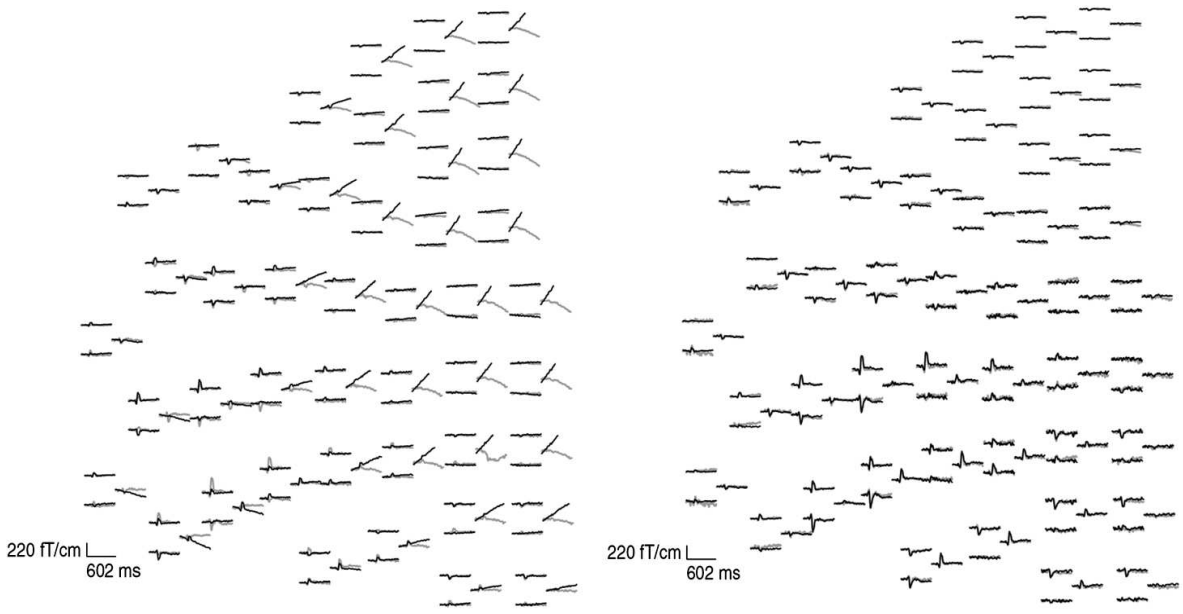

Figure 4.5, adapted from Applications of the Signal Space Separation Method (S. Taulu, J. Simola, M. Kajola):
Auditory responses at the left frontal quadrant of the sensor array.
Left: original waveforms of an auditory response recorded from two different head positions. Grey and black traces correspond to subject leaning to the left and to the right, respectively.
Right: standardized waveforms of an auditory response recorded from two different head positions. Grey and black traces correspond to standardizations made for subject leaning to the left and to the right, respectively.

In figure 4.5 the ability of SSS to align different head positions is shown. In this study the auditory response of a subject from two head positions has been measured, averaged and then converted to a standard head position. In the first measurement, the subject was leaning against the left side of the inside surface of helmet, and in the second measurement, he leaned against the right inside surface of the helmet.

The original unprocessed waveforms are shown overlaid on the left side of Fig. 15, and the morphology of the response is clearly altered by the different head positions. The right side of Fig. 15 shows the standardized signals from both measurements overlaid. These signals are the virtual signals.

4.2 Preprocessing of the anatomical data

The same day of the MEG experiment, anatomical MRI, DTI and fMRI of the subject were collected. The anatomical MRI has to undergo some pre-processing steps. AC-PC and Talairach transformations of the images are needed: the images were resampled to 1 mm resolution (isovoxel scaling) and transformed into ACPC and Talairach standard space. The coregistration will be then performed on the ACPC version of the anatomical scan. The source coordinates are expressed in this space but also can be expressed in the Talairach system.

The analysis of diffusion tensor imaging data is also subject of this thesis and will be discussed in the next section. The analysis of functional magnetic resonance data is however not included in this thesis.

4.2.1 Software used for MRI analysis

The entire analysis of the data obtained in the MR-scanner has been realized with BrainVoyager QX (Brain Innovation B.V., Maastricht, The Netherlands). BrainVoyager is a software for the advanced process and analysis of structural and functional MRI data. A recent development of the program allows the analysis of Diffusion Tensor Imaging (DTI) data and combined visualization with structural and functional MRI.

A very important feature, with respect to data analysis, is that there is a direct link between BrainVoyager and BESA. Through a procedure called coregistration, the MEG Head Coordinate system is matched to the individual MRI. This enables BESA to adjust all internally used coordinate systems to the individual brain, which will improve 3D maps, and the accuracy of source localization. Furthermore, source coordinates can be then

transmitted back from BESA to BrainVoyager to visualize dipole MEG models in the BrainVoyager space.

Integration between MEG and anatomical scans is not something new. Very famous softwares in the neuroscience field, like Spm, Fieldtrip, Brainstorm, are able to perform both, MEG and MRI analysis, and then to superimpose results obtained with both techniques.

The advantage with the integration BrainVoyager-Besa is the unification of two of the best programs, every one specialized in the respective field. Another advantage is that DTI and fMRI can also be analyzed in BrainVoyager, which is a remarkable feature. Superimposition of MEG source dipoles into these techniques is possible and their coregisteration with the anatomical data ensures coregistration with MEG.

Furthermore, moving data between different programs and different images formats is always critical and it is recommended to avoid it whenever possible. Since in BrainVoyager many different types of MR analysis can be done, the problem of transformation errors is minimized.

4.2.2 Anatomical MRI-preprocess, the Tailarach and the ACPC space

The Talairach space (Talairach and Tournoux 1998) is the most frequently used standard space for brain normalization. Spatial normalization reduces intersubject anatomical variability since in this space the location of brain structures is independent from individual differences in the size and overall shape of the brain. A brain can be transformed into this space by applying a Talairach transformation procedure. A Talairach transformation is controlled either by the specification of a few prominent landmarks or by an intensity-driven match of subject's brain to a template already located in Talairach space. BrainVoyager follows the first approach. It uses 9 anatomical landmarks defined in the specific brain to squeeze/stretch the brain into the Talairach space. This transformation works in two steps.

The first step is the so called AC-PC transformation. AC means anterior commissure and PC means posterior commissure are fiber tracts connecting the two hemispheres and relatively easy to see on most structural scans. In the Talairach system they are the brain landmarks, from these structures the system of reference is developed. In the AC-PC transformation a standard alignment of the brain to Talairach space is determined: the brain has to be set so that the anterior and posterior commissures are on a horizontal line. The AC point is located first, serving as origin of Talairach space. The brain is then rotated

around the new origin (AC) so that the PC appears in the same axial plan as the AC. The connection of AC and PC in the middle of the brain forms the y-axis of the Tailarach coordinate system. The x-axis runs from the left to the right hemisphere through AC. The z-axis runs from the inferior part of the brain to the superior part through AC. In order to further specify the x – and z- axis the y-z plane is rotated around the y (AC-PC) axis until it separates the left and right hemisphere (mid-sagittal plane). After these steps the brain is in the AC-PC space. Since it is a normal rigid body transformation , this space keeps the original size of the subject's brain intact while providing a common orientation for each brain.

For a full Talairach transformation, a cuboid is defined running parallel to the three axes enclosing precisely the cortex. This cuboid or bounding box requires specification of additional landmarks specifying the borders of the cerebrum and is then sub-divided by several subplanes into 12 sub-cuboids. In a final Talairach transformation step, each of the 12 subcuboids is expanded or shrunken linearly to match the size of the corresponding sub-cuboid of the standard Talairach brain. Talairach and Tournoux also defined the "proportional grid", to reference points within defined cuboids.

Talairach normalization ensures that the AC and PC obtain the same coordinates in each brain and that the subcuboids obtained by the AC PC points and the border of the cortex will have the same size. The important aspect of Talairach transformation is that correspondence is established across brains by linearly interpolating the space between important landmarks.

The technique of piecewise linear "warping" each brain into Talairach space is the same for every dataset, but of course the amount of variation applied to every brain is different, based on the difference in variation between of the specific brain and the Talairach brain. While Talairach transformation provides a recipe to normalize brains, regions, same coordinates in different individuals do not necessarily point to homologous brain areas. This holds especially true for cortical regions. For subcortical structures around the ACPC landmarks however the established correspondence is remarkably good.

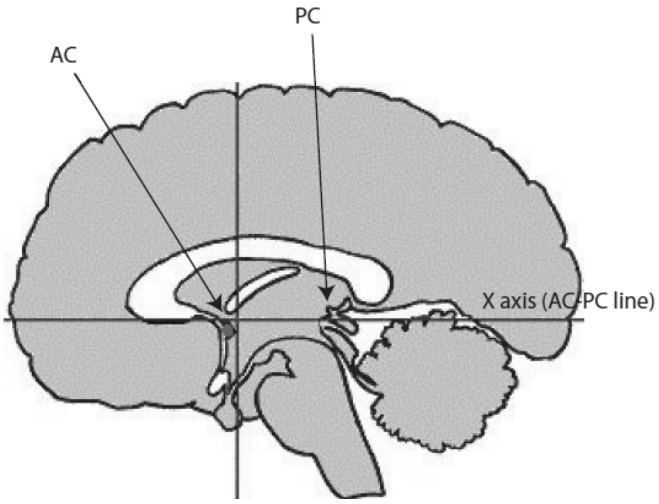

Figure 4.6:
Schematic of a sagittal brain view. The anterior and posterior commissures are shown.

4.3 Co-registration between MEG and MRI

The co-registration is achieved by importing in BrainVoyager the coordinates of the anatomical landmarks, the coils and the head shape, that we digitized before running MEG experiment and that define the head position with respect to the MEG device. Then the head-shape is matched with a surface reconstruction of the subject's head AC-PC aligned, and the necessary coordinate transformation between BESA and BrainVoyager is generated. This will enable BESA to adjust all internally used coordinate systems to the individual brain, which will improve 3D maps, and the accuracy of source localization. Furthermore, source coordinates can be then transmitted back from BESA to BrainVoyager to visualize dipole MEG models in the BrainVoyager space.

4.3.1 Coregistration procedure

Through this procedure, we will match the MEG Head Coordinate system (HC system) to the individual MRI. The HC system is a Cartesian coordinate system based on the three anatomical landmarks: the x-axis passes through left and right preauricular points (LPA, RPA), the y-axis passes through the nasion and is orthogonal to the x-axis and the z-axis is orthogonal to x and y. BESA's dipoles coordinates are natively expressed in spherical coordinates but can be expressed also in HC system or in the Tailarach system.

The coordinate of the digitized additional surface points, fiducial points (LPA, RPA, Nasion) and coils, expressed in the head coordinate system, are imported in BrainVoyager. Coregistration is performed in the surface module of BrainVoyager, with the surface

reconstruction of the subject's preprocessed individual anatomical MRI AC-PC aligned. Matching the MEG and MRI coordinate systems will define an affine transformation.

Fitting the points on the surface is a two step procedure. First, the location of the fiducial points (RPA, LPA, Nasion) are defined manually on the surface through visual inspection. The corresponding points on the MRI are visible since we put markers. BrainVoyager labels the defined points with a grey sphere (see Fig. 4.7) and automatically takes over the corresponding MRI coordinates for the nasion, the LPA and RPA to define its coordinates. When the three fiducial coordinates are defined, these points can be used to define a coordinate transformation MEG-MRI.

Fitting the head surface point cloud using the fiducials provides a first approximate alignment of the two coordinate systems. The fitting process can be improved by using all digitized head surface points and coils location. In this finer fitting several parameters can be set .

The "Optimize scales during fit" allow rescaling of x-, y-, and z-axes in order to account for small scaling inaccuracies that occur in many MR scanners. Furthermore, it is possible to assign a weight of respective reliability to the head surface points, fiducials and coils. It is also possible specify the distance in mm of all digitization points from the skin.

Playing with these parameters allows aligning the head surface points to the MRI as well as possible. As feedback the mean and maximum fitting error will be displayed.

Note that, even if we wouldn't have performed the head alignment among runs, the fitting process need to be performed only once for subject, since it establishes a transformation between the digitized points of the head and the MRI, while the position of the head with respect to the MEG device among the different runs is taken into account by the BESA program.

4.3.2 Coregistration issue

We put much effort in performing co-registration. Unfortunately the results were not as good as expected. In fact a consistent mismatch between the MRI data and the digitized points is observable in all the subjects.

If the fitting is performed mainly based on matching the three anatomical landmarks with the three markers, then the cloud of points from the skull doesn't fit the head (see Fig. 4.7) and match of coils-markers positioned on the coils (two in front and two behind the ear) also are bad. If vice-versa the coregistration is performed ignoring the fiducials and taking into account only the head points, then all the digitized points fit perfectly the surface but

the fiducials and coils are shifted toward down in the head-foot (H/F) direction with respect to the marker of at least 5 mm and more (see Fig.6). Interestingly, the shift was particularly evident since we put four additional marker on the coils position, which is a non-common praxis, that gave us a almost reliable feedback for the reliability of the three fiducials markers.

Since coregistration is a key point in the analysis I want to perform, much effort has been put in trying to solve this issue. This is subject of the next section.

4.3.3 Investigation of the Coregistration issue. Chemical shift hypothesis and phantom experiments

First of all, in order to verify our procedure, we tested the correctness of the Pholemus device, used for 3D-digitizing of fiducial points and the head surface, digitizing different points at known distance in different directions. Since the predefined locations and distances were perfectly reconstructed by the 3D digitization we can thus exclude that the digitization procedure is the cause of the problem.

In order to find the basis for the observed shift, we performed also several phantom experiments. In a first phantom experiment, several markers were applied on the surface of a oil-sphere. The markers and also additional points were digitized. Afterwards we took MRI of the sphere with the markers attached. Distortions were revealed. A distortion of 2-3% of the MRI image in Right-Left (R/L) and Anterior-Posterior (A/P) direction was observed, however this is normal and was not sufficient to explain the mismatch. The first phantom revealed also that all markers are shifted some millimeters downwards in the H/F direction.

A possible explanation given is the presence of a chemical shift artifact of the first kind on the position of the markers. Usually this artifact appears in the presence of fat and results in a shift in the spatial location of the fat voxels. Briefly, in the frequency-encode direction, the MRI scanner uses the frequency of the signal to indicate spatial position. Since water in organs and muscle resonate at a slightly different frequency than that of fat, voxels containing fat will not have the expected resonance frequency and will be spatially miss-registered, causing a shift in the spatial location in the frequency-encode direction. This frequency difference results from the different electron environments of the protons of water and fat, and is proportional to the magnetic field intensity. We supposed to have the same kind of artifact. Since the content of the markers and its composition is unknown and protected we can make only suppositions.

Several facts support this hypothesis. Firstly, the direction of the shift is only along the frequency-encode direction (the H/F direction) and the magnitude of the shift is different from the markers positioned "higher" (coils on the front) and "lower" (nasion, preauricular points). We have also some shift along the left-right axis for the preauricular fiducials, but this can be explained since the subject had to wear headphone inside the scan that probably "pressed" the markers and with the distortion of 2-3% in R/L direction.

We performed thus another phantom in the same way as described above. We collected two sets of data in the scanner, one with a frequency encoding direction as in the previous study and another one with inverted direction. Effectively the shift was reversed. An estimation of the shift was thus given as the half of the two shifts corresponding to the two opposite frequency encode directions: about 11 mm at level of the nose, about 5 mm at the level of the front.

Furthermore, the magnetic field of the MRI present at Cimec is particularly high (4T). Since chemical shift is proportional to the intensity of the field, this could be the reason why appositely thought markers, fail.

Moreover, when the coregistration is done only taking into account the points from the head surface, the source localization of S1 performed in BESA and then superimposed into the structural MRI of the subject, appears in the postcentral gyrus, the correct position, while using the coregistration that is based on the three anatomical fiducials, the functional localization of S1 is incorrect.

This chapter is however still open, further tests need to be done, maybe with different kinds of markers. Contacting the producer of the Markers, IZImed, did not give any satisfying answer. They declared that that they have not received any negative reports and that they have quality certificates for the same markers at magnetic field strengths of 0.5T, 1.5T, 3T and 7T in their database. Due to the carefully performed coregistration involving the possibility to verify the outcome with a lot of points from the skull and also four additional markers, it might be that this problem has not become a critical issue before. Moreover, since the chemical composition of the marker is unknown as the information is proprietary, we can make only suppositions about the behavior of these kind of markers in the MRI at Cimec.

The hypothesis, that the erroneous localization is the consequence of a chemical shift of the marker applied is very close at hand, but a final series of experiment is required.

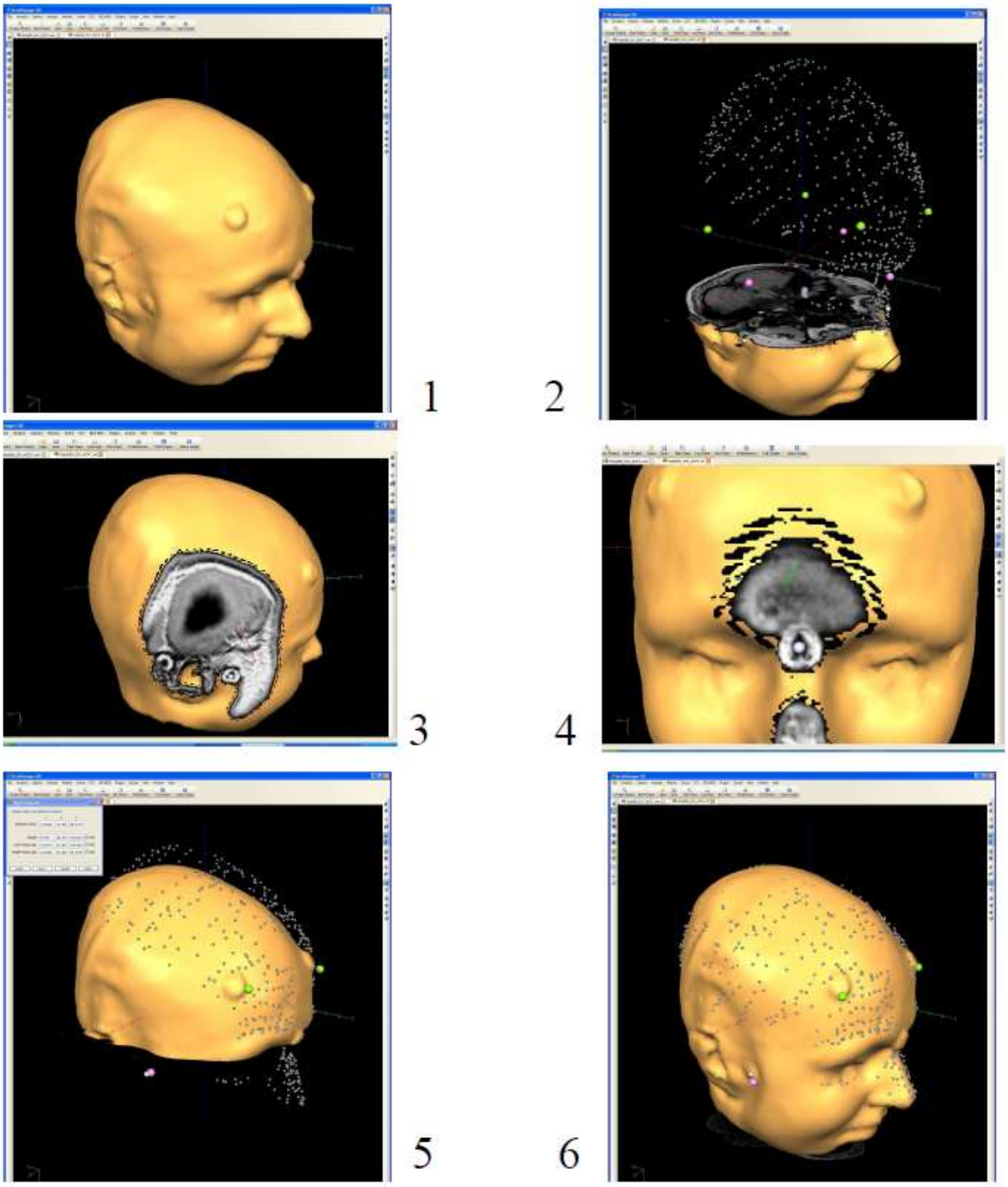

Figure 4.7: snapshots taken from the BrainVoyager surface module during coregistration procedure

1) Surface rendering of the ACPC transformed image. Markers are also visible.
2) The fiducials (pink), the coils (green) and the cloud of digitized head points are loaded into BrainVoyager.
3-4) The location of the fiducial points (RPA, LPA, Nasion) is defined manually through visual inspection. They are labeled with white sphere.
3) Assignment of the left preauricular point. The marker positioned at the place of the coils behind the left ear is also visible.
4) Assignment of the Nasion point
5) Fit based mainly on the three anatomical fiducials. The cloud of points from the skull and the coils don't fit.
6) Fit based on the digitized points from the skull: the digitized points correspond to the head shape, fiducials and coils are shifted toward " down" with respect to the marker of at least 5 mm.

4.4 Source analysis theory

In addition to the sub-millisecond temporal resolution that allows us to explore the timing of basic neural processes, MEG offers good spatial localization accuracy. Today, source analysis is usually an integral part of the analysis of MEG data. In the following sections the theoretical approach to the source localization by MEG is described. This has to be considered complementary to the forward problem depicted in chapter 1.

4.4.1 The inverse problem

The inverse problem in MEG refers to the problem of estimating the location and strengths of cerebral current sources that generate the measured distribution of the magnetic field.

It was shown by Helmholtz in 1853, that a current distribution inside a conductor G cannot be retrieved uniquely from knowledge of the electromagnetic field outside. There are primary current distributions that are either magnetically silent (B=0 outside G), electrically silent (E=0 outside G) or both. A simple example of magnetically silent source that produces an electric field is a radial dipole in a spherically symmetric conductor. An example of the opposite case is a current loop which is electrically silent but which produces a magnetic field. Moreover, because of the finite number of the sensors, the number of sources that can be localized is limited. Therefore, theoretically, an infinite number of source models would equivalently fit MEG observations, which reduces the predictive power on the system's behavior to null. A further problem lies in the fact that measured signals are always corrupted with noise. Small experimental errors can produce large inaccuracies in the solution: this problem is often referred to as an ill-conditioned problem.

In order to find the unknown current sources on the basis of noisy and incomplete measurements. A priori information is needed to constrain the space of feasible solutions. Constraints might be based for example on assumptions about the nature of the sources, e.g. number of sources, or on anatomical and neurophysiologic assumptions, e.g. defining the initial condition of the fitting in a defined area. It is evident that the accuracy and validity of the estimates depend at least to some extent also on the biological correctness of the assumptions and priors adopted in our models.

Two main types of inverse modeling approaches have been developed: the localization approach and the imaging approach. In the former method the observations are considered to be produced by the activity of a limited number of brain areas, whose locations can be estimated from the measured data. Each source in the global model accounts for the

activity of a brain region which is explicitly separated in space from other active regions in the model. Therefore, a corresponding number of dipoles are fitted to the measured data.
Imaging approaches have been developed more recently. This technique scans the brain for activity, that is, it computes the activity that a dipole would have that is successively placed at all possible locations.
The pertinence of either of these approaches is dictated by the neuroscience question investigated and the kind of data. In the case of this thesis the localization approach has been applied, the reasons of this choices will be explained later on.

4.4.2 Localization approach and least square dipole fitting

In the localization approach it is assumed that the measurements were generated by a small number of brain regions which are explicitly separated in space. Each source in the model accounts for a equivalent current dipole (ECD). Localizing a current dipole in the head implies that 6 unknown parameters have to be estimated from the data: 3 for location (the x, y, and z dipole position values), 2 for orientation (two angles are necessary to define dipole orientations in 3D space) and 1 for amplitude. Through algorithms, a data-fit cost function with dimension the number of parameters is minimized.
Theoretically, recent high-density systems with about 300 sensors would thus allow the unambiguous identification of 50 dipolar sources if it is assumed that the information recorded from the sensors in independent. However, it has been shown that estimating the 300 unknowns of a 50-dipole model from 300 observations would invariably result in overfitting any MEG data, i.e. the inverse model accounts for the noise components in the observations. Here, although a solution to the inverse problem exists and is unique, it is highly dependent on the noise components in the data and ends up violating the third condition of well-posedness, i.e. continuous dependency from the data. Trying to fit as many parameters as possible does not solve the ill-posed nature or the modeling problem in real, noisy conditions. It appears that MEG source localization are more stable considering inverse source models with far fewer dipole sources, typically less than five.
The number of dipole sources that is to be fitted to the averaged data is unknown and has to be estimated from the data. Increasing this number will lower the cost function because the recorded signals can be explained better. However, increasing the number too far, results in estimated dipole configurations that describe the noise in the data, rather than the evoked responses. Furthermore, the inverse solution becomes unstable when too many sources are fitted. Estimation of the number of dipole sources is an essential part of the

dipole localization problem. There is no standard way of determining this number. Estimates can be obtained by looking at the effective rank of the data using SVD or through information-theoretic criteria, but in practice experts often run several model orders and select results based on physiological plausibility. Caution is obviously required since a sufficiently large number of sources can be made to fit any data set, regardless of its quality.

Numerical approaches for the estimation of the unknown source parameters are generally based on the widely used least square (LS) technique, which attempts to find the set of parameter values that minimizes the square of the difference between the measured data and the magnetic field predicted from a fixed number of estimated sources using a forward model (see section 1.2).

For p dipoles we define the measure of fit in the least square (LS) sense as the square of the Frobenius norm:

$$J_{LS}(\{r_{qi},\Theta_i\},S) = \arg\min(\left\|M - A(r_{qi},\Theta_i)S^T\right\|^2)$$

where M is the averaged measured data matrix and A is the data matrix predicted by the forward model. The norm is the Frobenius norm that is defined for any matrix $A \in \Re^{n\times m}$ as

$$\left\|A\right\|_F = \sqrt{\sum_{i=1}^{n}\sum_{j=1}^{m}\left|a_{i,j}\right|^2}.$$

MEG signals are contaminated by nuisance components, e.g. environmental noise and physiological artifacts, which should not be explained by the model of brain activity. Therefore the forward model in presence of a nuisance term ε, may be presented as

$$M = A(\{r_{qi},\Theta_i\})S^T + \varepsilon.$$

Tuning the model parameters so that they perfectly fit the data would also result in explaining the remaining nuisance components, a general issue known as overfitting the observations. Therefore, signal pre-processing, like trial selection, averaging, filtering, etc. are necessary prior to any inverse modeling to reduce the contribution of nuisance to observations. The best-fit solution of the inverse problem is determined by minimizing the residual variance between the measured data and the forward calculated field:

$$J_{LS}(\{r_{qi},\Theta_i\},S) = \arg\min(\left\|M - A(r_{qi},\Theta_i)S^T\right\|^2) = \arg\min(\left\|\varepsilon_{LS}\right\|^2)$$

The fact that a dipole produces magnetic fields that depend linearly on current amplitudes S, while they depend non-linearly on source orientations and locations has been demonstrated by Baillet et al., 2001b [3] and is reflected in Eq.(8)-section 1.2 of this thesis.

It is because of this non-linearity that the inverse problem is generally treated by non-linear optimization methods, which can lead to solutions being trapped in local minima. Concretely, this will translate as a greater sensitivity of the search to its initial condition. In fact, non-linear searches that tend to be trapped in local minima of the LS cost, which are all the more numerous as the inverse model contains more elementary sources.

This least-squares model can either be applied to a single time sample or a block of time samples. When applied sequentially to a set of individual time slices, the result is called a "moving dipole" model, since the location is not constrained. Alternatively, by using the entire block of data in the least-squares fit, the dipole locations can be fixed over the entire interval. The fixed and moving dipole models have each proven useful and remain the most widely used approach to processing experimental and also clinical data in MEG/EEG.

4.5 Source analysis in the data

For each subject, source analysis was performed on the averaged runs of Left Motor condition and Right motor condition. Supra left and right conditions are not used in this thesis.

A single ECD was used to analyze the averaged data. This method allows the spatio-temporal modeling of neural sources assuming that one focal source generates the observed magnetic activity. It is widely used in studies handling with SEFs because for the early processing of somatosensory information the assumption is justified that there is only a single active source at a time.

The location, orientation, and moment of the dipole were calculated by an iterative least-square fit performed in the BESA source analysis module. The fit has been performed mainly on magnetometers, although also gradiometers have been used for comparison reasons.

Several digital filters were applied to the averaged evoked responses in order to find out how they affect the localization result.

4.5.1 S1 localization

The first step in this analysis of the sources is the localization of the source of the first component of the SEFs, the M20. I applied a loose initial condition: the dipole was positioned before perform the fitting in the correct hemisphere, i.e. the contralateral with respect to the stimuli side of the analyzed condition.

The earliest ” classical” component of the SEFs following median nerve stimuli are located in the somatosensory cortex, the posterior wall of the central sulcus. There is still disagreement about the specific regions involved, but the M20 component after median nerve stimulation is well considered to be generated in area 3b contralateral to the stimulated body part. This area owns favorable conditions of shallow depths and strong sources and according to several studies, its absolute localization of this single focal source is in the millimeter range. (Inui et al., 2004; Kakigi, 1994; Kawamura et al., 1996; Tecchio et al., 2000; Tiihonen et al., 1989).

For each subject the M20 component was individuated in time and the dipole fitted the data. A visual inspection of the correctness of the localization by coregistering the individual MRI of the subject was performed in order to verify the localization. Also the quality of coregistration was inferred by this comparison.

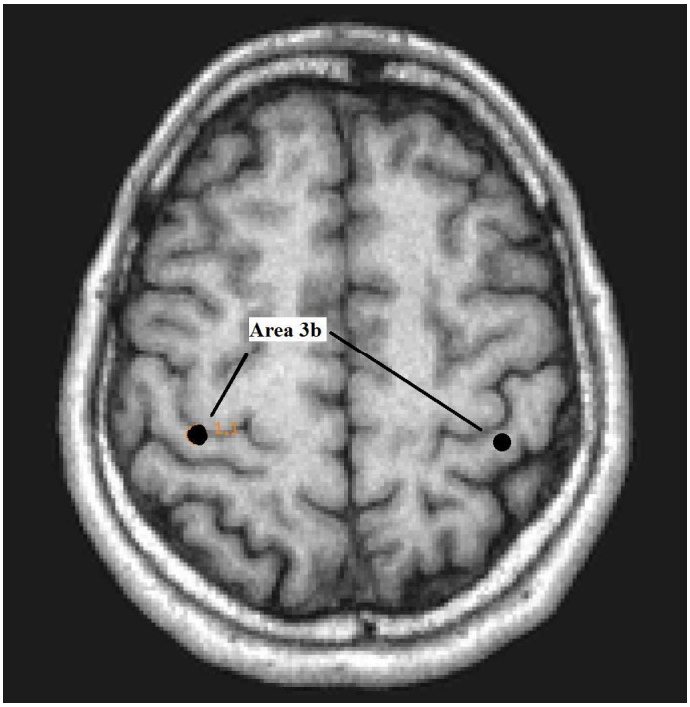

Figure 4.8:

Left and right area 3b

4.5.2 M15 localization

After localizing the M20, the dipole was fitted at every time point starting from about 5-6 ms before the M20 using the magnetometers signal. Using a sampling frequency of 5000 Hz the time step allowed is 0.2 ms. The dipole was fitted “going backward “in time, i.e. as initial condition of a dipole at a certain time point, the position of the dipole in the successive timepoint was taken (for example, as initial position of the dipole at the time point immediately before the M20, the M20 dipole position was used as initial condition,

and so on). The dipole localizations for the earliest time-points, the deepest ones, were however rather instable. i.e. very sensitive to the initial condition. The choice of this kind of initial condition is based on physiology. The maximum velocity conduction of a signal travelling along fibers reported in the literature is 100 m/s, that means that in 0.2 ms a length of at most 2 cm can be travelled. Let's assume that the signal doesn't "jump" from one location to the next within the head, but comes from somewhere in the vicinity of the previously or successively activated brain region. Thus, keeping the successive position as initial condition for the dipole fitting procedure, it won't compromise the reliability of the dipole localization.

The localization performed here, although not in all subjects, shows a dipole moving from the deep center of the head to the S1 in the 5-6 ms preceding M20. This is also reported in the recent scientific literature.

MEG is considered to be only sensitive to postsynaptic potentials in pyramidal neurons of the cerebral cortex that are lined-up mainly along tangential orientation. The common belief is that MEG is blind to deep and radial sources.

A theoretical simulation showed that the sensitivity profile of MEG does not exclude deep sources (Fagaly, 2006). Feasibility of recording SEFs from deep brain structures has been provided by Hashimoto et al. (1996), who recorded, in pigs, somatosensory evoked magnetic fields (SEFs) that were generated by neuronal populations at the level of the thalamus. This study indicates that, deep-lying structures in the brain can generate sufficiently strong MEG signals to be detected at a distance from the brain surface, at least in the pig head. Swine was chosen as a model for studying MEG signals from deep structures in the human brain because of a large size of the brain (about 6 cm long x 5 cm wide x 5 cm deep) with a well-developed convolution pattern of the cerebral cortex. The depth of a single equivalent current dipole representing a single focal region of active neuronal tissue was 21-28 mm below the exposed surface. Also other studies have been done using MEG on deep-lying areas for example Ioannides et al. (1995) [28], Tesche and Karhu (2000)[29].

The Elekta system is organized in 102 triplet of 2 orthogonal planar gradiometer and 1 magnetometer. Not all types of magnetic sensors have the same sensitivity to distant sources. In descending order of sensitivity to the depth of sources, magnetometers are most sensitive, followed by first-order axial gradiometers, second- order gradiometers and, finally, planar gradiometers. Magnetometers are more sensitive to deep sources but also to

noise. The “brain noise” in magnetic measurements is clearly stronger in the low- than high-frequency range consequently the relative signal-to-noise ratio in magnetometers is better for signals having high frequency components, like in our case.

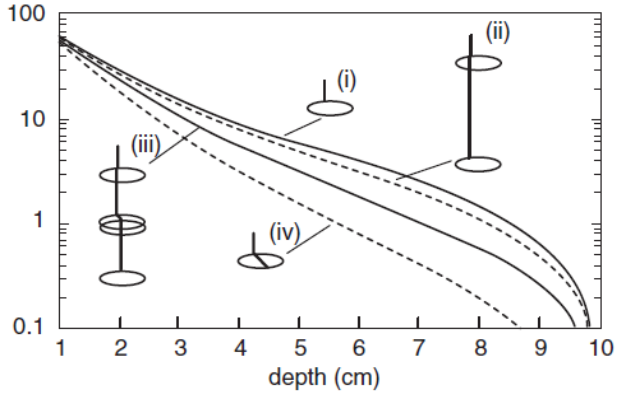

Figure 4.9, Adapted from *Magnetoencephalography in clinical neurophysiologic assessment of human cortical functions in Electroencephalography: basic principles, clinical applications, and related fields, Ernst Niedermeyer, F. H. Lopes de Silva, 2005:*

Dependence of signal strength (arbitrary units) on the depth of a current dipole when measured by different types of magnetic sensors: (i) magnetometer; (ii) first-order axial gradiometer; (iii) second order axial gradiometer; (iv) planar gradiometer.

4.6 Monte-Carlo simulation

Real, measured data exhibit a limited SNR, which is due to spontaneous background activity, environmental, and amplifier noise. The reconstructed dipoles represent the most probable source positions. Due to the noisy character of the input data there is a certain probability distribution around these positions, which corresponds to the noise level, i.e. the noise distribution of the data leads to scattered dipole positions in the source space around the most probable solution.

Monte-Carlo analysis is often used to examine the stability and accuracy of dipole solutions with respect to noise in the data (Medvick et al., 1989; Supek and Aine, 1993; Anderson et al., 1996). For Monte-Carlo analysis, noise is added to the data and the new data is then refitted with the original dipole solution. This is repeated many times with different noise realizations, resulting in a cluster formed by all solutions.

The noise level of the measured fields/potentials can be estimated by computing the standard deviation (SD) of signal pre-trigger or user defined latency ranges. By slightly moving each dipole from its best-fit position, the resulting field variation can be computed, compared to the noise level, and confidence ranges of the individual dipoles can be estimated.

In this thesis Monte-Carlo simulation was performed on the temporal window from the M15 to the M20 of each SEFs signal. The original SEFs data were exported from BESA to Matlab. Then, randomized noise with normal distribution and SD equal to the of the pre-stimulus baseline of the averaged SEFs, was calculated and added to the original signal. 100 of this new noisy signals were generated in Matlab then re-imported in BESA. Source analysis has been re-performed and for every time sample 100 solutions coordinate were obtained. Of these solutions, in Matlab, the volume of the ellipsoid containing the 90% of the points has been calculated trough a singular value decomposition (SVD). From the 90% confidence ellipsoid: volume, coordinates mean, coordinates standard deviation and coordinates depth, with respect to the best-fitted sphere used as head model for the fitting algorithm, were calculated. This analysis was performed only for the cases that presented a significant trajectory in the M15-M20 interval. It was conducted separately for gradiometer and magnetometers. The filter use is a low-pass band filter 250 Hz. The reason of this decision will be explained in the results section.

4.7 Diffusion MRI

In the cerebrum there is a histological distinction of two separate layers of brain tissue: the white matter, which contains long bundles of differentiated myelinated fibers running in parallel, and the gray matter, which contains a multitude of short fibers and neural cell bodies. Synapses abound in the grey substance connect different neurons and form networks on which information processing is based. In white matter there are no synapses and is the brain tissue through which messages pass between different areas of gray matter within the nervous system.

Conventional MRI cannot reveal detailed anatomy of the white matter since the contrast in the MRI-images reflects differences in chemical composition which is quite homogenous. Diffusion MRI is a recent technique able to reveal white matter inhomogenities, offering thus a unique insight into the structural organization of the brain white matter.

4.7.1 Principles of diffusion MRI: DWI and DTI

Diffusion MRI uses an excitation sequence for nuclear spins that is sensitive to the molecular diffusion of water, i.e. the molecular motions by thermal energy, the so called Brownian motion.

In pure water, diffusion is characterized as isotropic, meaning that its magnitude is equal in all directions. When a tissue, such the white matter, has an internal fibrous structure, the

diffusion becomes restricted and shows a more or less distinct anisotropy, meaning that the diffusion magnitude depends on the direction. Water will then diffuse more rapidly in the direction aligned with the internal structure, and more slowly as it moves perpendicular to the preferred direction. Diffusion in the direction of fibers is about three to six time larger than the one in the perpendicular direction.

Anisotropy effect can be exploited to map the orientation in space of the white matter tracks in the brain assuming that the direction of the fastest diffusion would indicate the overall orientation of the fibers. In diffusion MRI the obtained signal intensity depends on the degree of water diffusion. The mechanisms able to detect the water molecules positions, and therefore their diffusion, comes from dephasing phenomena accumulated by spins that move randomly with the presence of an applied magnetic field gradient. The diffusion weighting in an MR image reflects the random motion along the direction of the applied gradient. White matter tracks running in parallel to the applied gradient have their signal suppressed, while those running perpendicular will appear brighter in the image. Determination of diffusion directionality can bring important information about tissue structures.

The so called diffusion weighted MRI (DWI) consider a coefficient called Apparent Diffusion Coefficient (ADC) that is a mean average of the diffusion values within a voxel. Diffusion is detected only along the applied gradient axis, thus by combining X,Y and Z gradients, the ADC along any orientation can be measured and is expressed through contrast or colors of pixels.

The question is how to fully characterize the anisotropic diffusion and subsequently the fiber architecture. If the diffusion is isotropic the probability of finding a water molecule after a certain amount of time becomes spherical. If the diffusion is anisotropic we can assume that the diffusion process leads to an elliptical shape of the probability, with the longest axis aligned to the orientation fibers. This is the so-called diffusion ellipsoid whose shape and orientation represents the anisotropy in an effective way. In order to fully characterize the diffusion ellipsoid 6 parameters are needed: three numbers for the length of the axis and three vectors to define the orientations of the axis. This information can be obtained by measuring the ADC along a number of orientation (at least 6). To obtain the parameters a mathematical aide is necessary: a tensor D is used, that is a 3x3 matrix represented by 6 independent elements, which fully describe how molecular mobility in space varies along each direction and the correlation between these directions. It is the so

called diffusion tensor and the visualization of the diffusion tensors is referred to as diffusion tensor imaging (DTI).

Size, shape or orientation of the diffusion ellipsoids are the basic parameters which can be used to visualize 2D maps.

The most common measure quantifying anisotropy is the “Fractional Anisotropy” (FA). FA indicated how elongated the diffusion ellipsoid is by comparing the values of the three eigenvalues of the diagonalized tensor (length of the axis), without using its relative eigenvectors (directions). It has a range between 0-1. In this way an anisotropy map can be formed and it is called FA map. The eigenvectors and eigenvalue information can be incorporated to create color maps. The useful information is provided by the x, y and z components of the eigenvector with the largest eigenvalue. In the color map, three orthogonal axes are assigned to three principal colors (red, green, blue) and diffusion along intermediate directions can be visualized by appropriately mixing the three basic colors.

4.7.2 Principle of tractography

2D based color map can reveal only a cross section of white matter tracts, which often has convoluted structures in 3D space and is difficult to appreciate their 3D trajectories from the slice by slice inspection. Computer-aided 3D tracking technique can be very useful to understand the tract trajectories and their relationships with other white matter tracts or gray matter structures.

There are several types of tract reconstruction techniques. The most common is based on “line propagation” and is called deterministic approach since it provides only one solution (trajectory) from a given voxel and there is no a priori knowledge about the destination of the propagation. The tracking algorithm implemented in BrainVoyager belong to this class. A detailed description of this technique is beyond the scope of this thesis, some basic concepts of the deterministic approach are exposed in order to have a general overview and to allow the necessary understanding of the intrinsic limitations of this technique.

The starting point for tracking algorithm is usually defined manually on each subject’s FA map or directly on the anatomy and “seed points” from which the tractography procedure can commence. The tracking algorithm then “propagates” the line and several criteria of propagation exist. One of the most common criteria is following the direction of maximum FA from each seed point until FA falls below a set threshold (because the gray matter has a FA of 0.05-0.15, it is common to use FA>0.15-0.3 as FA threshold). Another criterion is the angle of transition from one voxel to a successive one. The angle can’t be too sharp.

Using this criteria tractography can allow for the reconstruction of all major white matter tracts of the brain.

4.7.3 Tractography limitations and validation

Although the 3D tract has a clear potential, it has also relevant limitations that need to be kept in mind when applying this technique.

A limitation comes from measurement errors, mostly related to motion of the patient which is correlated with scanning time.

Another major limitation refers to the acquisition of DTI and stems from the limited spatial resolution, which is usually in the order of 1-5 mm. The resolution is far larger than individual axons and unless axons form a large bundle with uniform fiber orientation, the voxel-by-voxel information is inevitably “averaged” information of the fiber orientations. This leads to the conclusion that as long as many axons enter into and exit from a voxel, it is impossible to obtain a single axonal path and thus cellular level connectivity. Furthermore, the tensor calculation assumes a uniform water diffusion property inside a voxel and thus a uniform tract organization, which may not be true. Voxels that fall between two unrelated fibers will have a fiber angle that is the population-weighted average of the two fibers angles (Partial volume effects). Moreover, because the tensor model cannot appropriately represent voxels with inhomogeneous populations, all tracking techniques based on the tensor model may fail in brain regions with significant fiber crossing. In this case there are two possible outcomes. One is false negative, in which tracking terminates in such regions since fiber crossing regions tend to have low anisotropy and random fiber orientation. The other outcome is false positive. This can be further divided into two classes: bias, in which tracking is shifted from the real path in a reproducible manner when it penetrates the problematic regions; and switching, in which tracking switches from a track of interest to an unrelated crossing tract.

Thus, validation is one of the most important questions in DTI, i.e. the question if the reconstructed tract is true. There are multiple validation issues: validation of data acquisition, of tensor calculation and of 3D reconstruction algorithm. Although these issues can be validated, the “biological“ validation, i.e. whether two locations are really connected by axons, remains an unsolved problem. The uncertainty about if a fiber tract has been reconstructed correctly, is partly due to the low resolution of the technique already described above. In addition the errors depend strongly on the brain area under investigation. E.g. if the coritcospinal tract in the medulla is reconstructed, at lower pons

level the result is accurate and precise and the tracking results are reproducible and agree well with the anatomical description. In contrast, if the corticospinal tract of the upper pons-cortex regions is reconstructed, the result is difficult to validate. In this region, every dedicated corticospinal tract run parallel with many other corticoefferent fibers and its location is debated even among neuroanatomists. Therefore, there are no general means of validating the tracking results. However, with an appropriate protocol we can reliably reconstruct the trajectory.

4.7.4 Process of DTI data

The analysis of DTI in the present thesis has been performed in BrainVoyager. In this section a brief description of the main steps and choices of the pre-process of DTI data is given.

For every subject the raw diffusion data are assembled in a new BrainVoyager project and the essential information is related to them, in particular the used gradient directions and relative b-values describing for each scanned volume the measured direction of diffusion.

The weighted images are then explored visually in order to detect and in case to discard eventual artifacts. Estimation of tensors is possible already in this space. Since we want to perform fiber tracking we will need to transform the data into 3D space and thus it is advisable to align the DWI data with a 3D scan of the subject, before calculating the tensor. It is possible to perform the coregistration between anatomical MRI with the DTI data directly with an anatomical already preprocessed AC/PC or TAL. In previous section we coregistered MEG data to the ACPC preprocessed anatomical data. In order to ensure coregistration of the DTI data also with MEG data, I coregistered the DTI data with the same anatomical ACPC-pre-processed used for MEG coregistration. Coregistration has been performed with the automatic alignment provided by BrainVoyager and then visually inspected and eventually manually adjusted. To transform the 2D DWI data into a 3D space a “sinc-interpolation” has been used.

Estimation of the diffusion tensors is then performed. Before I create a mask of the brain, in order to reduce computational burden and to allow a more clear visualization of the color coded map. For each voxel, the tensor estimation process results in three eigenvectors and associated eigenvalues and the calculated tensor information is saved into a file for later reuse. Diffusion tensor estimated at each voxel is the basis for calculation of useful maps as well as for fiber tracking.

4.7.5 Prior anatomical knowledge for tracking

Since tracking is strict related to brain regions, firstly a brief overview of the anatomical features of the target fibers is given.

A corticospinal tract is a collection of axons that travel between the cerebral cortex of the brain and the spinal cord. The corticospinal tract of the sensory pathway originates in the spinal cord. It transmits information to the ventral posterolateral nucleus (VPL) part of thalamus about pain, temperature, itch and crud touch. The thalamocortical sensory pathway proceeds from the VPL part of the thalamus to the somatosensory cortex S1. In this study the interest is in this thalamo-cortical tract.

The somatosensory fibers are very close to the motor pathway, since primary motor cortex lies just anterior to somatosensory cortex. The motor pathway originates from the spinal cord, passes to the medulla and the pons and to the midbrain and finally to the motor cortex.

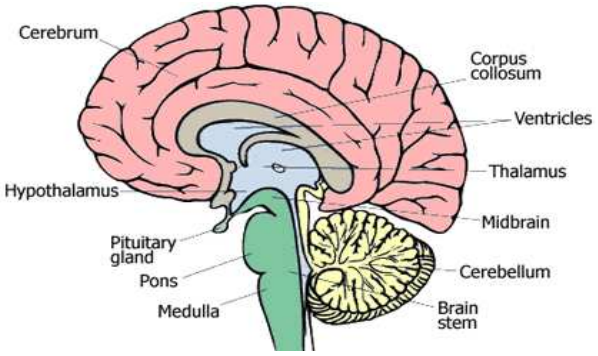

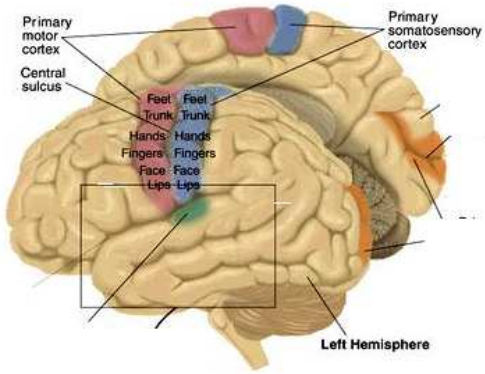

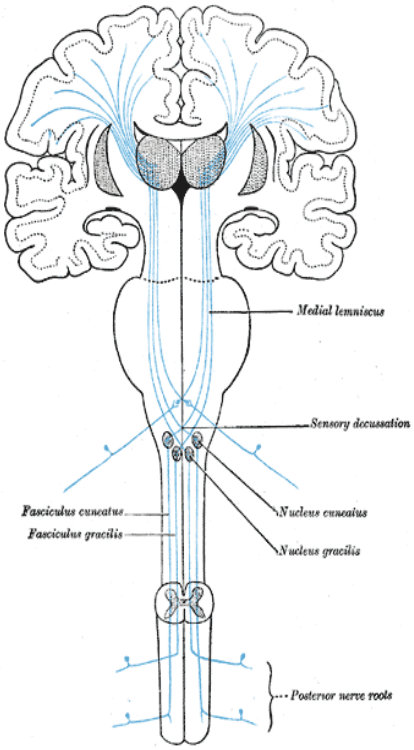

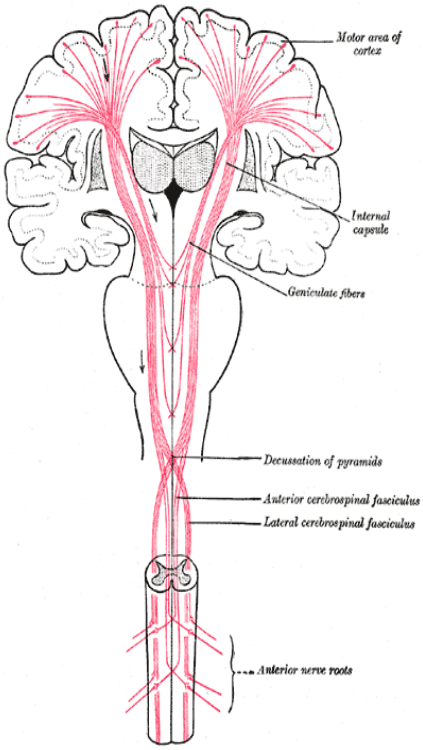

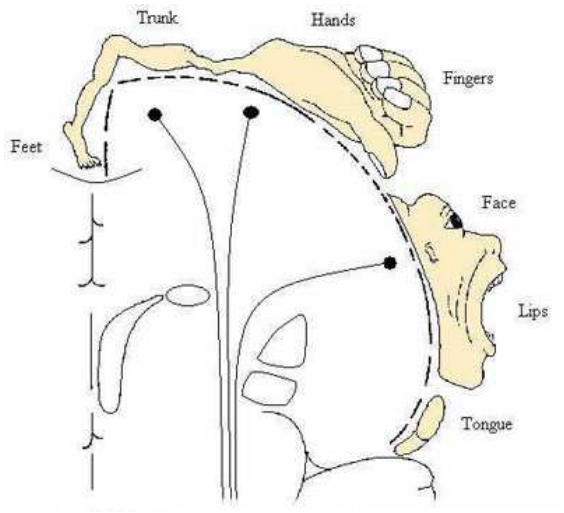

Figure 4.10
Above left: Major internal parts of the human brain.

Above right: Motor cortex, somatosensory cortex, central sulcus.

Central left: Schematic of the somatosensory pathway.

Central right: Schematic of the motor pathway.

Side: Schematic of fibers split in correspondence of the homunculus.

4.7.6 Thalamo-cortical somatosensory fiber tracking

Tracking is performed in BrainVoyager, that uses a deterministic algorithm. The DTI data are visualized superimposed to the previously coregistered anatomical scan of the subject. As already mentioned above, validation of the tracking in the upper pons-cortex regions is challenging because many different tracts are intermingled in this region. BrainVoyager allows an iterative real-time tracking, which I used to "play" with the data. However, for reproducibility reasons, a strict protocol for the final tracking was followed, based on a two-region approach. This protocol comes from the paper "Somatotopic Organization of Thalamocortical Projection Fibers as Assessed with MR Tractography" [22], a study that evaluated the course of sensory and motor thalamocortical projections based on tractography. According to [22], motor tracts rotate anteriorly as they travel through the centrum semiovale, and sensory tracts rotate posteriorly as they course through the centrum semiovale toward the cortex.

In the present thesis also both, motor and sensory fibers were tracked. The sensory and motor tracts can be viewed as a single entity since they run in parallel, apart from the regions in the vicinity of the cortex. Therefore it is useful to track them both in a first step in order not to mix them, and to assign them to either the motor or the sensory tract in a second step. Moreover, somatosensory and motor tract being in accordance with the described trajectory in [22]can be used to validate the results.

The starting point for the tracking is defined manually from each subject's FA or direction-coded map or directly from the anatomy. In this thesis the regions of interest (ROIs) were defined on the basis of the anatomical scans of the subjects superimposed with the direction-coded vector map. The visualization of the direction coded maps superimposed to the anatomical scans facilitated the identification of the different white matter regions as presented in the DTI and is useful to overcome small miss-location errors of the DTI due to errors in coregistration.

One of the most effective ways of dealing with errors by noise, partial volume effect and crossing fibers is tracking based on a priori anatomical knowledge in combination with a two-region approach. The two-region approach reconstructs only fiber bundles that pass through both regions at the same time thus minimizing the risk of obtaining false positives.

For the sensory tract, a ROI was placed at the dorsal pons. Pons is a structure located on the brain stem just below the thalamus and is chosen as ROI since is very easy to identify in anatomical scan due to its typical heart shape. The second ROI for the sensory tract was placed on the whole somatosensory sensory cortex. The sensory cortex is clear to identify

on the basis of morphologic features, as it lies just posterior to the central sulcus. The reasons why the whole somatosensory cortex has been chosen and not only the area corresponding to the hand is that the different fiber corresponding to the homunculus run parallel from the thalamus. They separate later, in the centrum semiovale. From these points the somatosensory fibers relative to the hand move towards the external part of the brain, for reaching their specific location in the somatosensory cortex according to the homunculus. These are difficult to track due to crossing of fibers, while the more internal fibers belonging to somatosensory cortex but relatives to other part of the body are not that affected by fiber crossing. Choosing only the S1 area of the hand thus wouldn't give good results.

When tracking the motor tract, two ROIs were defined, one covering the dorsal ventral pons and a another one covering the motor cortex. The motor cortex was identified on the basis of its clear morphologic features, as it lies just anterior to the central sulcus.

A fractional anisotropy value of 0.3 and an maximum rotational angle of 45º were chosen as stop criteria.

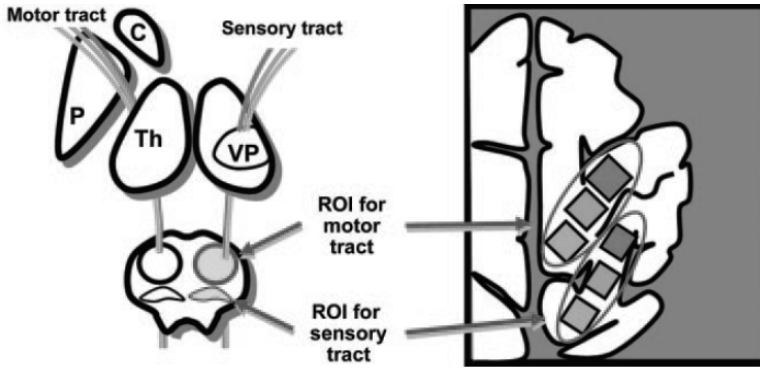

Figure 4.11:
Schematic illustrations of ROI settings for sensory and motor tractography.
The three regions in the cortical ROI represent the upper extremity region (the most external), the trunk region (the middle), the lower extremity region (the internal).
Where: Th=thalamus; VP=ventroposterior part of the thalamus; P=putamen; C=caudate nucleus.

Chapter 5

5.1 Results from MEG data pre-processing

5.2 Results from MRI pre-processing and coregistration

5.3 results from source analysis

5.4 Results from Monte-Carlo simulation

5.5 Results of tractography

5.6 Superimposition of the tracked fibers with Monte-Carlo simulation

Results from MEG data pre-process

In table 5.1, 5.2 the results of MEG pre-processing are shown. The number of averaged trials depend on the number of discarded trials during the artifact rejection. The original number of trials per condition was 3000 trials per subject. Some subjects have more than 3000 trials since we collected one additional run (200trials per condition). This was the case when we saw a quite noisy signal and the subject was still willing to collaborate.

In figure 5.2 a typical SEF obtained from the average of the selected trials is shown.

Table 5.1: Left Motor

Subject	n. trials	N20 [ms]	x [mm] (Tail)	y [mm] (Tail)	z [mm] (Tail)
1	2931	18	47.2	-23.7	37.6
2*	3172	20	49.2	-23.4	42.6
3	3106	19.2	46.9	-18.1	51
4	2862	19.4	46.2	-23.2	43.9
5	3066	18.8	37.4	-14.5	47.5
6	2364	18.2	49	-19.2	37
7	3104	19.6	38.8	-24.9	39.7
8	2948	17.8	35.5	-16.4	54.3
9*	2923	20.2	42.8	-22.6	45.6
10	2512	20.2	44.7	-18	43.8
11	2865	19.6	39.5	-15.2	44.8
12*	2915	20	46.1	-25.3	47.1
13*	2616	18.8	34.9	-29.7	38.6
Average	2875	19.2	42.9	-21.1	44.1
SD		0.8	5.1	4.5	5.2

Table 5.2: Right Motor

Subject	n. trials	N20 [ms]	x [ms] (Tail)	y [ms] (Tail)	z [ms] (Tail)
1*	2936	17.8	-43.7	-21.1	36.8
2*	3188	19.6	-45	-23.5	41.9
3	3098	19.2	-45.6	-20.9	48.3
4	2882	19.6	-41.7	-25.4	38.2
5	3081	18.8	-39.1	-19.1	49
6*	2426	18.6	-47.7	-27	42.8
7*	3113	20	-40.6	-19.1	43.2
8	2952	18.2	-42.4	-18.3	45.8

9	2916	20.2	-43.1	-26.1	42.6
10*	2518	20.4	-48.6	-22.3	45.7
11*	2865	20.2	-45.8	-18.8	36.6
12	2912	19.6	-44.3	-29.5	45.7
13	2634	18.8	-43.2	-24.8	36.9
Average	2659	19.3	-43.9	-22.8	42.6
SD		0.8	2.7	3.6	4.3

Table 5.1-5.2: for every subject the number of averaged trials for left and right condition are showed. Thirds column shows the time point of the M20 component and the following columns show the coordinates of the dipole localized from the averaged data at the M20 in Tailarach coordinates for the magneotmetrs. In the last two rows average and standard deviation (SD) among subjects of the coordinates are shown.
*represent the cases where significant movement of the dipole was detected

5.2 Results from MRI-preprocessing and coregistration

All the subjects underwent the MRI session, except one subject who is therefore not presented in this thesis. The subject was excluded from the MRI scan because of metallic pieces in the mouth. It is however noteworthy that the results of this subject in terms of dipole analysis showed a clear shift of dipole location from the thalamus to primary somatosensory cortex .

For all the presented subjects ACPC and Tailarach transformation of the anatomical scan were performed. After reconstructing a mesh modeling the head in ACPC space, coregistration with the headshape obtained from 3d digitizationwas performed by using the fitting algorithm provided in BrainVoyager. The markers we put were not taken into account (for more details see section 4.3). The goodness of the coregistration was then judged by goodness of the S1 localization and the symmetry showed by the left and right S1.

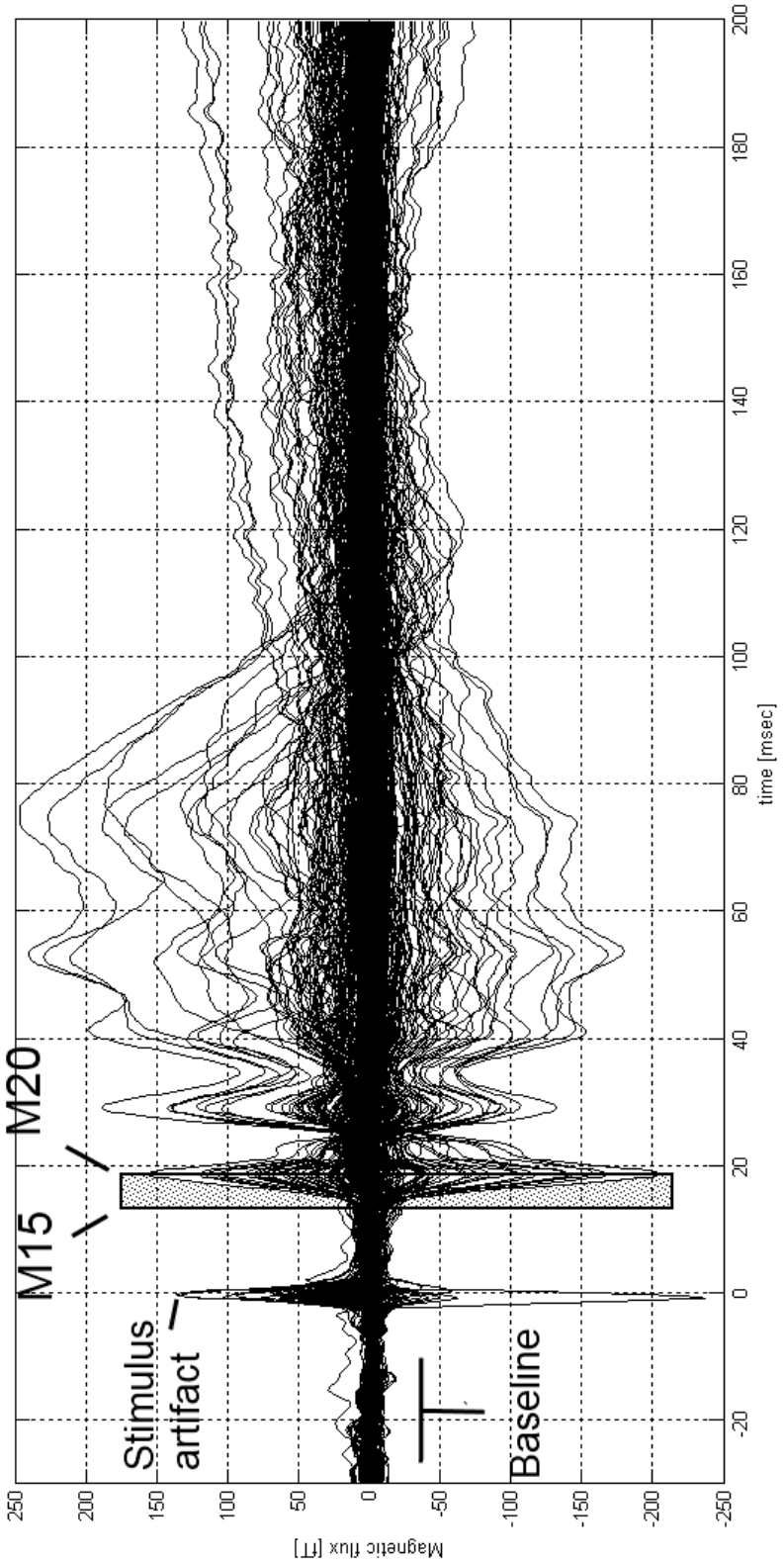

Figure 5.2: Example of a somatosensory evoked field (SEF) obtained from the average among trials of one condition.

5.3 Results from source analysis

- M20 component localization

The third column of table 5.1 and 5.2 shows the time of the M20 component. The components reveal substantial temporal inter-subjects variability, particularly for the recording of SEF at median nerve since it depends on the length of peripheral nerves and this changes with body heigth.

A dipole was fitted to the topography of the M20 component. The obtained sources coordinates are shown in Table 5.1 and 5.2 in Tailarach coordinates. The correspondence of the Tailarach with functional and neuroanatomical brain regions can be easily verified in the on-line Tailrach atlas (www.tialrach .org). All the coordinates showen in Table 5.2 and 5.2 are well located in or close to primary somatosensory cortex according to Tailarach atlas. A part for subject 8 whose signal was very noisy and S1 localization failed. The noise seemed to be related mainly to the subject and less strongly to technical noise. Accordingly the signal needs to be cleaned with more sophisticated artifact rejections techniques. Since the somatosensory cortex is well recognizable in anatomical scans, these results are also in accordance with visual inspection of the localization.

- *M15-M20 source localization*

Source localization was performed for data points starting from the M20 peak backwards investigating the dipole localization for the 6 ms preceding the M20. For the dipole fit, a priori information on the number of the sources taken from the literature was used. In the literature a single dipole has been suggested to be appropriate to describe the M20 response, i.e. a single source can be regarded as sufficient. Additionally, the initial location of the dipole fitting approach is crucial. Going forward in time the outcome of a previous source location step will serve as starting point for the localization of the topography of the next sample. Since the fitting was performed going back in-time, source localization results for a later time point served as starting point for the analysis of a previous step.

Among the 24 total SEFs obtained from the preprocessing part, for 10 of them the fitted dipole moved from the center of the head toward S1, i.e. a clear pattern and ordinate movement is recognizable. An example is showed in figure 5.3. It is assumed that in subjects showing no shift of dipole sources the thalamic activity was too low to be detected or the dipole orientation was unfavorable to create any significant contribution.

From now on the results reported are referred to these 10 “positive” cases.

As reported in the literature, SEF stimulation does not only elicit evoked responses, but also causes oscillatory activity in various frequency that might go up to 700 Hz. I thus studied the source localization for different frequency bands. Up to this point all the registered frequencies of the raw data have been conserved, i.e. 0.1-1000Hz. Since there is no clear information about the role of the frequency on source localization, source analysis was performed in different frequency bands

Indeed, the trajectories of the moving dipoles modeling the brain activity related to the M15 and the M20 componente in the same subject were different for different filter setting. However, no clear pattern which related frequencies- trajectories among subjects could be established.

In general I could identify the following rules:

- by cutting the signal with a low-pass filter 700 Hz, the trajectory doesn't change with respect to unfiltered signal 0.1-1000Hz.
- by applying a high-pass filter around 70-Hz/100 Hz the moving was severely diminished or disappears.
- by taking only the frequencies above 70/100 Hz the moving was severely diminished or disappears. By including piecewise higher frequencies the dipoles start to "move".
- the most regular and well-defined movement was presented for low-band filter around 300-250 Hz. This was shown also in accordance with the DTI tracked fibers.

5.4 Results from Monte-Carlo simulation

The Monte-Carlo simulations where used to infer the confidence volumes of dipole source localizations and to compare their extent with the geometry of the fiber tracts obtained by DTI.

For two cases Monte-Carlo analysis was performed in three different frequency bands: 0-250 Hz, 250-450 Hz, 450-750Hz. The volumes of the 90% confidence ellipsoids were smaller for the first lower band with respect to the second. In the third band the trajectory were almost without significance. On the basis of these findings, deeper analysis was conducted in 5 cases in the band range between 0-250Hz. Given the time needed to do the analysis of the confidence volumes, I've chosen only the five most representative cases.

In all the subjects analyzed the trajectory followed by the confidence ellipsoids correspondent to the different time points, is the same followed by the original dipoles.

The volumes of these ellipsoids are in accordance with what is expected from MEG theory, i.e. the volumes of the confidence ellipsoids grows non linearly with the depth of the

dipole source. The 2-3 ms preceding the M20 localization, the sources are very close to the area S1, i.e. superficial, and the volume of the confidence ellipsoid is very small. For what regards the deepest and earliest sources localized, the volumes grow with the deep of the sources. The relationship deep of the sources /volume is non linear. The depth was calculated as the radial distance of the mean coordinates of the ellipsoids from the sphere used as geometry of the head. The size of the volumes also at depth levels are meaningful, i.e. they depict a defined area.

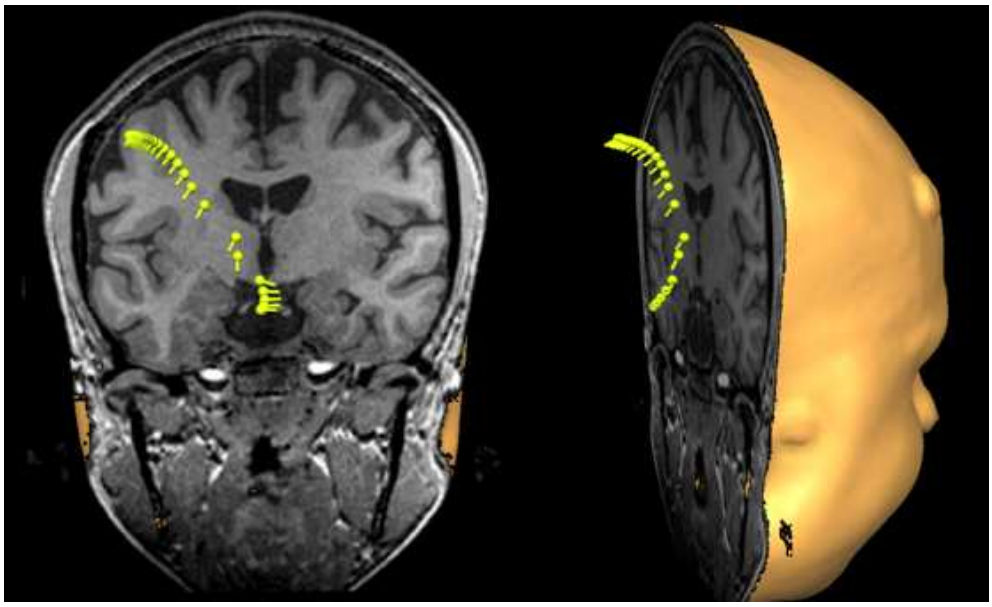

Figure 5.3
Example of dipoles moving trajectory

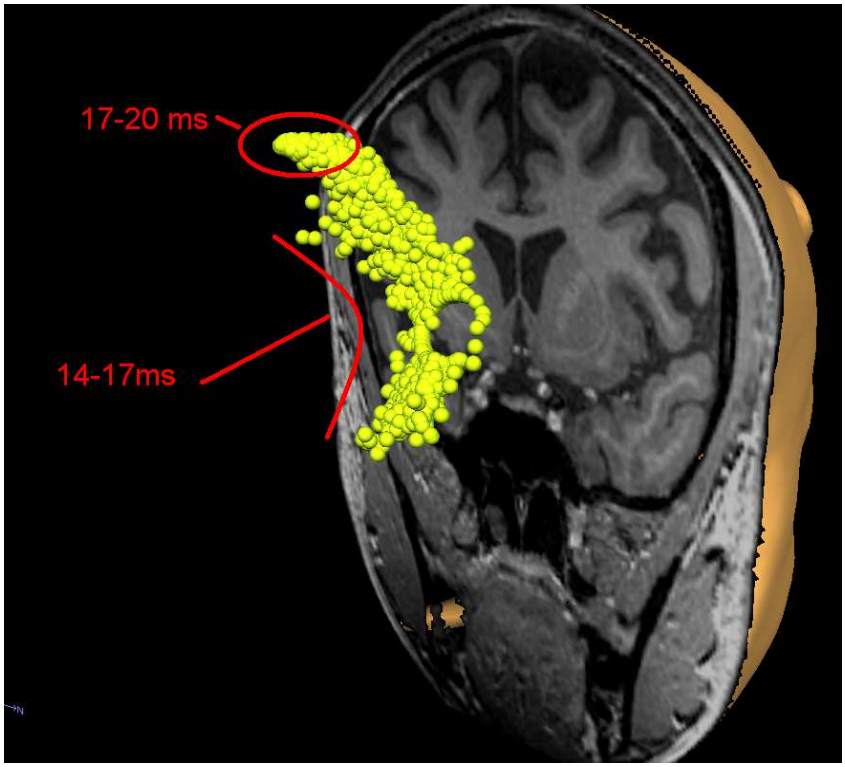

Figure 5.4:
Example of results obtained with Monte-Carlo results. The data original data are represented in Fig. 5.3

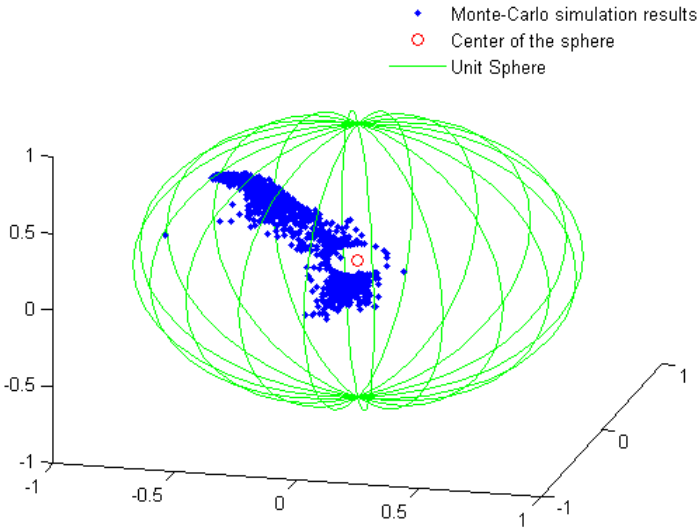

Figure 5.5:
The clouds of the dipoles as generated by Monte-Carlo simulation in Matlab space. The unit sphere is the sphere model used as approximation of the head by the fitting algorithm. Around the center of the sphere for radiality of the sources, dipole can't be fitted. Note that the points showed here are the same showed infigure 5.4-5.3 superimpsoed on subject's MRI.

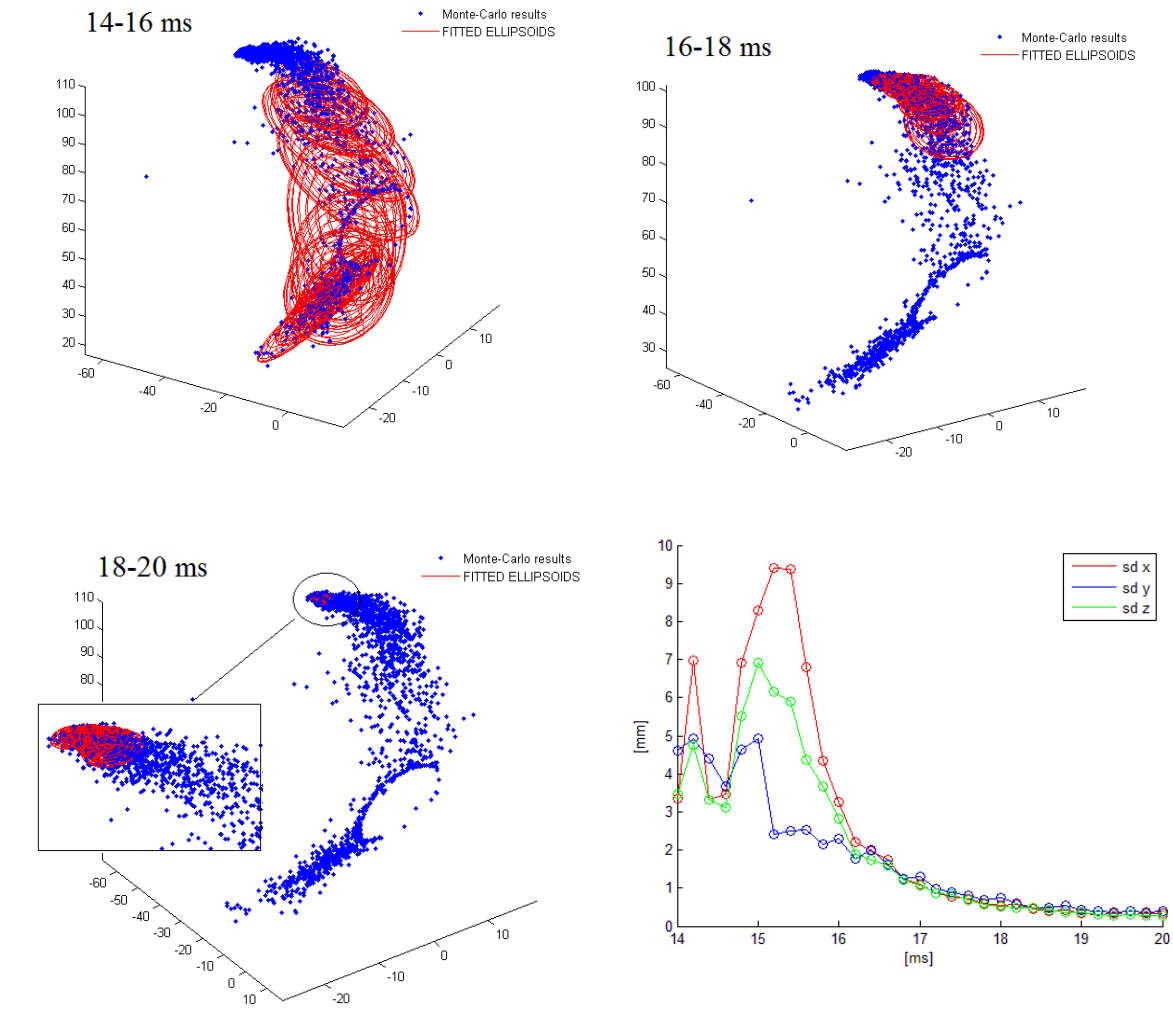

Figure 5.6: The cloud of points generated for every time point is fitted through SVD to a 90% confidence ellipsoid. The results are shown in the MATLAB space for different time intervals. In the last schematic the standard deviation of the volumes is shown and reflect the growth of the volumes with the depth of the sources. Note the peak of SD in correspondence to the time points where the dipole are close to the center of the sphere.

5.5 Results of tractography

For subjects showing a movement in dipole position between the source configuration for M15 and M20, fiber tracking was performed. However, tracing of the thalamo-cortical fiber has been not so easy as depicted in paper [12]. Biological validation of the fibers it is a crucial issue that has not fully been solved. As explained in section 4.7, a two-regions approach was used and motor and sensory fiber has been tracked.

For exposition reasons we can divide the fiber in three significant part as shown in Fig 5.6.

The first section of the fiber is relative to tracking in the deepest part of this analysis. In this case, the fibers start from the pons and are easy to track due to the low fiber crossing and the good alignment of the fibers which essentially go upwards in parallel. However at that point, motor and somatosensory fiber are difficult to distinguish since they run as a unit.

The second part is the fiber at central at level of the centrum semiovale. Fibers start to separate, here according to [] somatosensory fibers rotate posteriorly while motor fibers rotate anteriorly. In this part fibers still travel parallel and tracking is straightforward. However reproducibility and biological validation is critical since a lot of fibers travel through this area and it is difficult to distinguish them. By playing with iteractive tracking it's possible to track almost everywhere in this area and also a small changing in the ROI definitions change the path of the fibers in this area. Thus, it is not so easy to validate the results.

The third part of the tract is at the level of the cortex where the repartition is "internal" to the fiber, i.e. the somatosensory fibers spread for reaching the sensory homunculus and the same happens to motor fibers. This area is thus difficult to track, due to the present of many different small fibers which travels in different directions. The somatosensory area related to the hand is placed external to the somatosensory area and could not be traced.. For the motor cortex this limit was evident but however the tracing in the part immediately below the cortex is confused. The results obtained are thus only approximated.

5.6 Superimposition of the tracked fibers with Monte-Carlo simulation

The results of the Monte-Carlo simulation were superimposed to the fibers.

The superimposition had sufficiently good results only for the central part of the fiber. In the upper part, close to the primary cortex area, starting from the S1, the trajectory followed by the dipoles doesn't follow the expected pattern but moves anterior, in the direction of motor cortex. Since in this area is difficult to track, is not to discard the

eventuality the indeed fibers belonging to the hand area follow the pattern depicted by the dipoles.

For what regard the central part, a superimposition of fiber-dipoles has been found. Not in all subjects, but even if there was no superimposition of the two certain similarity in the two pattern is encountered.

For what regard the third lowest region, no superimposition was found. We can assume that MEG limitations in localizing deep and radial sources plays a predominant role since these region is very depth and central in the sphere to which the subjects head has been approximated.

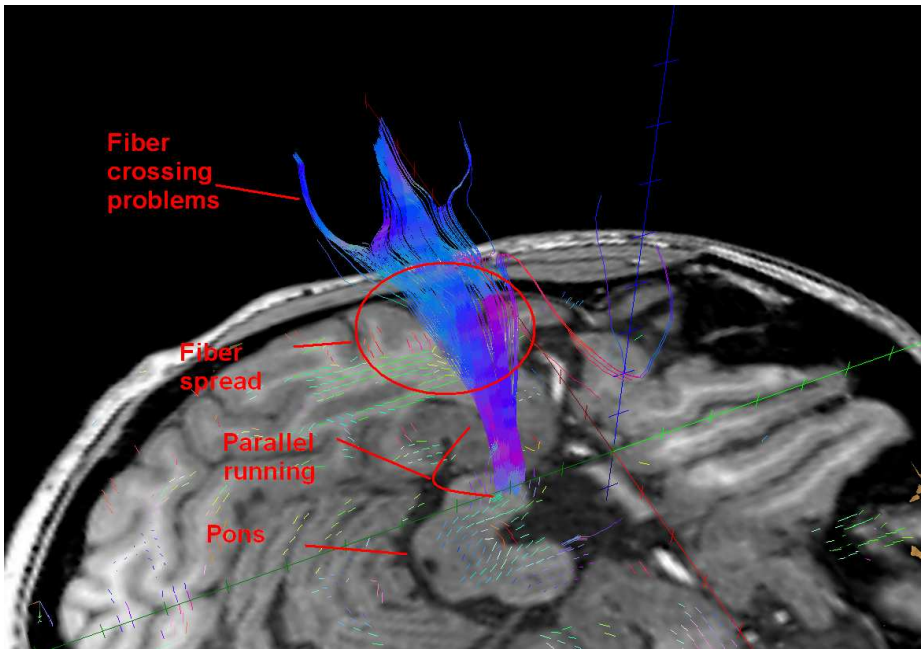

Figure 5.6: DTI limits.

Figure 5.7: Results of the superimposition of DTI and Mote-Carlo data.

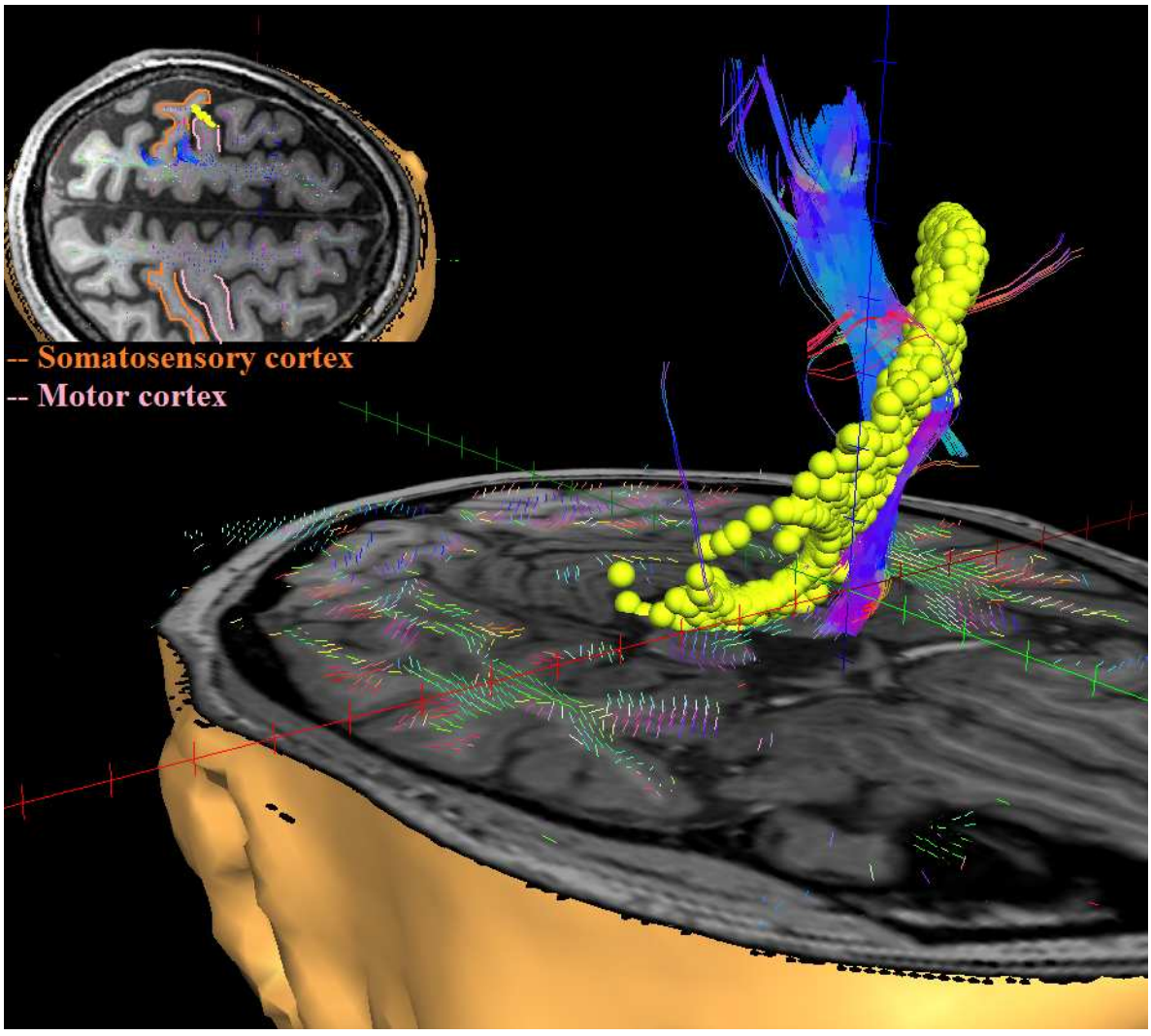

Chapter 6

6.1 Discussion of the results and conclusion

6.1 Discussion of the results and conclusions

The starting point of this study was what had been reported in [12], i.e. the detection of the propagation of neural activity along the thalamo-cortical fiber tract using MEG. To this aim, the somatosensory system was activated by applying electrical stimulation to the medianus nerve. The first important thing to emphasize is that with respect to [12] I have done a good step forward. Thanks to my improved experimental setup, i.e. the much higher sample frequency (5000 Hz instead of 1000 Hz), the big number of averaged trials and the higher number of subjects (14 instead of 3), and the combination of functional data recorded by MEG with anatomical data obtained from MR I obtained comprehensive information and a high level of data quality. Accordingly, I could find a number of cases showing reliably and with high accuracy a spreading of activation along the thalamo-cortical tracts. The question why the spreading of activation could only be recorded in some subjects can have several answers: one explanation could be the different SNR in the subjects. It could well be that in case of high SNR the thalamic activity is buried in the brain noise not related to somatosensory processing and thus cannot be localized. Another reason could be the geometry of the head and the topology of the thalamus and its location in the head. Since in a spherical head, deep sources as well as dipolar sources with a radial dipole orientation create only negligible magnetic brain activity, it could be that subject specific shape and location of the thalamus is crucial for recording a signal from this area. However, it is noteworthy that only in one subject the movement of the dipole was found for left and right stimulation.

The Monte-Carlo simulation executed in order to verify the localization accuracy of the dipoles along the thalamo-cortical tract with respect to the noise in the MEG data, confirmed the results: while for different noisy signals the trajectory remained the same, the volume of the confidence ellipsoids indicating the localization accuracy depicted from the 90% of the noisy dipoles, grows non-linearly with the depth of the source location. This is in accordance with MEG theory, which predicts that the magnetic field detected is inversely proportional to the cubic of the depth.

In order to test whether MEG can infer thalamo-cortical signal propagation, the trajectory of the moving dipole was compared to the thalamo-cortical fiber trac as reconstructed by DTI technique. Since the source localization in MEG is limited and depends strongly on the noise level of magnetic activity the comparison between fiber tract and dipole trajectory needs to take into account the localization error, i.e. the comparison was executed on the results obtained from the Monte-Carlo simulation. Results show some

parallels between the courses of the fiber tract and the dipole trajectory but also considerable deviations. Therefore, still a clear conclusion cannot be drawn and a differential interpretation of the findings is required. The discrepancy between fiber tract and dipole trajectory can be explained by the limitations of MEG source localization and DTI based fiber tract reconstruction. For brain region close to the center of the head DTI works well, because fiber tracts are dense and propagate along defined directions. In contrast MEG source localization is limited for deep sources and dipoles with radial orientations yielding unreliable source reconstruction results. In the central part of the fiber the match of the fiber-dipole works quite well and there is decent agreement between the dipole trajectory and the fiber tract. For what regards the trajectory close to the primary cortex dipoles deviate from the course of the fiber. This mismatch might be due to the problem of fiber tracking of highly diverging fibers like they can be found in cortical regions.

An alternative hypothesis explains the thalamo-cortical dipole trajectory not by the propagation of neuronal activity along the afferent somatosensory pathway, but by the superposition of subsequent activation of thalamus and primary somatosensory cortex. The magnetic field generated by exclusive activation of the thalamus can be modeled by a dipole located in this area. Likewise, the field generated by the activation of the primary somatosensory cortex can be perfectly explained with a dipole in SI. However, when thalamus and primary cortex are activated simultaneously the localization of the dipole depends largely on the relative contributions of the thalamic and the cortical activity to magnetic field. The major argument against this hypothesis is that in this case the dipoles movement should propagate from one to the other following a straight line. The straight trajectory could be demonstrated with a simulation study performed with the “BESA” program simulator: two dipoles were placed in the brain, one in the cortex and the other one in the thalamus, the simulator generated artificial signals from the known position of the sources by solving the forward problem. In the simulation the relative contribution of the thalamic and the cortical source was systematically varied. The artificial signal was then transferred to BESA source analysis module and analyzed with source analysis algorithm, i.e. the inverse problem is solved. Indeed the solution by putting only one source as a priori information by solving the inverse source problem yielded a dipole moving in a straight line from the thalamus to S1. By contrast, the trajectories recorded in the experiment don’t follow a straight line and thus the alternative explanation is very

In order to come to clear decision whether MEG can detect thalamo-cortical spreading of activation further studies and analysis are thus required. Recently we collected the same kind of data from a patient who has a congenital anomality in the route of thalamo-cortical fibers tract. If the dipole source obtained for the early evoked fields follows indeed the course of fiber tract the question can be clearly answered

More generally, integration of DTI with MEG source analysis has so far only used rarely. Although the combination of different methods seems to be promising there are also limitations which make these two techniques difficult to match. If further studies will prove that MEG can detect signal propagation from the depth of the brain, this will open new applications for MEG.

[1]Vrba J., Robinson S.,2001. Signal Processing in Magnetoencephalography. Methods Vol. 25(2), pp 249-71.

[2] Del Gratta C., Pizzella V., Tecchio F., Romani, G., 2001. Magnetoencephalography - a noninvasive brain imaging method with 1 ms time resolution. Rep. Prog. Phys. Vol. 64, pp. 1759-1814.

[3] S. Baillet, J.C. Mosher, R.M.Leahly , 2001. Electromagnetic brain mapping. Signal Processing Magazine, IEEE, Vol. 18, No. 6., pp. 14-30.

[4]M. Hämäläinen, R. Hari, R. Ilmoniemi, J. Knuutila, and O. Lounasmaa, 1993. Magnetoencephalography. Theory, instrumentation and applications to the noninvasive study of human brain function, Rev. Mod. Phys., vol. 65, pp. 413-497.

[5] C. Del Gratta, V. Pizzella, K. Torquati, and G.L. Romani, 1999. New trends in magnetoencephalography, Electroencephalogr. Clin. Neurophysiol. Suppl., vol. 50, pp. 59-73.

[6] Clarke, J.,1996. SQUID Sensors: Fundamentals, Fabrication and Applications. Weinstock, H. Ed., pp. 1–62, Kluwer Academic, Dordrecht.

[7] Hansen P. C., Kringelbach M.L., Salmelin R., 2010. Meg: An Introduction to Methods, Oxford Edition.

[8] Kakigi R ., 1994. Somatosensory evoked magnetic fields following median nerve stimulation . Neurosci Res , Vol. 20, pp. 165 – 174 .

[9] Hari R., Forss N., Magnetoencephalography in the study of human somatosensory cortical processing. Philos Trans R Soc Lond B Biol Sci 354(1387):1145-1154.

[10] R. Gobbele et al., 1994. Different origins of low- and high-frequency components (600 Hz) of human somatosensory evoked potentials. Electroencephalogr. Clin. Neurophysiol., Vol. 115, pp. 927-937.

[11] Curio G. et al., 1994. Localization of evoked neuromagnetic 600 Hz activity in the cerebral somatosensory system . Electroencephalogr. Clin. Neurophysiol., Vol. 91 , pp. 483 – 487 .

[12] Kimura T, Ozaki I, Hashimoto I, 2008. Impulse propagation along thalamocortical fibers can be detected magnetically outside the human brain. The Journal of Neuroscience, 28(47), pp.12535-8.

[13] A. A. Ioannides, P. B. C. Fenwick, L. Liu, 2005. Widely Distribute Magnetoencephalography Spikes Related to the Planning and Execution of Human Saccades. The Journal of Neuroscience, 25(35), pp. 7950-7967.

[14] C.J. Poletto, C.L. Van Doren,1999. A High Voltage, Constant Current Stimulator for Electrocutaneous Stimulation Through Small Electrodes. IEEE Transaction on Biomedical Engineering , 46(8), pp. 929.

[15] T. Yamamoto, S. J. Williamson, L. Kaufman, C. Nicholson, R. Llinas,1988. Magnetic localization of neuronal activity in the human brain, Vol. 85, pp. 8732-8736.

[16]C. Papadelis, S. Eickhoffì, K. Zillesand A. Ioannides, 2010. BA3b and BA1 activate in a serial fashion after median nerve stimulation: direct evidence from combining source analysis of evoked fields and cytoarchitectonic probabilistic maps. NeuroImage, Vol. 54(1), pp. 160-73.

[17] Liu A.K., Dale A.M., Belliveau J.W.,2002. Monte Carlo simulation studies of EEG and MEG localization accuracy. Hum Brain Mapp. ,Vol. 16(1), pp.47-62.

[18]R. Kakigi et al.,2000. The somatosensory evoked magnetic fields. Progress in Neurobiology, Vol. 61, pp.495-523.

[19] Ikeda H, Leyba L, Bartolo A, Wang Y, Okada YC, 2001. Synchronized spikes of thalamocortcal axonal terminals and cortical neurons are detectable outside the pig brain with MEG. J Neurophysiol, Vol. 87, pp. 626–30.

[20] Papadelis, C., Poghosyan, V., Fenwick, P.B., Ioannides, A.A., 2009. MEG's ability to localize accurately weak transient neural sources. Clin. Neurophysiol.,Vol.120 (11), pp. 1958–1970

[21] Braun C. et al., 1997. Confidence interval of single dipole locations based on EEG data. Brain Topography, Vol.10, N.1

[22]K. Yamada et al., 2007. Somatotopic Organization of Thalamocortical Projection Fibers as Assessed with MR Tractography, Radiology, Vol. 242, pp. 840-845.

[23]Kamali A., Kramer L.A., Butler I.J., Hasan K.M., 2009. Diffusion tensor tractography of the somatosensory system in the human brainstem: initial findings using high isotropic spatial resolution at 3.0 T. Eur Radiol., Vol.19(6), pp.1480-8.

[24] J. Heon Hong, S. Min Son, S. Ho Jang, 2010. Identification of spinothalamic tract and its related thalamocortical fibers in human brain. Neuroscience Letters, Vol. 468,pp.102–105.

[25] Mori, 2007. Introduction to Diffusion Tensor Imaging. Elsevier.

[26] Toga A.W., Mazziotta J. C.,2002. Brain mapping : the methods (2nd Ed.) , Academic Press Inc .

[27] H. Johansen-Berg,T. E. J. Behrens, 2009. Diffusion MRI: from quantitative measurement to in-vivo neuroanatomy. Academic Press Inc.

[28] Ioannides , A. A. , Liu , M. J. , Liu , L. C. , Bamidis , P. D. , Hellstrand , E. , & Stephan , K. M ., 1995. Magnetic field tomography of cortical and deep processes: examples of “real-time mapping” of averaged and single trial MEG signals. Int. J. Psychophysiol, Vol. 20 , 161 – 175 .

[29] Tesche , C. D. , & Karhu , J., 2000. Theta oscillations index human hippocampal activation during a working memory task . Proc Natl Acad Sci U S A , Vol. 97, pp- 919 – 924 .